## Experimental Assessment of Microbial Fuel Cells for Treatment and Nutrient Recovery from Different Wastewaters

# EXPERIMENTAL ASSESSMENT OF MICROBIAL FUEL CELLS FOR TREATMENT AND NUTRIENT RECOVERY FROM DIFFERENT WASTEWATERS

by

Hadeer Abdalla

A Thesis presented to the Faculty of the
American University of Sharjah
College of Engineering
In Partial Fulfilment
of the Requirements
for the Degree of

Master of Science in
Civil Engineering

Sharjah, United Arab Emirates

May, 2022

**Declaration of Authorship**

I declare that this thesis is my own work and, to the best of my knowledge and belief, it does not contain material published or written by a third party, except where permission has been obtained and/or appropriately cited through full and accurate referencing.

Signed……Hadeer Abdalla…….

Date……18/05/2022…..……

## Approval Signatures

We, the undersigned, approve the Master's Thesis of Hadeer Samir Abdalla

Thesis Title: Experimental Assessment of Microbial Fuel Cells for Treatment and Nutrient Recovery from Different Wastewaters

Date of Defense: 10 May 2022

| **Name, Title and Affiliation** | **Signature** |
|---|---|
| Dr. Kazi Fattah<br>Associate Professor, Department of Civil<br>Thesis Advisor | |
| Dr. Mohamed Abdallah<br>Associate Professor, Department of Civil and<br>Environmental Engineering, University of Sharjah<br>Thesis Co-Advisor | |
| Dr. Md. Maruf Mortula<br>Professor, Department of Civil Engineering<br>Thesis Committee Member | |
| Dr. Fatin Samara<br>Professor, Department of Biology, Chemistry and<br>Environmental Sciences<br>Thesis Committee Member | |
| Dr. Irtishad Ahmad<br>Head<br>Department of Civil Engineering | |
| Dr. Lotfi Romdhane<br>Associate Dean for Graduate Affairs and Research<br>College of Engineering | |
| Dr. Fadi Aloul<br>Dean<br>College of Engineering | |
| Dr. Mohamed El-Tarhuni<br>Vice Provost for Research and Graduate Studies<br>Office of Research and Graduate Studies | |

## Acknowledgments

First and foremost, I am thankful to Allah the almighty, for giving me the opportunity to undertake this study and, the ability and knowledge to complete the Master's thesis. I would like to express my gratitude to my supervisor, Dr. Kazi Fattah for his support, patience, and his precious advice. Without his guidance and constructive feedback, I wouldn't have been able to successfully complete my thesis. I also wish to express my utmost appreciation to Dr. Mohamed Abdallah for his invaluable assistance and his continuing encouragement throughout my journey. I have been extremely fortunate to work under the supervision and mentorship of Dr. Kazi and Dr. Mohamed, where I learned from their invaluable experiences and rich knowledge.

I would like to express my gratitude to the American University of Sharjah, for providing me with this opportunity and funding my research. I also want to express my gratitude to the University of Sharjah central laboratories for providing me with the facilities to conduct my experimental research. I would like to particularly express my sincere appreciation to Ms. Loubna Chaabi, whom I consider my older sister. I am very thankful for your technical and personal support as well as guidance throughout the masters. I would also like to genuinely acknowledge the efforts of my dear friend and lab partner, Nisreen. She dedicated her time and efforts to help with the experimental work, for that and more, I will forever be indebted. I also would like to thank all the researchers and staff who have taken the time to discuss and enrich my research work.

To my friends whom I consider my second family, who had turned all the anxiety and hard times into cheerful moments, thank you for being there at every moment of the past few years, no words will ever be sufficient to express my gratitude. I would like to particularly thank, Zakiya, Wedad, Sara Smadi, Rawan, Mariam, and Abdul-Rahman, whom the completion of the thesis would not have been possible without you. I also want to extend my thanks to Anwar, Aamal, Reem, Maha, Sarah Sinno, Sarah Sami, Zahraa, and Zainab. The key to my success were my parents, whom their warm prayers, unwavering love, support, encouragement, and faith in my capabilities provided me with the strength to pursue my master's degree. Your pride in me is what made me feel the value of reaching this milestone. To my sister and brothers, you have been and always will be the joy of my life.

**Dedication**

To my family…

**Abstract**

Wastewater is an abundant renewable source of nutrients such as nitrogen and phosphorus. However, current recovery methods require large amounts of energy and chemicals. Consequently, these processes pose economic and environmental burdens and is therefore often not implemented. Microbial fuel cells (MFC) are one of the bio-electrochemical wastewater treatment technologies that has potential for nutrient recovery as it can reduce chemicals cost while at the same time treat the wastewater and produce electricity. However, there is limited knowledge of the optimum operation mode of MFCs and the effect of the substrate on nutrient recovery. This study investigates the efficiency of struvite formation for nutrient recovery in a MFC using various wastewater substrates, such as, urine, centrate, and greywater (phase I) and different operating modes (phase II). In phase II of the experimental run the system was operated by recirculating the treated anolyte to the cathode compartment. The performance of the 700ml-volume dual-chamber cells was assessed based on electricity output, organics removal in terms of soluble chemical oxygen demand (sCOD), and struvite recovery. The highest sCOD removal efficiency of over 95% was achieved with the centrate-fed cell. The sCOD removal efficiency increased by 24% from the single operation (phase I) to the recirculation stage (phase II). The highest maximum power density generated from the urine, centrate, and greywater fed MFCs for phase I were found to be 1.7, 1.5, and 0.95 $mW/cm^2$, and 1.18, 0.82, and 0.73 $mW/cm^2$ for phase II, respectively. The urine-fed 700ml cell produced the highest struvite precipitate quantity (1.5g), followed by centrate (1.3g) and greywater (0.3g) in phase I, while the urine sample yielded 1.7g in phase II. The highest phosphate recovery efficiencies of over 55% (phase I) and 20% (phase II) were found for the cell treating urine, while efficiencies of other substrates were 36% (for centrate) and 48% (for greywater. Morphological and chemical analysis of the precipitate formed confirmed that the nutrients were recovered primarily as struvite. The results of this study verify the potential for implementing MFCs for nutrient recovery and anolyte recirculation.

**Keywords: Bio-electrochemical systems; microbial fuel cell; nutrient recovery; substrate; operation mode.**

## Table of Contents

## List of Figures

## List of Tables

## List of Abbreviations

| | |
|---|---|
| BES | Bio-electrochemical Systems |
| COD | Chemical Oxygen Demand |
| DAQ | Data Acquisition |
| DO | Dissolved Oxygen |
| EC | Electrical Conductivity |
| EDS | Electron Dispersive Spectroscopy |
| EPA | Environmental Protection Agency |
| FTIR | Fourier Transform-Infrared Radiation Spectroscopy |
| LSV | Linear Sweep Voltammetry |
| MFC | Microbial Fuel Cell |
| ORP | Oxidation-Reduction Potential |
| PAO | Phosphorus Accumulating Organisms |
| $Pds_{max}$ | Maximum Power Density |
| PEM | Proton Exchange Membrane |
| PTFE | Polytetrafluoroethylene |
| SEM | Scanning Electron Microscopy |
| TN | Total Nitrogen |
| TP | Total Phosphorus |
| TS | Total Solids |
| VS | Volatile Solids |
| UAE | United Arab Emirates |
| UMFC | Up-flow Microbial Fuel Cell |

| | |
|---|---|
| USDA | United States Department of Agriculture |
| WWTP | Wastewater Treatment Plant |
| WHO | World Health Organization |
| XRD | X-ray Diffraction |
| XRF | X-ray Fluorescence |

List of chemical species:

| | |
|---|---|
| $Al^{3+}$ | Aluminum |
| $CO_2$ | Carbon Dioxide |
| $Ca^{2+}$ | Calcium |
| $H^+$ | Hydrogen Ion |
| FePC | Iron Phthalocyanine |
| $Mg^{2+}$ | Magnesium |
| $MgCl_2$ | Magnesium Chloride |
| MgO | Magnesium Oxide |
| $MnO_2$ | Manganese Oxide |
| NaOH | Sodium Hydroxide |
| $NH_4^+$ | Ammonium |
| $NO_3$ | Nitrate |
| $PO_4^{3-}$ | Orthophosphate |
| Pd | Palladium |
| Pt | Platinum |
| $O_2$ | Oxygen |

# Chapter 1. Introduction

## 1.1. Overview

Traditional non-renewable energy sources, such as fossil fuels and natural gases, are being depleted due to excessive consumption. During its use, these fuels undergo combustion to produce energy leading to the release of carbon dioxide ($CO_2$) and other harmful greenhouse gases. Despite their crucial function and environmental merits, conventional wastewater treatment plants (WWTPs), particularly biological processes, are energy-intensive, consuming approximately 0.75% of the global electricity demand [1], [2]. The need for sustainable wastewater treatment solutions have promoted the shift toward energy-neutral/positive methods. Bio-electrochemical systems (BESs), also known as microbial electrochemical technologies, are emerging techniques that utilize microbes capable of directly converting the chemical energy of biodegradable organics in wastewater to electricity. It has been found that using wastewater for energy production can potentially replace coal, as it can generate an equivalent quantity of energy [3].

### 1.1.1. Microbial fuel cell

The microbial fuel cells (MFCs) are a type of BES whereby electrical energy is produced from the catalytic activity of microbes consuming the organics present in wastewater [4]. MFCs are considered a renewable energy source and an innovative wastewater treatment system with no electricity input. The MFC history dates back to the late 1990s, and since then, the technology has gone through massive developments and significant upgrades, with power outputs increasing over a thousand-fold [5]. Nevertheless, the MFC technology remains under development and has been actively investigated and improved towards full-scale applications.

Figure 1-1 shows the working mechanism of an MFC; two electrodes (anode and cathode) are separated by a membrane, typically a proton exchange membrane (PEM). An anaerobic oxidation reaction occurs in the anodic chamber resulting in the formation of an electrogenic biofilm. Such a process drives the forward reaction and facilitates the release of electrons which travel through an external circuit to the cathode [6]. This process is achieved via electroactive microorganisms that degrade the organics in the substrate and extracellularly transfer electrons. The reduction reaction is further

continued in the anodic chamber, where $CO_2$ is released, and the produced ions ($H^+$) are conveyed through the PEM to the cathodic compartment. The cathodic reaction occurs when the $H^+$ near the cathode, and the electrons are transferred to the terminal electron acceptor ($O_2$), which gets reduced to water.

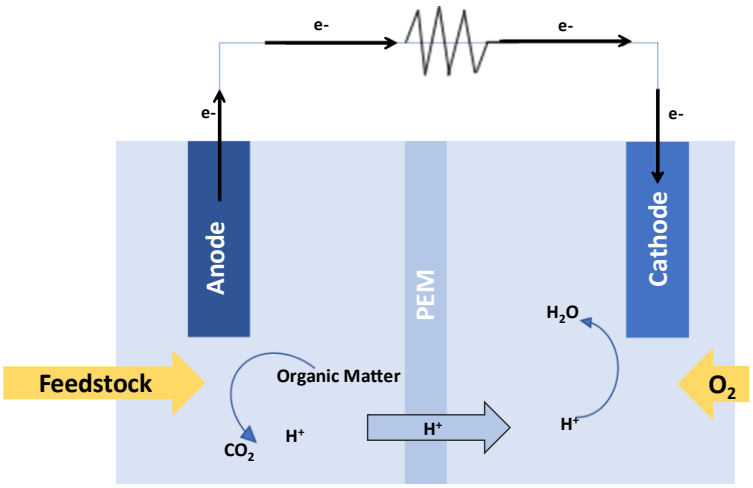


Figure 1-1: Schematic diagram for the working mechanism of microbial fuel cells.

A wide range of substrates can be utilized in the MFC, effectively treating and fueling the cell [7]. Carbon sources for the MFC microorganisms include municipal wastewater, sludge from municipal or industrial sources [8], glucose, sucrose [9], and acetate [4], among others. Equations 1, 2, and 3 are examples of the reactions occurring in the anodic and cathodic chambers using acetate as a feedstock [10].

$$\text{Anodic chamber: } CH_3COO^- + 2H_2O \rightarrow 2CO_2 + NH_3 + 7H^+ + 8e^- \quad (1)$$

$$\text{Cathodic chamber: } O_2 + 4e^- + 4H^+ \rightarrow 2H_2O \quad (2)$$

$$NH_3 + H_2O \rightarrow NH_4^+ + OH^- \quad (3)$$

### 1.1.2. Nutrient recovery

Conventional wastewater treatment has mainly focused on the quality of treated effluent rather than utilizing the water as a resource, for example, through nutrient recovery. Research interests have shifted toward investigating potential resource recovery from wastewater as it is an abundant nutrient source [11]. Municipal wastewaters received at WWTPs constitute substantial nitrogen (20 to 35 mg/L) [12] and phosphorus (4 to 11mg/L) [13] loads. Considering the high energy content and abundant nutrients and chemicals, wastewater can be regarded as a valuable renewable source for energy

harvesting and nutrient recovery. Traditional WWTPs are transitioning to become resource recovery facilities to promote sustainability in this vital sector [14].

Phosphorus, a substantial element present in wastewater, is typically mined from phosphate rocks which are a non-renewable resource and is expected to be depleted over the next century [15]. In addition, the minable phosphorus resources are limited to specific regions, including China, Morocco, Russia, and the United States, which account for 75% of the total reserves. The leading cause behind phosphorus depletion is the increasing demand for fertilizers associated with population growth and the need to grow more food. Nutrients, such as phosphorus and nitrogen (as ammonium), can be recovered using struvite ($MgNH_4PO_4 \cdot 6H_2O$) precipitation. Struvite, also known as MAP (magnesium, ammonium phosphate), is characterized as a precipitate with low impurities; hence, it is regarded as a valuable fertilizer. Struvite crystals are initiated by the nucleation stage, where the combination of ions occurs, followed by the crystal growth stage [16]. The general reaction occurs according to Equation 4 [17].

$$Mg^{2+} + NH_4^+ + H_nPO_4^{3-n} + 6H_2O \rightarrow MgNH_4PO_4 \cdot 6H_2O + nH^+; \text{ where } n = 0, 1, \text{ or } 2 \quad (4)$$

The formation of struvite is affected by several factors, mainly pH, magnesium to phosphorus molar ratio, and the presence of competing ions [14]. The nucleation of MAP depends primarily on the pH, which may reach as high as 11, and the most favorable pH is in the range of 8-9 [17]. Moreover, nucleation of struvite requires the presence Mg:N:P = 1:1:1 (equimolar ratios). As a result of the variation of these ions in wastewater, where Mg is the limiting ion, the addition of reagents to reach the required molar ratios is imperative for the initiation of struvite nucleation. Typically, such reagents are added at high dosages to account for competitive ions, such as $Ca^{2+}$ and $Al^{3+}$, that may react and decrease the final quantity of struvite [16]. The reagents utilized in this process, i.e., Mg sources such as magnesium chloride and magnesium oxide, reduce the economic viability of struvite recovery in WWTPs.

Practical application of the struvite precipitation process has been hindered by the high cost of the chemical buffers required. The use of recovered struvite in agricultural applications is a promising solution; nevertheless, the application as an economical fertilizer has not been investigated sufficiently [17]. Recently, very few studies have examined the use of MFCs to recover nutrients as struvite. The ammonium transported from the anodic to the cathodic chamber via diffusion process can eliminate the need

for buffering agents. It increases the pH in the cathodic compartment providing the optimum conditions for struvite recovery by increasing the buffering capacity.

## 1.2. Problem Identification

The advancement of the MFC technology for wastewater treatment toward commercialization has been restricted despite three decades of ongoing research and experimental work. The full-scale application of the MFC is a challenge mainly due to the costly components and relatively low electricity output. Moreover, many research studies investigated the treatment of simple substrates, e.g., acetate or wastewater, using MFCs; nevertheless, the varying characteristics of the latter have produced an unstable power supply. Nutrient-rich wastewaters have been rarely studied and compared in the MFC literature. Furthermore, to successfully implement field-scale MFCs, further research is required to emphasize the sustainable attribute of the MFCs as WWTP operators are shifting toward resource recovery and value-added materials. Limited research has been performed on the nutrient recovery mechanisms using MFCs. In particular, few studies have investigated the potential of MFC for nutrient recovery as struvite crystals. To date, there is no consensus over optimum MFC configuration for the recovery of struvite.

## 1.3. Thesis Objectives

Based on the outlined knowledge gap, this study aims to investigate the performance of MFCs in struvite recovery, organic treatment, and electricity harvesting from various substrates. The specific objectives of the present study are to:

- Investigate the treatment efficiency and electricity generation of a modular, dual-chamber MFC using different substrates, i.e., urine, centrate, and greywater.
- Study the potential struvite recovery from MFCs through different operating modes, i.e., batch single-stage and sequencing two-stage (using recirculated anolyte) modes.
- Assess the effect of urine as feedstock on struvite nucleation and recovery.

## 1.4. Research Contribution

The present research aims to fill a critical gap in the literature by studying different operating modes of the MFC for nutrient recovery while maintaining stable energy

output and treatment efficiency. A novel sequencing configuration of an MFC treating wastewater and recovering struvite is proposed and evaluated. Moreover, a key contribution of this work is to assess and compare the performance of MFCs with nutrient-rich substrates that have not been studied in the literature. The outcomes of this research intend to develop an understanding of nutrient recovery in the form of struvite from MFCs and identify an optimum operating mode toward maximizing the sustainability and economic benefits of the technology.

## 1.5. Thesis Organization

The thesis dissertation is organized as follows:

Chapter 2: Background and Literature Review

This chapter includes a review of previous work on the MFC and its tested operation mechanisms and substrates, in addition to the nutrient recovery, using conventional methods and MFCs.

Chapter 3: Methodology

The experimental framework, operating conditions, measurements, and analytical tests are thoroughly described in this chapter.

Chapter 4: Experimental Setup

This chapter includes the assembled experimental setup with details of the specific MFC unit design, configuration, cell components, and used materials.

Chapter 5: Results and Analysis

The chapter presents the substrate characterization results and all experimental findings pertaining to the MFC treatment and electricity generation. Moreover, the experimental results of struvite recovery are thoroughly discussed. Lastly, the effect of different cell operating modes and substrates on struvite recovery are analyzed.

Chapter 6: Conclusion and Future Work

This chapter summarizes the findings and conclusions drawn from the thesis work, as well as future recommendations to improve the MFC technology toward sustainable implementation.

# Chapter 2. Background and Literature Review

This chapter covers the literature on MFC technology, including the different implemented configurations, operating modes, and utilized substrates for energy harvesting and treatment efficiency. Moreover, recent advances in nutrient recovery, in particular struvite precipitation, using MFC are also summarized; finally, a discussion of the limitations associated with current nutrient recovery technologies is also addressed.

## 2.1. Microbial Fuel Cell

### 2.1.1. Electrode material

A typical design of an MFC includes an anode, cathode, and membrane, which can be constructed using different materials, as summarized in Table 2-1. Electrode materials are continuously developed to account for the limitations in the currently used materials. Mostly, carbon-based materials are relatively more expensive, while other materials, such as stainless, steel, and graphite rods, are limited by their relatively small surface area [19]. Several studies tested the performance improvement of MFC in terms of electrochemical activity when using catalysts, such as metals (e.g., palladium (Pd), platinum (Pt)) and compounds ((manganese dioxide ($MnO_2$) and iron(II) phthalocyanine (FePC)) [20]–[23]. Carbon electrode materials deposited with Pt catalyst were found to have relatively higher power density and maintained stable operation of the MFC when compared to other catalysts. Moreover, the effect of waterproofing has been reported to increase the long-term stability of MFC in terms of power output using polymers such as polytetrafluoroethylene (PTFE). Moreover, to prevent short-circuits between electrodes and separate chemical reactions in addition to transfer of ions between the anodic and cathodic compartments [24]. Furthermore, the membrane serves as a barrier to inhibit crossover between the anode and the cathode and a barrier that prevents electron acceptor (i.e., oxygen) transfer from the cathodic compartment to the anode. In MFCs, PEMs are the most commonly used separator due to their moderately high conductivity toward cations and low internal resistance [25]. Several examples of PEM are shown in Table 2-1. Nevertheless, Nafion, manufactured by DuPont, is the most widely used PEM, which is characterized by the high conductivity.

Table 2-1: Common materials used in the components of a microbial fuel cell.

| Component | Material | Reference |
|---|---|---|
| Anode / cathode | Graphite; graphite felt; carbon paper; carbon cloth; carbon felt; glassy carbon; carbon brush; stainless steel | [10], [19], [26], [27] |
| Membrane | Nafion; polyethylene; Ultrex | [8],[16],[21],[22] |

### 2.1.2. Configuration

The design of a conventional MFC reactor can be a single-chamber, double-compartment, or an up-scaled version of these two configurations by increasing the compartment size or by cell stacking [28]. Single-chamber MFCs are configured by placing the anodic electrode on one side of the chamber, and the cathode is kept apart from the anode and exposed to air [29]. While single-chamber MFCs have been found to be more straightforward in terms of operation and scale-up, lab-scale experiments are commonly conducted using dual-chamber MFCs. Nawaz et al. [30] designed a dual-chamber with graphite rods for electrode materials to treat wastewater produced by the beverage industry [30]. Operating the MFC reactor revealed treatment efficiency of 84% based on chemical oxygen demand (COD) removal and a power output per unit volume of 15 $W/m^3$. Jiang et al. [31] constructed a single compartment air-cathode MFC using carbon-based electrodes [31]. The study intended to achieve a stable power output and eliminate precipitate accumulation on the cathode surface by utilizing a sponge electrolyte to separate the anode and cathode. The examined MFC configuration was able to maintain a power output of $100W/m^3$.

Multiple studies explored the performance of large-scale MFCs. The concept of large-scale MFCs is based on enlarging the dimensions of a single MFC reactor, including all its main anode and cathode components. Most of the reviewed literature developed single-chamber MFC systems with a rectangular design, as they entail simpler designs and are a cost-effective option compared to other alternatives. Fewer dual-chamber setups were tested under continuous-flow mode and included mostly up-flow reactors.

The tested rectangular-shaped MFCs had a relatively satisfying power output and treatment efficiency when compared to the tubular design based on the reviewed literature. A study that operated 1.6 L MFC constantly for three months yielded a maximum power output of 22 $W/m^3$ (695 $mW/m^2$) beside 90% removal efficiency of acetate [32]. A comparable outcome was revealed by another study operating an MFC

continuously for 212 days which had achieved a relatively low maximum surface power density ($Pd_{max}$) of 4 mW/m$^2$ [33]. Moreover, Hiegemann et al. continuously operated the MFC system for nine months which was reported to achieve a COD removal efficiency of 67% and a maximum power output of 82 mW/m$^2$ [34]. Another study continuously operated a 1L MFC system for 70 days while maintaining a neutral pH [35]. The power density output ranged from 2 to 10 W/m$^3$ and achieved 81% COD removal efficiency. The MFC performance in terms of electricity output and treatment efficiency was hindered due to the accumulated biomass on the anode. A large-scale tubular air-cathode MFC was conducted in a semi-continuous flow mode with a vast anode volume of 45 L [36]. A low power output of 110 mW/m$^3$ was reported, with a relatively low COD removal efficiency of 21.7%.

The literature has also covered the continuous flow stacked MFC with a volume exceeding 1L towards electricity improvement. Liang et al. [37] stacked fifty 20-L MFC units in order to construct a 1000-L MFC reactor [37]. Such assembly allows achieving a COD removal rate of 80% and volumetric $Pd_{max}$ of 125 W/m$^3$. High external resistance was found to impact the energy recovered from the system significantly. Another study stacked four 5-L bipolar flat plate cells for 34 days [38]. Poor MFC performance was reported as a result of a potential reversal in the cathode, membrane bending, and oxygen reduction rate. Nevertheless, lowering the pH of the cathode, positioning the membrane to inhibit movement, increasing the flow rate, and improving the oxygen concentration enhanced the cathode performance and produced a volumetric power density of 144 W/m$^3$. Another MFC with six 12-L cell stack modules experiment was operated continuously for six months, reaching a volumetric $Pd_{max}$ of 42.1 W/m$^3$ [39]. Two separate configurations were examined: (1) independent circuit connection (each cell connected with a separate resistor) and (2) parallel circuit connection (multiple units connected to a single resistor). The former setup was considered outstanding, as the current reversal caused a lower power density in the last. This finding was similar to another study utilizing a six-cell anaerobic baffled MFC stack [40]. The range of the maximum power density in both series and parallel was between 200 mW/m$^2$ and 270 mW/m$^2$, on the other hand, the individual unit produced 267 mW/m$^2$. This observation concluded that the connection type does not influence electricity generation, and a particular unit can acquire a high-power density.

More studies were focused on studying the connection type of the stack (individual, series, or parallel) and its influence on the overall performance. For individual against series connections, a study compared the overall performance of individual cells with in-series stacked systems shown in Figure 2-1 [41]. Single cells in the 20- and 40-unit produced a $Pd_{max}$ of 79 mW/m$^2$ and 4.2 mW/m$^2$, respectively, approximately 93% and 99% higher than the series connection, which can be attributed to the high internal resistance. For individual and parallel connections, a study stated that tubular reactors outperformed individual MFCs when connected in parallel [42]. This behavior was based on reduced organic content along the reactor, causing an increased over-potential when connected in parallel. Rahimnejad et al. [43] explored the performance of a 4-cell stacked MFC operated for three days [43]. In the case of individual MFCs, $Pd_{max}$ was 490 mW/m$^2$, although a 75% increase was observed in $Pd_{max}$ (2,003 mW/m$^2$) for the parallel connection stack.

a)

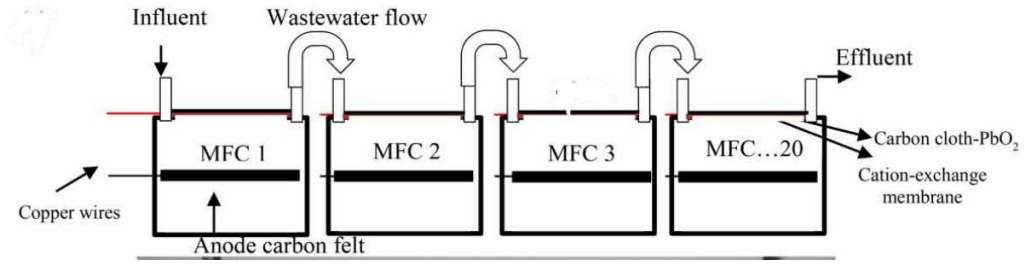


b)

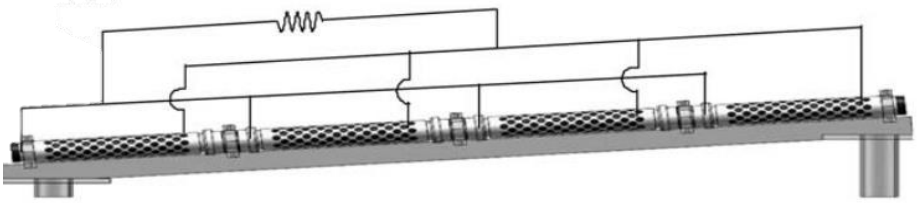

Figure 2-1: Schematic of stacked microbial fuel cells in a) series [41] and b) parallel connections.

### 2.1.3. Influence of substrate type

The substrate supporting the MFC cell was considered as a crucial operational parameter affecting the power production rate. A vast set of substrates, ranging from simple compounds to complex organic mixtures, were utilized in the literature. Although simple substrates were found to be effective for instant results, substrates containing complex organic matter support the growth of the diverse microbial community. The majority of the revised studies used acetate to fuel the MFC, with

fluctuations in results. Acetate is a simple substrate used to benchmark various cell elements, designs, and operating conditions [44]. When applied as feed, acetate could generate a 24% higher $Pd_{max}$ than domestic wastewater, ranging between 286 mW/m$^2$ and 218 mW/m$^2$, respectively [45]. Besides, power generation of up to 308 W/m$^3$ and COD removal efficiency of up to 99% were obtained using sodium acetate [32], [46]. Furthermore, the $Pd_{max}$ generated by the acetate substrate was 29% higher than that of glucose, 39% higher than dextran, 15% higher than starch, and 11% higher than butyrate [45]. However, in the same experiment, the MFC cell attained the lowest COD removal efficiency when acetate was used at the level of 8% compared with the other substrates (32, 10, 22, and 26% for glucose, butyrate, dextran, and starch, respectively). Another study evaluated the performance of fermentable glucose and glycerol and non-fermentable as acetate and lactate substrates and stated that glycerol affords the best results [47]. It was concluded that fermentable substrates promote the biodiversity and growth of the cathodic community, leading to improved overall process performance. Synthetic wastewater was found to be the second most employed substrate due to its consistency and flexibility in controlling its strength, pH, and conductivity [48].

Many studies have also used domestic wastewater to examine the actual operating parameters. A study compared the MFC performance with synthetic and municipal wastewaters, recording a $Pd_{max}$ of 125 W/m$^3$ when synthetic wastewater was used [37]. Nevertheless, in the case of municipal sewage, a remarkable increase in internal resistance was detected, and the cell yielded fluctuating results ranging between 7 W/m$^3$ and 60 W/m$^3$. Another finding was reported by Yu et al. [49], who obtained much lower power outputs ranging between 116 mW/m$^2$ -149 mW/m$^2$ with domestic wastewater compared with that in synthetic wastewater, ranging between 191 mW/m$^2$ -754 mW/m$^2$ [49]. The obtained lower power production was likely attributed to the change in ionic strength and microbial community [50]. In the same study, the volumetric $Pd_{max}$ generated by pig slurry-spiked feed was 62% greater than synthetic wastewater ranging between 5623 mW/m$^3$ and 2138 mW/m$^3$, respectively [51].

## 2.2. Nutrient Removal and Recovery

### 2.2.1. Conventional technologies

Struvite recovery is essential to mitigate eutrophication caused by phosphorus accumulation in water bodies and provide a renewable resource of phosphorus and

other nutrients, as discussed earlier. Considering the emerging trend towards utilizing sustainable and renewable resources, research efforts have been focused on investigating struvite recovery technologies. Different methods and techniques were being used for phosphorus removal. Chemical precipitation by adding metals such as iron and alum-phosphorus precipitate are popular phosphorus removal techniques [52]. Continuous stirring tanks were the most used for phosphorus recovery as struvite crystals [17]on a lab scale.

Stirred tank reactors are characterized by a simple configuration that facilitates control of the experiment. The reactor is equipped with a mixer for creating a homogenous media and aiding in nucleation and growth via enhancing the transfer of ions of the struvite crystals [28]. Moreover, struvite shape is affected by mixing conditions; turbulent solutions create irregularly shaped crystals [17]. Several studies selected the optimum mixing speed to opt for high struvite formation. Taylor et al. [29] observed an increase in struvite formation by 30% when the mixing rate was increased (160 rpm to 240 rpm). Fouling on mixer blades was detected at lower mixing speeds which reduces the crystal quality [53], and at rates higher than 500 rpm, the growth of struvite crystals is inhibited [54]. Energy consumption for stirring the solution was a limitation of the system. Therefore, several modifications were attempted to replace conventional mixers. An airlift system was operated in continuous mode, which resulted in 98% phosphate removal from formed struvite crystals [55]. Saidou et al. [56] utilized air bubbling for mixing the system and studied the effect of air flowrate on struvite formation in the reactor. The findings revealed that 10 L/min to 25 L/min achieved the highest struvite crystal formation, and beyond that range, struvite crystallization was inhibited, and operation costs increased.

Although chemical precipitation facilitates high struvite formation and phosphorus removal, nevertheless it has several limitations: increase of additive ions as a result of adding metals [57], high cost of chemical reagents, an increase of sludge [58], low purity of final product, and overall instability of the process [59]. Herna and Garrido-baserba [60] asserted that most operation costs were attributed to added chemicals and inappropriate selection of magnesium source for struvite formation. Other utilized technologies for phosphorus removal as struvite crystals include fluidized bed reactor (chemical precipitation), ion exchange methods (i.e., adsorption), and BES. MFC

system, a type of BES technology, provides optimum conditions for struvite formation, particularly pH conditions [61]. Therefore, the recovery of phosphorus using microbial fuel cells is an emerging technology. Moreover, several pilot-scale and full-scale struvite recovery systems have also been implemented such as such as the Pearl in Ostara, AirPrex , and PHOSPAQ are widely used [62]. The Ostara nutrient recovery system (shown in Figure 2-2) utilizes chemical doses, fluidization energy, and loading rate control to achieve struvite crystallization via an up-flow fluidized bed. The limiting element, which is Mg, is added in the form of magnesium chloride ($MgCl_2$) while the pH is controlled by the addition of NaOH. The Ostara technology runs by mean of the Pearl process as shown in Figure 2-2 obtained from [62]. The Ostara process has been widely implemented and was reported to achieve 90% P removal and an average of 28% removal of nitrogen [62]–[64].

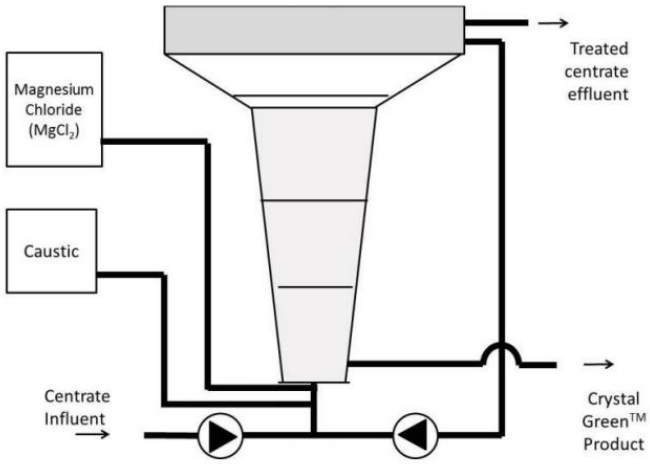


Figure 2-2: Schematic of the Ostara pearl process plant adopted from [62].

The Airpex was developed with the aim of Phosphorus recovery using a Continuous stirred-tank reactor (CSTR) where struvite precipitation experiments are conducted [65]. The pH adjustment is undertaken by air stripping, and $MgCl_2$ is used as a magnesium source. An aerated zone in the middle of the reactor lifts sludge upward by air bubbles, and in the outer part of the reactor, the sludge settles after reaching the surface (tranquil zone). Moreover, the precipitated struvite is continuously removed from the bottom of the CSTR. The Process diagram of Airprex is illustrated in Figure 2-3, which is adopted from [62]. In Germany and the Netherlands, this technology has been reported to remove 80-90% of phosphorus from sludge digestate in full-scale operations.

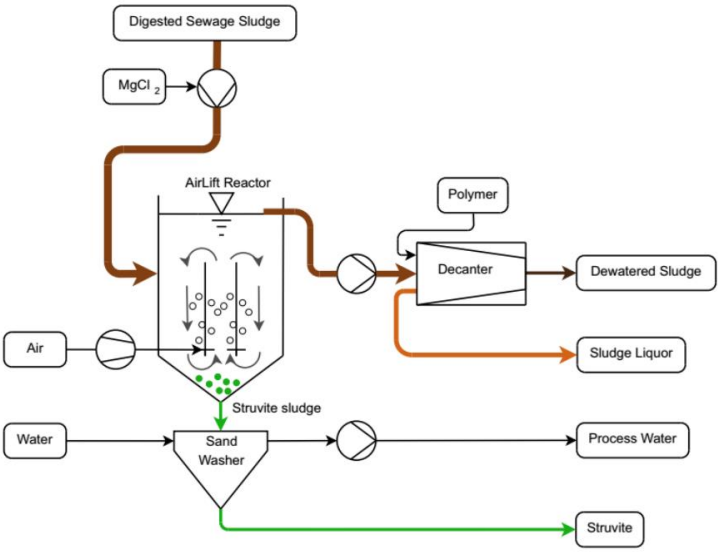


Figure 2-3: Schematic of the Airprex struvite recovery plant adopted from [62].

The PHOSPAQ technology is a full-scale plant for struvite recovery based in the Netherlands [66]. An aerated reactor is utilized where the pH is controlled at 8, and magnesium oxide (MgO) is added. A hydrocyclone and a press screw are used to gather the struvite from the bottom of the reactor, as shown in Figure 2-4. The PHOSPAQ technology has been implemented in the United Kingdom (UK), where it was found that P recovery reached 85% [62].

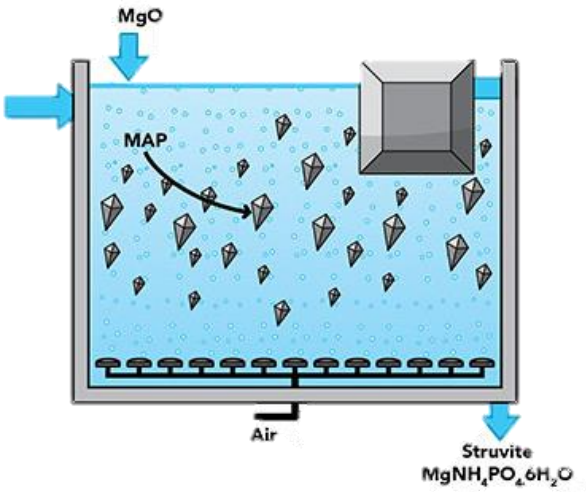


Figure 2-4: Schematic of the PHOSPAQ working mechanism adopted from [66].

### 2.2.2. Microbial fuel cells

The implementation of nutrient recovery in conventional wastewater treatment shall improve the sustainability of modern treatment techniques. Nutrient recovery using

MFCs has been explored widely in the literature using various substrates, as summarized in Table 2-. Various studies performed such a system under batch operating mode. Pepè Sciarria et al. [67] studied the energy and Phosphorus recovery of MFC from digestate. The system generated 14.2 $W/m^3$ and showed up to 90% phosphorus recovery when seawater bitterns were added and 44.7% COD removal efficiency [67]. Sharma and Mutnuri[68] assessed the performance of MFCs using urine in terms of energy generation and nutrients recovery. The results revealed that the system could potentially generate 0.68 $W/m^2$ and contribute to 70.0%, 50.0%, 54.3%, and 94.2% removal efficiencies for COD, $NH_4^+$-N, $NO_3^-$, and orthophosphate, respectively [68]. Orner et al. [69] also evaluated the feasibility of power generation and struvite precipitation of MFCs using side stream effluent of a wastewater treatment plant. The results found that the process can remove up to 53% of total nitrogen, produce $0.3W/m^2$, and remove COD at 45%-53% based on operating conditions [69]. Fischer et al. [70] attempted recovery of orthophosphate from digested sludge which typically dissolves in high concentrations (80 mg/L –300 mg/L) upon the AD process. A two-chamber MFC was used for the recovery of orthophosphate in the form of struvite, where 82% was recovered with a power output of 3.1 µW [70]. Also, [71]–[74] performed MFCs in batches to evaluate the biological treatment of synthetic wastewater. Almatouq and Babatunde [71] concluded that the system could achieve up to 192 $mW/m^2$ power density, 90% COD removal, and 84% total phosphorus precipitation. Almatouq and Babatunde [72] obtained a slightly higher power density of 198 $mW/m^2$ and 38% phosphorus recovery. Similarly, Happe et al. [73] recovered 34.8% of phosphorus using MFC. Tao et al. [58] reported a maximum ammonia and phosphate recovery of 70.2 and 92.8%, respectively, for both single and dual-chamber MFCs, with different power intensities of 560 $mW/m^2$ and 528 $mW/m^2$, respectively.

Other studies operated MFCs under different flow modes. Kim et al. [75] studied the efficiency of electricity generation and nutrient recovery (struvite) from a hybrid system containing multiple consequential MFCs, a struvite precipitation reactor, and a sedimentation tank. The study utilized synthetic wastewater as a substrate that was continuously fed into the system. The COD and total phosphate (TP) removal efficiency were obtained as 70 and 95% removal efficiency, respectively, with a power output of 2 mW [75]. Ye et al. [76] investigated the nutrient recovery potential of a double-chamber MFC under various operation modes, different aeration conditions, and using

multiple types of separators. The results showed that maximum recovery of nitrogen at 98.8% can be achieved when a forward osmosis separator is used. In comparison, a cation exchange membrane separator can yield a maximum phosphorus recovery of 94.9%. Moreover, the maximum voltage of 386.4 mV, 641.4 mV, and 591.9 mV can be generated from the MFCs operating under batch, self-circulation, and single-continuous modes, respectively [76]. Merino-Jimenez et al. [77] showed struvite recovery up to 94% containing magnesium ammonium phosphate and magnesium potassium phosphate crystals from a continuous flow of urine to an MFC with a total maximum power yield of 2.1 mW [77]. Similarly, You et al. [61] examined the feasibility of treating urine using MFCs under continuous operating mode. The results showed a potential phosphate recovery of 82%, along with COD removal and maximum power density of 20% and 14.3 $mW/m^3$ [61].

Few studies tested out the MFC efficiency in recovering phosphorus in the form of struvite are summarized in Table 2-2. Kim et al. [75] examined the efficiency of a hybrid reactor (MFC and a sedimentation tank) to generate electricity as well as recover struvite from synthetic wastewater influent. The experimental results revealed a COD and phosphates removal efficiency of 90% and 94%, respectively. Nevertheless, the observed power output was low in the hybrid reactor (0.033 mW/ 4.34 $mW/m^2$) compared to operating MFC alone (2 mW). The low power output in the hybrid system was a result of resistance of charge transfer as a result of residual organic presence. Sharma and Mutnuri [68] followed a similar approach to recover struvite; dual compartment MFC was used for the treatment of urine, and the treated effluent was directed to another tank for the chemical precipitation of struvite. Ye et al. [76] successfully operated a dual compartment MFC to remove phosphate and utilized chemical precipitation within the cell for recovery of the nutrient. The findings revealed that effective phosphorus removal was achieved by microbial absorption and the addition of NaOH in the anodic compartment. You et al. [61] assembled a three-stage hybrid reactor consisting of stacked MFCs, a precipitation tank, and another set of stacked MFCs. The results showed that 80% and 20% of the phosphate and COD were removed, respectively. Additionally, the power density of the two MFC stacks reached 14.3 $W/m^3$ and 11.8 $W/m^3$. Happe et al. [73] utilized a triple-compartment MFC to remove phosphorus from iron phosphate, which yielded 67% recovery.

Table 2-2: Literature summary of microbial fuel cell applications in nutrient recovery.

| Substrate | Inoculum | Operation Mode | Power Yield | COD Removal Efficiency (%) | Nutrient Recovery (%) | Reference |
|---|---|---|---|---|---|---|
| Synthetic wastewater | Sludge | Continuous | 2.0 mW | 70 | 95: TP* | [75] |
| Municipal wastewater | Anaerobic sludge | Batch<br>Self-circulation<br>Single-continuous | 386.4 mV<br>641.4 mV<br>591.9 mV | 81.2 | 83-95: $PO_4^{3-}$<br>97-99: $NH_4^+$ | [76] |
| Digestate | - | Batch | 14.2 $W/m^3$ | 27-44 | 90: $PO_4^{3-}$ | [67] |
| Urine | Digestate | Batch | 0.68 $W/m^2$ | 70 | 94.2: Ortho-P<br>50: $NH_4^+$<br>54.3: $NO_3$ | [68] |
| Wastewater | Shewanella putrefaciens and Geobacter metallireducens microbial cultures | Batch | 0.3 $mW/m^2$ | 45-53 | 52: TN** | [69] |
| Synthetic wastewater | Activated and anaerobic digester sludge | Batch | 192 $mW/m^2$ | 62-90 | 84: TP* | [71] |
| Urine | Activated sewage sludge | Continuous | 1.3-2.1 mW | 16.2-18.1 | 80.8-94.0: MAP+MKP*** | [77] |
| Synthetic wastewater | Activated sludge | Batch | 198 $mW/m^2$ | 70-90 | 38: P | [72] |
| Urine | Activated sewage sludge | Continuous | 11.6-14.3 $mW/m^3$ | 20 | 82: $PO_4^{3-}$ | [61] |
| Synthetic wastewater | Sewage sludge | Batch | - | - | 34: P | [73] |
| Synthetic wastewater | Anaerobic sludge and aerobic sludge | Batch | 528-560 $mW/m^2$ | 66-79 | 70.2: $NH_4^+$<br>92.8: $PO_4^{3-}$ | [74] |
| Digested sludge | Yeast | Batch | 3.1 µW | - | 82: $H_3PO_4$ | [70] |

* TP: Total phosphorus

** TN: Total nitrogen

*** MAP: magnesium ammonium phosphate; MKP: magnesium potassium phosphate

Moreover, Zang et al. [13] proposed the recovery of struvite in a precipitation reactor, followed by treatment and energy harvesting in an MFC. The experiment yielded promising results as the phosphorus recovery (by addition of magnesium) was 94.6% in addition to COD removal and power density of 64.9% and 0.9 $W/m^2$, respectively. Similarly, Fischer et al. [70] utilized a single-chamber MFC to mobilize phosphate present in the digested sludge resulting in phosphorus recovery of up to 84%.

There were several early attempts of identifying the viability of struvite formation and phosphorus using an MFC reactor alone [13], [70], [78]–[80]. Tao et al. [74] investigated the possibility of struvite formation in single and dual chamber MFC reactors. The results revealed a higher accumulation of struvite in the cathodic chamber (dual compartment cell) compared to the single MFC, as well as the presence of phosphorus accumulating organisms (PAOs). Hirooka and Ichihashi [78] investigated the performance of a single-chambered MFC after the accumulation of precipitate on the cathode surface. It was concluded that after removal of precipitate and conducting dissolution treatment of cathode electrode, the power output returned to the original value measured as current (4.3 $A/m^2$). In a similar matter, Ichihashi and Hirooka [78] achieved 27% phosphorus recovery (from struvite precipitate) using a single air cathode MFC.

Pepè Sciarria et al. [67] conducted an experiment using a single MFC to recover struvite and further conducted crystallization tests on the effluent using sea bittern. Using an MFC alone, 35.7% phosphate removal was achieved in addition to 44.7% COD removal and a volumetric power output of 14.2 $W/m^3$. A dual-compartment configuration MFC was tested for treatment of synthetic wastewater by initially adding it to the anode chamber and then reintroducing it to the cathodic compartment [74], [80]. Moreover, struvite crystals were recovered from anodic and cathodic compartments without the utilization of external precipitation reactors. The maximum obtained removal efficiency of phosphorus and COD were 95% and 90%, respectively. Nevertheless, the power output experienced a decrease and irregular resistance as the cathode had experienced scaling due to precipitate on the surface of the cathode. Merino-Jimenez et al. [77] also attempted to recover struvite crystals using an MFC reactor and added seawater/ $MgCl_2$. It was reported that the addition of seawater/ $MgCl_2$ increased struvite recovery from 21 to 94% but did not impact the power production of the MFC (1800 µW).

Table 2-2: Summary of studies on phosphorus recovery using microbial fuel cells.

| Reactor | Substrate | Phosphorus Recovery Efficiency (%) | pH | Power Density ($mW/m^2$) | Voltage (mV) | COD Removal (%) | Reference |
|---|---|---|---|---|---|---|---|
| Single air cathode | Synthetic wastewater | 94.1 | 7.0 | 4.3 | - | 91 | [75] |
| Double-chamber | Synthetic wastewater | 94.0 | 8.1-8.4 | - | 386-641 | 81 | [76] |
| Single air cathode | Digestate | 35.7 | 8.5 | 430 | 500 | 45 | [67] |
| Double-chamber | Urine | 94.2-99.0 | 6.3 | 123 | 645 | 70-82 | [68] |
| Double-chamber | Synthetic wastewater | 95 | 7.5-9 | 180 | - | 60-90 | [71] |
| Tubular single chamber | Urine | 94 (struvite) | 9.0-9.3 | 1800 (μW) | - | 18 | [77] |
| Double-chamber | Synthetic wastewater | 38 | 8.0 | 72.0 | 550 | 70-90 | [72] |
| Stacked | Urine | 80 | 6.6-9.3 | 652 (μW) | 4200 | 20 | [61] |
| Triple chamber | Sludge | 67 | 7.5 | - | 300 | - | [73] |
| Single/Double -chamber | Synthetic wastewater | - | 7.3/7.2 | 560/528 | 443/524 | 66/79 | [81] |
| Single air cathode | Synthetic wastewater | 55 | 7.3-8.6 | 4.3 ($A/m^2$) | - | - | [78] |
| Single air cathode | Swine wastewater | 27 | 7.8-8.4 | 2.3 | 300 | 91 | [82] |
| Single air cathode | Urine | 94.6 | 8.0-9.0 | 900 | 500 | 65 | [13] |
| Single air cathode | Digested sludge | 84 | 7.0-9.5 | - | 700 | - | [70] |

## 2.3. Summary

In this chapter, a comprehensive review of the literature was conducted on the applications of the MFC technology, in particular the utilization of the cell for struvite recovery. Comparisons between conventional (i.e., chemical precipitation) and the MFC technology were presented. Conventional nutrient recovery methods are associated with multiple disadvantages, including the high cost of chemical buffering reagents, low purity of struvite, and increased sludge formation. The studies performing struvite recovery using MFC were faced with issues such as the cathode scaling, which led to unstable power output and a decrease in power density. Overall, there is a lack of knowledge on the optimum MFC configuration and substrate for struvite recovery, in addition to a low understanding of the phosphorus removal mechanism in the cell. Therefore, the present experimental research aims to investigate different operating modes of the MFC to identify the optimum configuration and substrate for struvite recovery.

# Chapter 3. Methodology

In this chapter, the pursued experimental plan is detailed, in addition to an in-depth discussion of the operational parameters, analytical measurements, computations, materials, and methods utilized in the present work.

## 3.1. Research Plan

This section summarizes the stages experimental program, operating conditions, and substrates investigated. Figure 3- 1 illustrates the framework followed in the present experimental work. Upon the characterization of the selected substrates and the design and assembly of the MFC cells and lab setup, the experimental work was divided into two main phases: batch single-stage and dual-stage sequencing mode, followed by cathodic-nutrient recovery. A detailed discussion of the experimental setup is provided in Chapter 4.

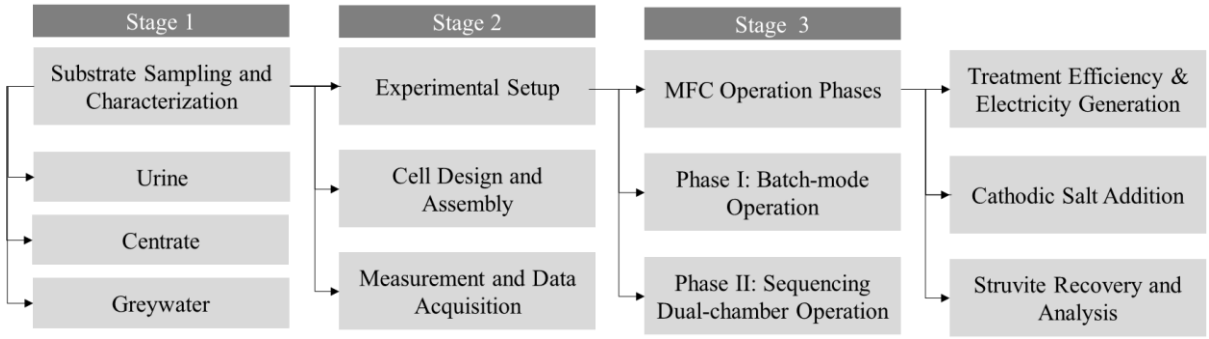


Figure 3- 1: Scope of work for the planned experimental study.

## 3.2. Experimental Operation

The MFC was operated in two phases with three different substrates, as summarized in Table 3-1. The following sections detail the examined substrates and operation modes.

Table 3-1: Experimental variables and operation stages of the current study.

| Parameter | Variable | Operation Phase/Cell |
|---|---|---|
| Configuration | Single batch operation | Phase I (Cell I) |
| | Sequencing two-stage mode | Phase II (Cell II) |
| Substrate | Urine (U) | Cells I/II-U |
| | Centrate (C) | Cells I/II-C |
| | Greywater (G) | Cells I/II-G |

### 3.2.1. Microbial fuel cell operation

The MFC experimental protocol involved two phases, each with a different operation mode. Urine was used as the feedstock to evaluate and compare the two phases, while centrate and greywater were only utilized during phase 1 as the performance in the MFC operation was uncertain and has not been studied in the literature. Figure 3- 2 shows the experimental protocol with a detailed description of each stage. The first phase was operated in batch mode, and it involved evaluating the performance of the MFCs in terms of treatment efficiency and electricity harvesting. The MFC was operated with a buffer solution on the cathode side and the substrate in the anode compartment. At the end of phase I, struvite was recovered in the cathodic compartment of the tested cells. Effluent catholyte samples were filtered using (microfiber filter paper 125 mm, 2 microns). The filtered catholyte was tested for nutrient removal, whereas a sample of the anolyte was tested for COD removal efficiency.

The second phase involved recirculating the treated anolyte to be utilized as a buffer in the cathode chamber while adding fresh substrate in the anodic chamber. The treatment efficiency and power output were evaluated similarly to the preceding phase. Upon the decline of the electricity output from the MFC, the struvite precipitation experiment was repeated for the recirculated anolyte. Phase II was operated to allow continuous operation of the MFC and to examine the potential nutrient recovery from the treated anolyte without disrupting the biofilm on the anodic side. Therefore, recirculating the anolyte will both serve as a buffer solution and a source for nutrient recovery.

### 3.2.2. Substrates

Fresh urine, centrate, and greywater were the main substrates that were examined during the different phases of the experiment. The urine samples were collected from healthy young volunteers, mixed using Dlab OS20-Pro digital mixer, and stored in 10 L jerry cans under 4$^{o}$C, as shown in Figure 3- 3. The urine samples were employed within one week of collection and returned to room temperature prior to use in the cells. The centrate samples were collected from the supernatant of an anaerobic digester at Al-Rawabi WWTP in Dubai, United Arab Emirates. The collected centrate was left to settle further, and the supernatant was mixed and stored below 4$^{o}$C, as depicted in Figure 3- 3.

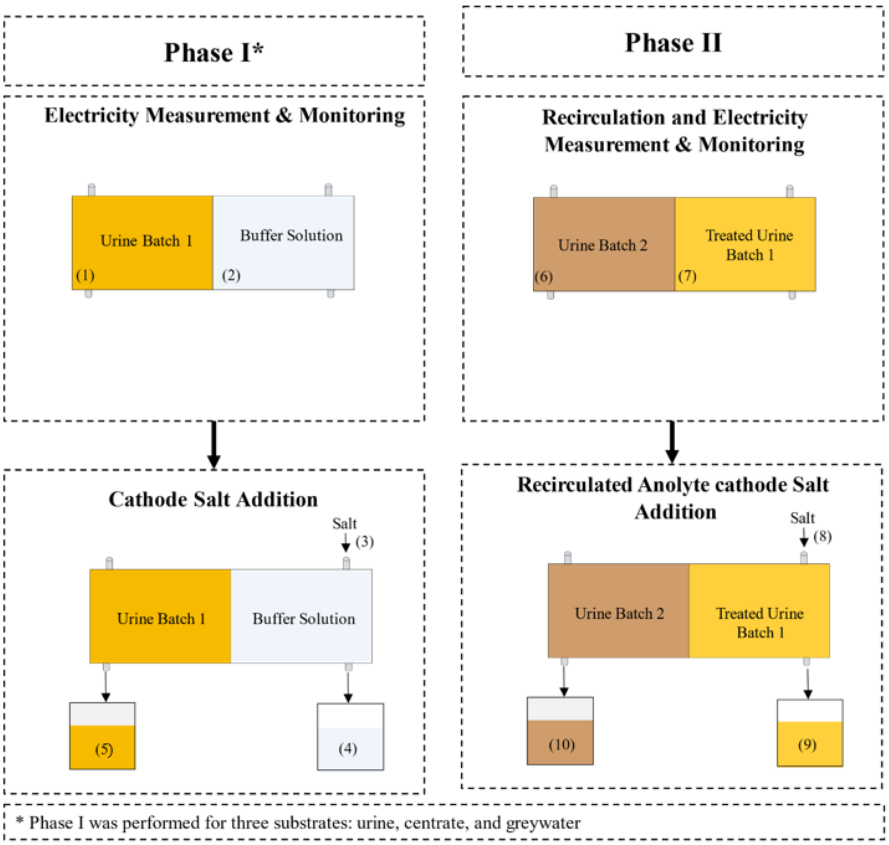


Figure 3- 2: Experimental operation for phases I and II.

(1) is the first batch of urine addition to the anode, (2) is the addition of buffer solution to cathode compartment, (3) is the addition of the $MgCl_2$ and commencement of precipitation reaction, (4) is the decanted buffer solution with precipitate, (5) is the treated first batch of urine, (6) is the addition of a second batch of urine to the anodic chamber, (7) is the recirculation of treated urine to cathode chamber as a buffer solution, (8) the addition of $MgCl_2$ and struvite precipitation experiment, (9) decanting of the buffer solution with precipitate, and (10) is the decanting of the treated urine batch 2.

The greywater shown in Figure 3- 3 was composed of laundry and dishwasher wastewater at a 1:10 ratio. The mixing ratio was obtained from the literature based on the greywater characteristics, particularly the organic load of dishwasher and laundry wastewaters [83]. All substrates were characterized based on the tests detailed in section 3.3.

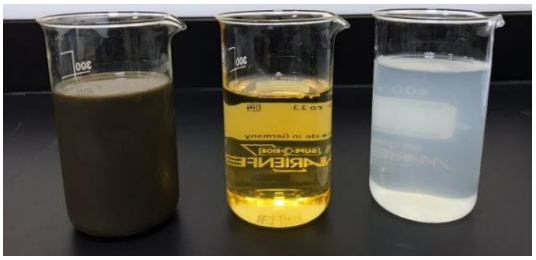

Figure 3- 3: Samples of the examined substrates: centrate, urine, and greywater (from left to right).

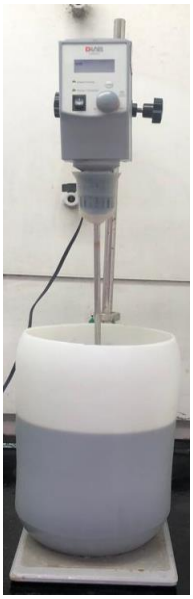

Figure 3- 4: Lab mixing setups for the examined substrates.

### 3.2.3. Electrochemical characterization

The performance of the MFC in terms of energy generation was assessed based on the electrical parameters calculated using Equations (5) to (9).

$$I = \frac{U}{R} \tag{5}$$

$$P_E = UI \tag{6}$$

$$Pd_{max} = \frac{UI}{A} \tag{7}$$

$$Pd_{max,v} = \frac{UI}{V} \tag{8}$$

$$J = \frac{I}{A} \tag{9}$$

where I is the electric current (Ampere, A), U is the electric potential across the electrodes (Volt, V), R is the external resistance (Ohm, Ω), $P_E$ is the power of the circuit (Watt, W), $Pd_{max}$ is the maximum surface power density ($W/m^2$), $Pd_{max,v}$is the maximum volumetric power density ($W/m^3$), A is the surface area of the electrode ($m^2$), V is the volume of the reactor ($m^3$), and J is the current density ($A/m^2$). The treatment efficiency was determined by testing the concentrations and removal efficiencies of COD, $PO_4^{3-}$, $Mg^{2+,}$ and $NH_4^+$. The treatment efficiency (R), which is the percentage removal of a pollutant, was measured as the difference between the influent concentration of COD, $C_{in}$ ($g/m^3$), and COD concentration in the effluent $C_{out}$ ($g/m^3$) relative to $C_{in.,}$ as shown in Equation 9.

$$R = \frac{C_{in} - C_{out}}{c_{in}} \times 100 \quad (10)$$

The surface power density was calculated based on the surface area of the cathode. Using the potentiostat shown in Figure 3-5 (PGSTAT by Metrohm), polarization curves of the cell potential versus current (U vs. I) were generated by alternating the circuit resistance and obtaining the relative cell voltage. Moreover, power curves were obtained by plotting the power versus current ($P_E$ vs. I). Nova software was used to calculate the power and current densities [84], in addition to generating the polarization curves. The linear sweep voltammetry (LSV), the most commonly used method, was utilized at a current range of 100 to 100 mA, while the scan rate and step size were set to 0.02 V/s and 0.00244 V, respectively [85].


Figure 3-5: Potentiostat used for polarization experiments of the examined microbial fuel cells [84].

### 3.2.4. Struvite recovery

In the current experimental work, the MFC reactors were utilized to recover struvite from urine, centrate, and greywater. The precipitation experiment was carried out in the cathodic chamber of the MFC. The $PO_4^{3-}$, $Mg^{2+,}$ and $NH_4^+$ were measured (detailed in section 3.3.1.5) to determine the limiting nutrient of the examined substrates and to attain an equimolar ratio amongst the aforementioned parameters. The magnesium, which is typically the limiting chemical, was increased by adding $MgCl_2$ (SRL Chemicals). The pH of samples was continuously monitored and maintained between 8 and 9.5 [17] using diluted NaOH pellets. Moreover, the electric conductivity (EC) was also observed as it provided an indication of the struvite nucleation and crystallization reactions completion [86]. Furthermore, continuous stirring was maintained inside the cathodic compartment. The precipitation experiment was stopped

as the pH of the samples stabilized. The samples containing struvite precipitate were filtered as shown in Figure 3-6 and dried in the oven at 50°C. The samples were tested using XRF and FTIR to identify the precipitate composition, whereas SEM was utilized for morphology analysis.

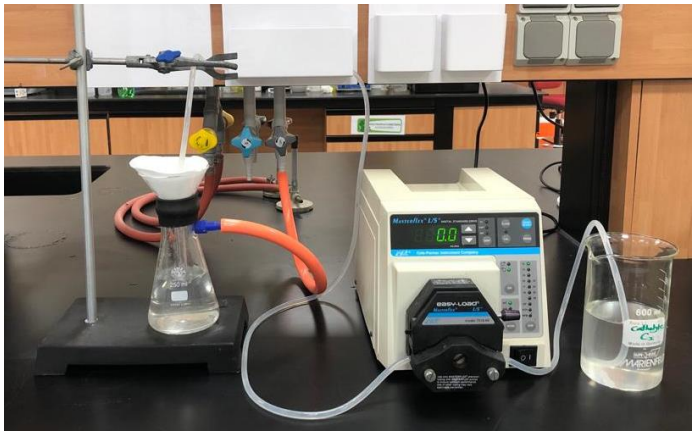

Figure 3-6: Filtration apparatus for struvite extraction.

## 3.3. Analytical Methods

### 3.3.1. General characterization

A general characterization was conducted for the substrate samples, including solid contents, pH, alkalinity, oxidation-reduction potential (ORP), EC, COD, dissolved oxygen (DO), and several chemical parameters, including $PO_4^{3-}$, $Mg^{2+}$, and $NH_4^+$. All measurements were conducted in duplicates and verified by a triplicate in case of non-concise results to ensure meeting the quality assurance of the tests.

#### *3.3.1.1. Solids content*

The solids content test was conducted according to Standard Methods No. 2540 [54] to obtain the moisture content and the different solids fractions, including total and volatile solids. The samples were filtered using (microfiber filter paper 125 mm, 2 microns) and the volume used for the three substrates was 15 mL. Total solids (TS) were measured by initially heating samples at 100 $^oC$ in the oven for 24 hours. The TS was calculated as shown in Equation 11.

$$\mathrm{TS(mg/L)} = \frac{w_0 - w_1}{\text{Volume of Sample}} \times 100 \qquad (11)$$

Where $w_0$ is the weight of crucible and sample before heating (g) and $w_1$ is the weight of crucible and sample after heating (g).

To measure volatile solids (VS), the samples were ignited in a furnace at 550 ºC for at least 4 hours using furnace, and the volume of the sample was measured. The VS was calculated according to Equation 12.

$$\mathrm{VS(mg/L)} = \frac{\mathrm{w_0} - \mathrm{w_1}}{\mathrm{Volume\ of\ Sample}} \times 100 \qquad (12)$$

Where W1 is the weight of crucible and sample before heating and $W_2$ is the weight of crucible and sample after heating at 550$^{o}$ C (g). Figure 3-7 shows the examined samples prior to conducting the total solids test and after ignition.

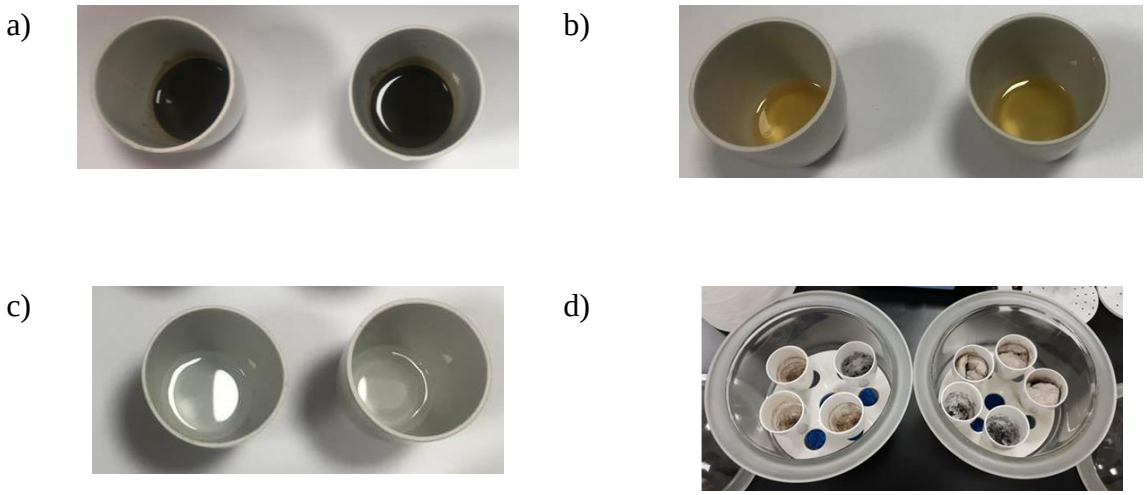


Figure 3-7: Different samples in the measurements of solids contents before ignition for a) centrate, b) urine, and c) greywater, and d) after ignition.

#### *3.3.1.2. pH and alkalinity*

The pH of the substrates was measured using HACH HQ40d digital multi-meter and IntelliCAL$^{TM}$ pH PHC101 probe. The electrode probe is calibrated with the corresponding solution and rinsed with deionized water. The alkalinity of samples was measured based on the HACH burette titration test (method 8221). The samples were added to an Erlenmeyer flask and diluted using distilled water before alkalinity measurements. The volume of each sample was chosen to be 50 mL based on the expected alkalinity values and corresponding volumes provided in the method procedure. The utilized acid for this procedure was sulfuric Acid ($H_2SO_4$) with a concentration of 0.02N (HACH cat. 20353). Figure 3-8 shows the apparatus used for the pH and alkalinity tests in the present study.

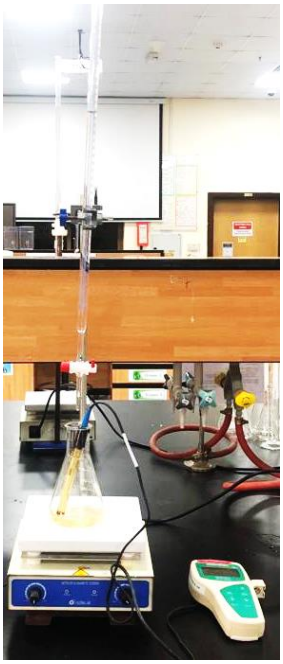

Figure 3-8: Titration apparatus for the alkalinity tests.

#### *3.3.1.3. Oxidation reduction potential (ORP) and electrical conductivity (EC)*

Electrochemical parameters such as ORP and EC were measured, where the former indicates the oxidation and reduction capability of a substance, while the later measured the ability of the studied samples to convey current. The ORP test was conducted using HACH HQ40d digital multi-meter with the IntelliCAL$^{TM}$ ORP-REDOX MTC101 probe. The electrode probe was also calibrated with the corresponding solution and rinsed with deionized water. On the other hand, EC was measured using the ScichemTech$^{R}$ SCT-BEN-CON-1 conductivity meter. Figure 3- 9 shows the digital meters utilized for ORP and EC tests.

a) b)

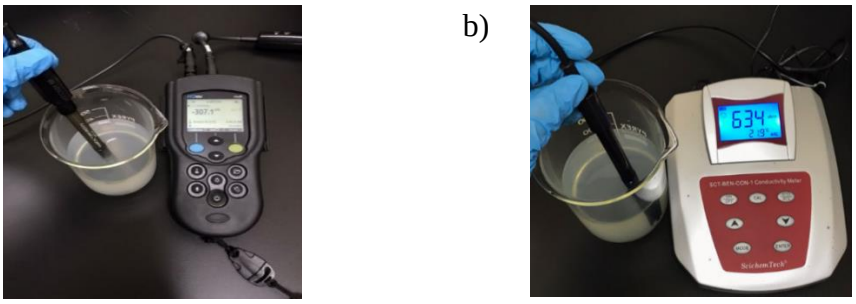

Figure 3- 9: Probes and digital meters for the measurements of a) oxidation-reduction potential, and b) electrical conductivity.

#### *3.3.1.4. Chemical oxygen demand (COD) and dissolved oxygen (DO)*

The COD is an indicator of the organic content, which can identify the treatment efficiency. Figure 3-10 shows the measurements and devices for the digestion and

colorimetric measurement of the COD. The COD was measured by adding a 0.2 mL of the collected sampled to the COD vials (8000 HACH kit; high range: 0 to 15,000 ppm) in addition to preparing a blank sample (deionized water). The samples were left for digestion at 148° C for two hours using the digester (Model No. DR 2200). The digested vials were left for 15 minutes too cool inside the digester then removed and measurements were taken using spectrophotometer (Model No. DR 3900) when the vials reached room temperature. The same procedure was followed for measuring the soluble COD, nevertheless the samples were filtered beforehand using (microfiber filter paper 125 mm, 0.45 microns).

a)

b)

Figure 3-10: Testing apparatus for the measurements of: a) soluble chemical oxygen demand, and b) dissolved oxygen.

#### *3.3.1.5. Chemical parameters*

Three chemical parameters were measured for all samples, including $NH_4^+$, $PO_4^{3-}$, and $Mg^{2+}$. The ammonium test was performed as per the HACH method (LCK 301). The test was conducted by adding 0.2 ml of the sample into the reagent, and a 15-minute reaction time was required. To attain accurate values, the cuvette outside was wiped and cleaned, then placed into the spectrophotometer holder (Model No. DR 3900). Moreover, the $PO_4^{3-}$ test was conducted according to the HACH method LCK 350. Similar to the ammonium test, 0.4 ml of the sample was added to the cuvette, and a reading was taken using the spectrophotometer. Prior to the analysis, the cuvettes were placed in the digester (Model No. DR 2200) for 30 minutes at 120° C to ensure sample dissolution. Finally, the $Mg^{2+}$ was tested as reported by the HACH method (LCK 326). The reagent (3.5 ml) was mixed with 0.5 ml of the sample, poured into a cuvette, and

obtained readings using the spectrophotometer. Figure 3-11 shows the testing kits and devices utilized for measuring the chemical parameters of monitoring the chemical properties of the collected samples.

Figure 3-11: Chemical colorimetric test analyses of the collected samples.

### 3.3.2. Qualitative analysis

Struvite detection in the precipitate was identified using spectroscopic and microscopic techniques. X-ray fluorescence (XRF), Scanning Electron Microscopy (SEM), and Fourier Transform-Infrared Spectroscopy (FTIR) were utilized to analyze the precipitate and identify the purity of the struvite crystals.

#### *3.3.2.1. X-ray fluorescence (XRF)*

XRF spectrometer is an instrument used for the chemical analysis of minerals, sediments, soil, etc. The equipment is effectively used for bulk chemical analysis of major elements, including Mg, Al, Ca, P, and k, and trace elements, including Rb, Cu, Zn, and Cr. The analysis depends on the interaction between the atoms present in the sample and the radiation of the machine. The incident beam inside the machine illuminates the samples and depending on the chemical composition of the sample; energy is either scattered or absorbed into the sample causing the agitation of particles. The agitation targeted electrons to be ejected from atoms and replaced by other electrons in the outer orbital. As a result, x-ray emissions are released in a wavelength range depending on the characteristics of the particles, hence identifying the fractions. In this research, XRF was used to determine the composition of the precipitated struvite.

#### *3.3.2.2. X-ray diffraction (XRD)*

XRD data will be attained for identifying the components of the precipitate, and the results will be compared to the standard MAP pattern by Bruker D8 Advance XRD shown in Figure 3-12. A beam is directed at the samples from different angles to enable atom interaction which yields the chemical composition of the precipitate. The results

consist of diffraction graphs where the intensity of the peaks can be compared to a standard MAP pattern database. Bragg law is used to define the working mechanism of the XRD as shown in Equation 13.

$$n\lambda = 2\,d\sin\theta \tag{13}$$

Where n is an integer representing the reflection order, λ is the wavelength, d is the spacing in a planar model of the crystalline structure, and θ is the angle of x-ray beam scattering. The step size is 0.2 degrees with 0.2 seconds per step for angles between 5 and 85 degrees.

Figure 3-12: X-ray diffraction device for precipitate characterization.

#### *3.3.2.3. Scanning electron microscopy- energy dispersive xray (SEM-EDS)*

The morphology and structural heterogeneity for the surface of resulting struvite crystals were determined using SEM with EDS, as shown in Figure 3-13 (Tescan VEGA XM variable pressure SEM). The SEM instrument uses an electron beam probe to analyze the surface of samples to the nanoscale. It produces high magnification images with high resolution. Moreover, the SEM-EDS mainly focuses on retrieving information of the particle surface, and the generated 3D images reflect the scattered electrons.


Figure 3-13: Scanning electron microscope for struvite morphology analysis.

#### *3.3.2.4. Fourier Transform-infrared spectroscopy (FTIR)*

The precipitate was analyzed using the Thermo Scientific™ Nicolet™ iS5 FTIR shown inFigure 3-14. The FTIR is based on infrared radiation, which is located in the range between visible light and microwaves. The chemical structure of molecules was measured based on absorbed infrared radiation. It also recognizes unknown compounds and molecules via matching to a known database. Moreover, FTIR provides information about the energy of the molecules by studying the vibrational behavior.


Figure 3-14: Fourier transform-infrared spectroscopy for the chemical bonds in the studied samples.

# Chapter 4. Experimental Setup

## 4.1. Microbial Fuel Cell Design

A set of three dual-chamber MFCs was designed and fabricated, as illustrated in Figure 4-1. Each cell was constructed using acrylic materials with an effective volume of the anodic and cathodic compartments of 700 mL each. The two chambers were separated by a PEM (Nafion 117, Fuel Cell Store) with a membrane area of 64 $cm^2$. The electrode areas were 65 $cm^2$ each, where a plain carbon cloth was used as the cathode, and a carbon cloth with a 40% Pt gas diffusion layer (Fuel Cell Earth) constituted the anode. Titanium wires were used for electrical connections of the carbon-based electrodes. Sampling, inlet/outlet, and gas ports were arranged at both chambers. Phosphate buffer solution was used as the catholyte, which contained 8.5g sodium chloride, 1.9g disodium hydrogen phosphate, and 0.4g potassium dihydrogen phosphate. As a source of microbial cultures, yeast was added to the anolyte solution at a concentration of 1.28 mg/L.

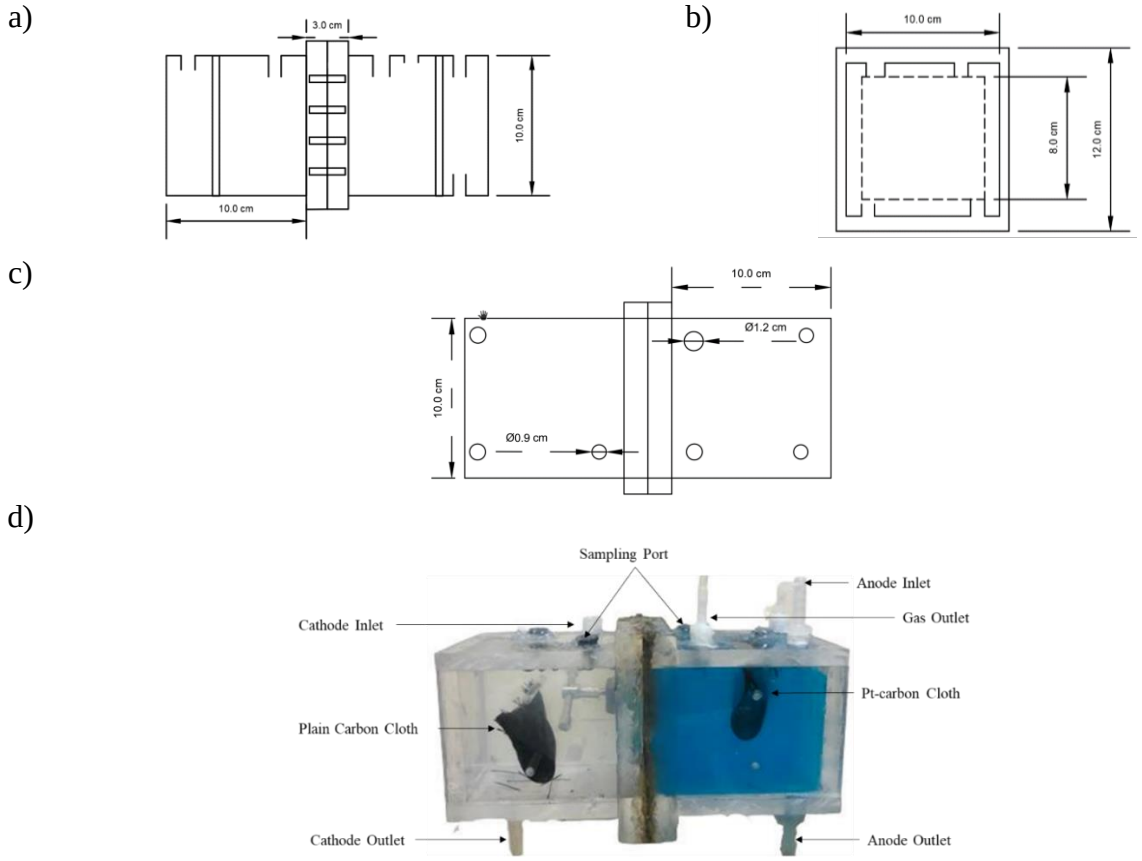


Figure 4-1 : Sketch of the designed microbial fuel cell: a) side view, b) front view, c) top view, and d) lab-scale dual-chamber unit with various cell components.

## 4.2. Experimental Configuration

The experimental setup comprised the MFC units, inline measurement devices, and monitoring system, as illustrated in Figure 4-2. The MFC voltage was monitored throughout the experiment via LabVIEW monitoring and control software connected to a data acquisition (DAQ) system from National Instruments (CDAQ-9178 installed on a COMPACTDAQ Chassis). The voltage readings were recorded every 30 minutes for all MFC reactors and were frequently validated through manual measurements by a voltmeter (UNI-T UT33C). The polarization curves were obtained using NOVA software based on the potential and resistance variation measured using potentiostat readings (Metrohm PGSTAT).

a)

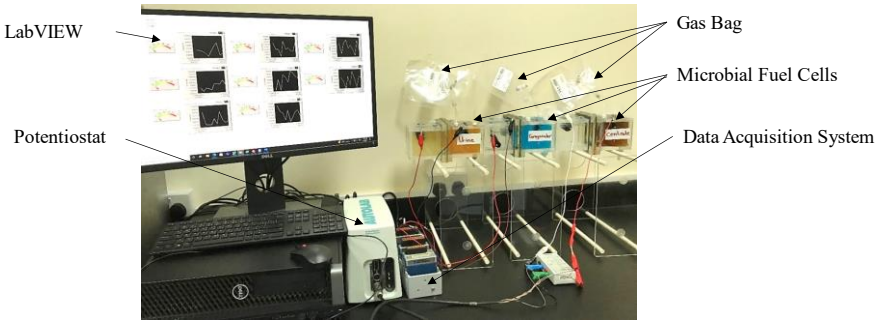


b)

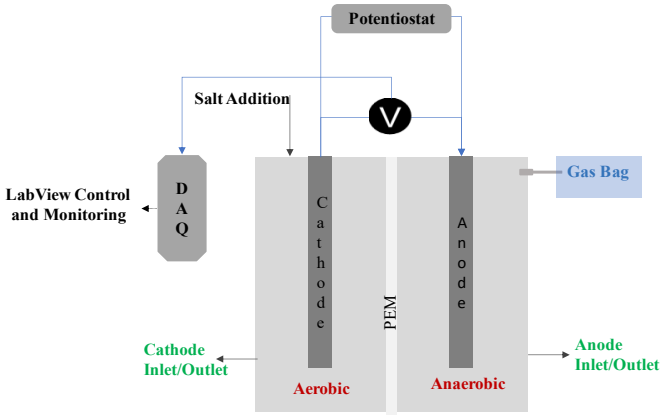


Figure 4-2: Lab-scale experimental setup: a) actual photo, and b) detailed schematic.

## 4.3. Monitoring of Experimental Setup

Figure 4-3 shows the block diagram and front panel of the cell connections for the voltage readings. The actual anode and cathode connections were defined on the block diagram (DAQ Assistant) and connected to the analog input voltage module. The LabVIEW was programmed to demonstrate the recorded measurements in the form of line graphs and meter scales Figure 4-3 b), in addition to exporting the raw voltage data as a CSV file.

a)

b)

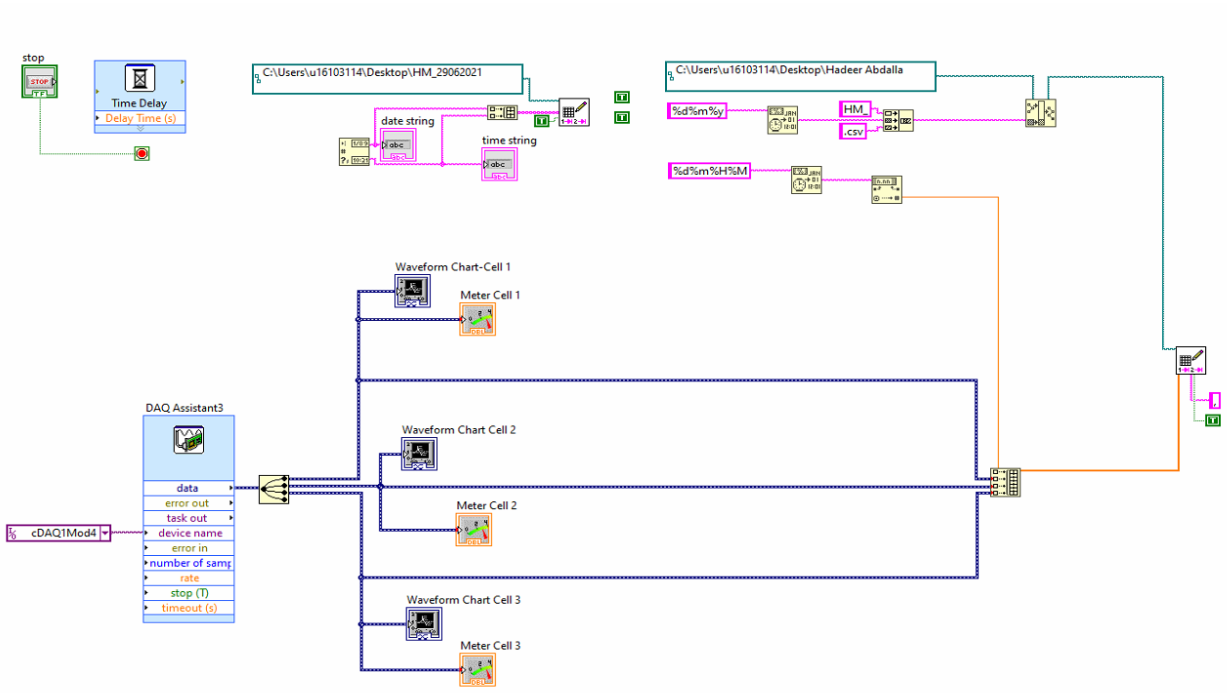


Figure 4-3: Front panel and block diagrams of the experimental voltage readings setup using LabVIEW.

# Chapter 5. Results and Analysis

## 5.1. General Characterization

Three substrates, urine, centrate, and greywater, were collected and analyzed in this study. Table 5-1 shows the general physiochemical characteristics of the examined samples. In terms of the TS content, urine had the highest value of 40 mg/L, which was due to the high salt concentration [87]. Moreover, the higher VS concentration in the urine indicated a high organic content that could promote microbial activity and increase electricity generation. Moreover, the urine contained the highest fraction of readily biodegradable organics at 41%, followed by the centrate at 34%, while the greywater had the lowest fraction (8%) due to the non-biodegradable detergents.

Table 5-1: Summary of the parameters measured for general characterization of substrates.

| Substrate | pH | EC (µS/cm) | TS (mg/L) | VS (mg/L) | COD (mg/L) | S-COD (mg/L) | DO (mg/L) | ORP (mV) | Alkalinity (mg $CaCO_3$/L) | Mg (mg/L) | $NH_4^+$ (mg/L) | $PO_4^{3-}$ (mg/L) | Mg:P |
|---|---|---|---|---|---|---|---|---|---|---|---|---|---|
| Urine | 8.9 | 17.8 | 40 | 34.0 | 1,343 | 548 | 61.9 | 96 | 2,440 | 2.8 | 1390 | 1,698 | 1:105 |
| Centrate | 8.1 | 15.4 | 23 | 15.8 | 4,135 | 1,390 | 67.2 | 415 | 1,260 | 3.5 | 578 | 71 | 1:7 |
| Greywater | 7.6 | 15.5 | 1.3 | 0.9 | 210 | 17 | 56.5 | 197 | 3,060 | 4 | 400 | 14 | 1:1.5 |

The electrochemical analysis of the substrates showed that the centrate had the highest ORP, which could lead to a higher tendency of electron transfer between the catholyte and anolyte indicating increase in current. Moreover, the EC measurement revealed that the three substrates were highly conductive, with urine being slightly higher (17.8 µS/cm), followed by greywater and centrate with EC values of 15.5 and 15.4 µS/cm, respectively.

High ammonia, phosphorus, and magnesium contents were found in the urine and centrate, with the highest concentration in the urine samples. Moreover, the increased ammonia content in the stored urine may have occurred due to urea hydrolysis, through which it is converted to ammonia and bicarbonate aiding in increase of pH once transferred to cathode chamber. Therefore, the storage of urine prior to treatment using MFC facilitates the pH increase which provides the optimum condition of struvite recovery as it increases from pH 8 to up to 9.3 [88]. Moreover, Li et al. [89] found that the pH of mixed greywater ranged between 6.3 and 8.1. The used substrates were alkaline, with the urine being within the recommended pH range of 8-9.5 for optimal nutrient recovery [88]. Furthermore, the collected urine samples were pale yellow and

turbid in appearance likely due to large concentrations of phosphates. In addition, greywater was deficient in phosphate and ammonia, which can be attributed to the use of phosphorus-free detergent in the laundry water and the exclusion of feces and urine. In the literature, the $NH_4^+$ in the greywater and centrate was reported in the range between 1.7 and 34.3 [89] and 82 to 86 mg/L [90], whereas, the $PO_4^{3-}$ ranged from 0.11 to 22.8 [89] and 59 to 222 [90] mg/L, respectively.

The COD and sCOD were measured for urine, centrate, and greywater to determine the total and soluble organic matter concentration. The COD was highest in the centrate (4135 mg/L), followed by urine (1343 mg/L) and greywater (210 mg/L). Nevertheless, the soluble fraction of COD was highest in urine, measured at 40% of the total COD, followed by centrate (34%) and greywater (8%). Furthermore, the COD concentration of the stored urine was found to range from 3,900 [91] to 11,300 mg/L [68], which was higher than the results obtained in the current study. The high COD values of urine in the literature can be attributed to the method of collection, where the urine is typically separated and collected from a urinary. The COD of the centrate was found to range from 201 [92] up to 4,750 mg/L [93]. The centrate COD concentration in the literature varied significantly based on the type of the source wastewater. Similarly, the greywater characteristics showed significant variation in the literature depending on the living habits of the population involved and the cleaning products used [94]. The COD of greywater in the literature was found to be as low as 100 mg/L reaching 3,000 mg/L when the concentration of kitchen waste was relatively high [95].

The parameters shown in Table 5-1 were mostly in agreement with previous studies examining similar samples. For instance, the ORP of greywater was found to be in the range of 130 to 350 mV in the literature, while its alkalinity ranged between 3267 and 3407 mg $CaCO_3$/L which is higher than the obtained result in this study [96]. The measured EC for urine was 40% greater than that reported in previous studies at 11.14 µS/cm [68], indicating higher nutrients levels in the collected urine samples [97].

## 5.2. Treatment Efficiency

The treatment efficiency of the anolyte (urine, centrate, and greywater) was determined in terms of sCOD, $NH_4^+$, $PO_4^{3-}$, and $Mg^{2+}$ as described in sections 3.3.1.4 and 3.3.1.5. Figure 5- 1 demonstrates the removal efficiency of Cell-I-U, Cell-I-C, and Cell-I-G. In all cells, $NH_4^+$showed the highest removal efficiency among the nutrients as it could be

easily converted to free ions under alkaline conditions, where it can potentially enhance nutrient recovery. The high removal efficiency of $NH_4^+$ at the cathodic chamber of Cell-I-U could also be attributed to the accelerated urea hydrolysis of ammonium ions as a result of urine storage [61]. The removal efficiencies of $PO_4^{3-}$ and $Mg^{2+}$ at the cathode of Cell-I-G were in close proximity at 76.4 and 74.7%, respectively. On the other hand, the treatment efficiency of $Mg^{2+}$ was the lowest among the recovered nutrients in all cells, as it is typically considered the limiting nutrient in most of substrates [61], [67]–[69], [71]–[73], [75], [77]. The sCOD removal at the anolyte of Cell-I-G was the lowest due to the complex organic compounds contained in greywater resulting in a relatively longer lag period and shorter stable electricity generation phase, as reemphasized later. In contrast, the sCOD removal of Cell-I-C was found to be the highest, which could be attributed to the high soluble organic content of the centrate leading to the maximum electricity yield. Overall, the centrate achieved the highest sCOD removal as it was reduced from 1,390 to 32 mg/l, which agreed with the electricity output results. On the other hand, greywater had the lowest sCOD removal efficiency of 58.8%. Moreover, the sCOD fraction of urine decreased by 75.3%, which is in line with the findings of [68] where a 70% sCOD removal was reported in the application of MFC with urine.

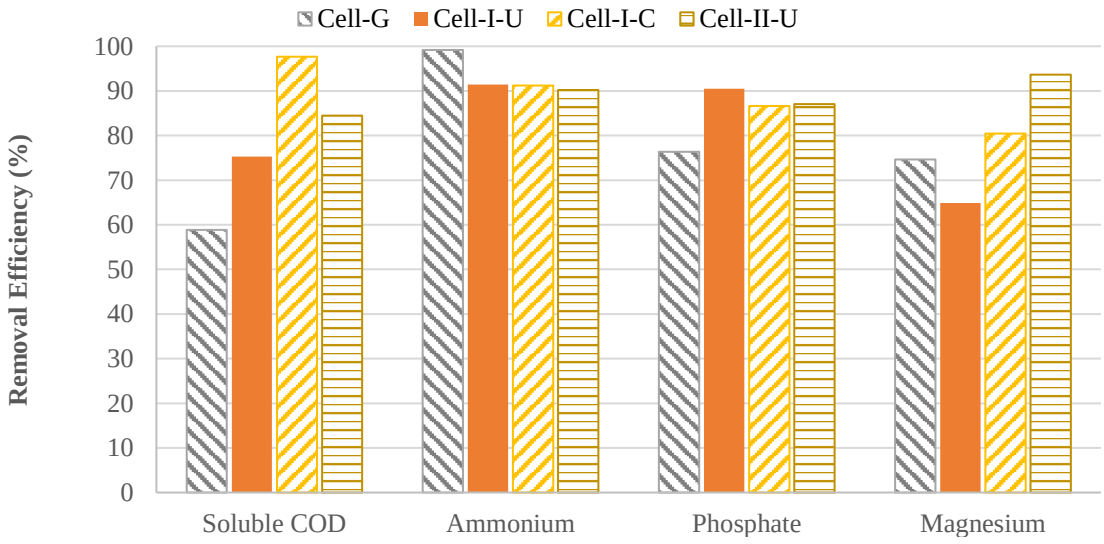


Figure 5- 1: Removal efficiency of sCOD, $NH_4^+$, $PO_4^{3-}$, and $Mg^{2+}$ in Cell-I-U, Cell-II-U, Cell-I-C, and Cell-I-G.

Table 5-2 summarizes the final effluent quality of Cell-I-U, Cell-II-U, Cell-I-C, and Cell-I-G in terms of sCOD, $NH_4^+$, $PO_4^{3-}$, and $Mg^{2+}$. In terms of sCOD, Cell-I-G had the lowest effluent concentration (7 mg/L) compared to Cell-I-U which had 99 mg/L

with a removal efficiency of 60%. The removal efficiency of sCOD increased to 24 and 22% in the 2nd phase for Cell-U and Cell-I-C, respectively. Moreover, the $Mg^{2+}$ concentrations in Cell-I-U, Cell-I-C, and Cell-I-G were 48, 77, and 61 mg/L, respectively which are lower than the allowable limits by the world health organization (WHO) and United States department of agriculture (USDA) [98], [99]. Furthermore, the phosphate concentration in Cell-I-U (106 mg/L), Cell-I-C (67 mg/L), and Cell-G (123 mg/L) were high compared with the United States environmental protection agency (EPA) limits of 1 mg/L although the removal efficiency ranged between 76 and 87% [100]. For the $NH4^{+}$, the effluent of Cell-I-G had the lowest concentration (50 mg/L), followed by Cell-I-C (641 mg/L) and Cell-I-U (661 mg/L), in which they were found higher than the recommended effluent quality of total nitrogen (TN); 10 mg/L. Although the removal efficiency of phosphates and ammonium was relatively high, further examination of the nutrient recovery using MFCs was required as discussed later (section 5.4).

Table 5-2: Summary of the effluent quality and removal efficiency of Cell-U, Cell-C, and Cell-G for the examined operation phases.

| MFC | Parameters* | | | | | | | | | |
|---|---|---|---|---|---|---|---|---|---|---|
| | sCOD | | | | $NH_4^+$ | | $PO_4^{3-}$ | | $Mg^{2+}$ | |
| | Phase I | | Phase II | | Phase I | | Phase I | | Phase I | |
| | Eff. Conc. (mg/L) | Rem. Eff. (%) | Eff. Conc. (mg/L) | Rem. Eff. (%) | Eff. Conc. (mg/L) | Rem. Eff. (%) | Eff. Conc. (mg/L) | Rem. Eff. (%) | Eff. Conc. (mg/L) | Rem. Eff. (%) |
| Cell-U | 99 | 60 | 85 | 84 | 661 | 90 | 106 | 81 | 48 | 65 |
| Cell-C | 32 | 75 | 48 | 97 | 641 | 91 | 67 | 87 | 77 | 80 |
| Cell-G | 7 | 98 | 4 | 75 | 50 | 99 | 123 | 76 | 61 | 75 |

* Eff. Conc.: Effluent Concentration; Rem. Eff.: Removal Efficiency

## 5.3. Electricity Generation

The voltage readings for the MFC reactors were recorded daily in closed circuit mode. Figure 5-2 and Figure 5-3 depict the corresponding cell potentials for phases I and II, respectively. As previously described in 2.3, phase I aimed to investigate the electricity generation and struvite recovery from the cathodic chamber, while phase II involved the recirculation of the treated anolyte to the cathode compartment, followed by struvite precipitation in the cathodic chamber. Cell-I-U and Cell-I-C lasted approximately 15 days in the acclimatization phase, during which the voltage spiked up to 130 mV for the former and 200 mV for the latter. On the other hand, Cell-I-G stayed in the lag phase

for a longer duration (23 days) due to the complex composition, particularly the high concentrations of detergents, of the collected greywater. Cell-I-C achieved the highest voltage readings, which could be attributed to the high sCOD concentration of the centrate (1,390 mg/L) compared to the relatively lower sCOD of the urine (548 mg/L) and greywater (17 mg/L). A substantial increase in the voltage readings for Cell-I-C was observed on day 16 at 188 mV, which peaked on day 32 with a maximum potential value of 590 mV. Sudden voltage increase has been investigated in the literature and attributed to changes in pH [101]. Moreover, Cell-I-U demonstrated a gradual voltage increase from day 16, starting at a potential of 63 mV and reaching the highest reading (381 mV) on day 28. On the other hand, Cell-I-G experienced a substantial surge in voltage reading on day 24 increasing from 13 to 439 mV (the highest recorded voltage). Although the voltage readings of Cell-I-U had the lowest range (261 to 364 mV) during the stationary growth phase, the MFC maintained stable voltage readings for a longer duration (18 days), compared to 11 days for Cell-I-G and 7 days for Cell-I-C. The extended stable electricity output or stationary phase for Cell-I-U resulted from the readily biodegradable organics present in the urine. It should also be noted that the three MFCs had a sudden increase in the electricity output during the expected biofilm formation stage (day 5 to 10); the electricity had increased to 193 mV for Cell-I-C, 132 mV for Cell-I-U, and 127 mV for Cell-I-G. Such a slight increase in electricity production had resulted from the consumption of readily biodegradable matter by the electrogenic bacteria.

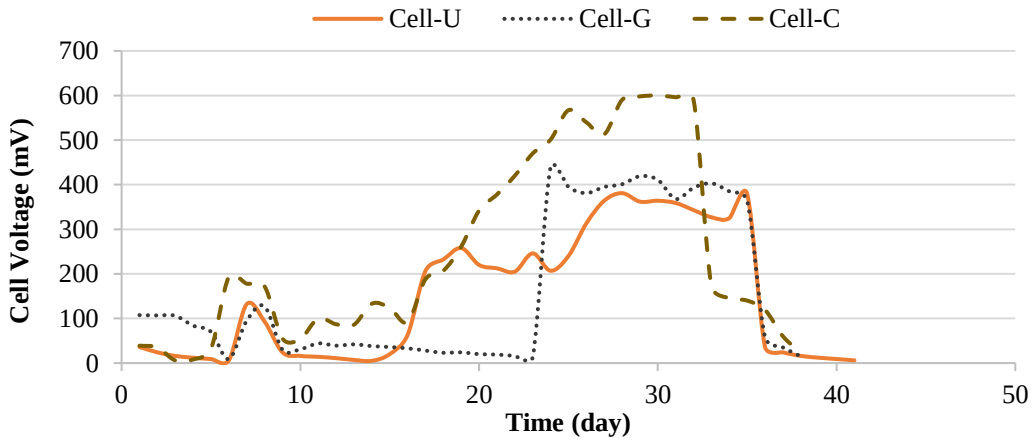


Figure 5-2: Daily voltage readings of Cell-U, Cell-C, and Cell-G for phase I of operation.

Phase II of operation revealed similar trends for Cell-II-U, Cell-II-C, and Cell-II-G reactors during the biofilm forming stage. The three cells experienced an acclimation

period of 13 days on average, followed by an increase in voltage between days 14 and 15. Similar to phase I, Cell-I-C had the highest voltage of 345 mV. In contrast to phase I, Cell-II-U achieved the least performance with maximum voltage of 256 mV, whereas Cell-II-G obtained a cell potential of 343 mV. The low performance of Cell-II-U could have been caused by the relatively high pH of the catholyte (recirculated treated urine from phase I); a pH of 9.3. Overall, Cell-II-C lasted for ~40-day period and remained in the stationary stage for 22 days which was three times more than Cell-I-C (7 days). Such longer stationary period could be explained by the bacteria which were already acclimatized to the substrate during phase I. Moreover, Cell-II-G was found to have an overall better performance in terms of the average voltage output during the stationary phase, where the potential ranged between 224 and 343 mV over a 31-day period; almost three times more than Cell-I-G (11 days). Although the maximum potential output of phase II for the three substrates was lower compared to phase I, the stable electricity output stage lasted longer (9-31 days).

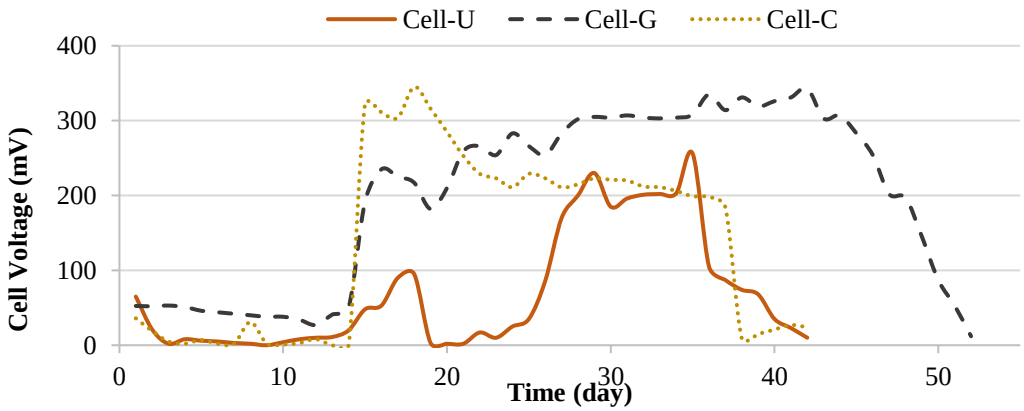


Figure 5-3: Daily voltage readings of Cell-U, Cell-C, and Cell-G for phase II of operation.

The polarization curves of Cell-I-U, Cell-I-C, and Cell-I-G (shown in Figure 5-4) reveal a maximum power density ($Pd_{max}$) of 1.7, 1.5, and 0.95 mW/cm$^2$, respectively, while Cell-II-U, Cell-II-C, and Cell-II-G had a $Pd_{max}$ of 1.18, 0.82, and 0.73 mW/cm$^2$, respectively. The results obtained in this experimental work were found to be higher or within those reported in the literature, as shown in Figure 5-5. Sharma and Mutnuri [68] reported a maximum power density of a urine-fed MFC of 0.068 mW/cm$^2$, which was 96% smaller than that of Cell-I-U (1.7 mW/cm$^2$). Based on the reviewed literature, no study had utilized centrate or greywater as feedstock for operating MFCs; nevertheless, Pepè Sciarria et al. [67] and Fischer et al. [70] used digestate in batch MFC experiments. Pepè Sciarria et al. [67] reported a power density of 1.42 mW/cm$^2$ for a digestate

sample, whereas Fischer et al. [70] found a maximum power output of 0.031 mW. The results of Pepè Sciarria et al. [67] were in close proximity to the power density of Cell-I-C (1.5 mW/cm$^2$). In comparison, the power output reported by Fischer et al. [70] was significantly lower than the present experiment (97.5 mW in Cell-I-C).

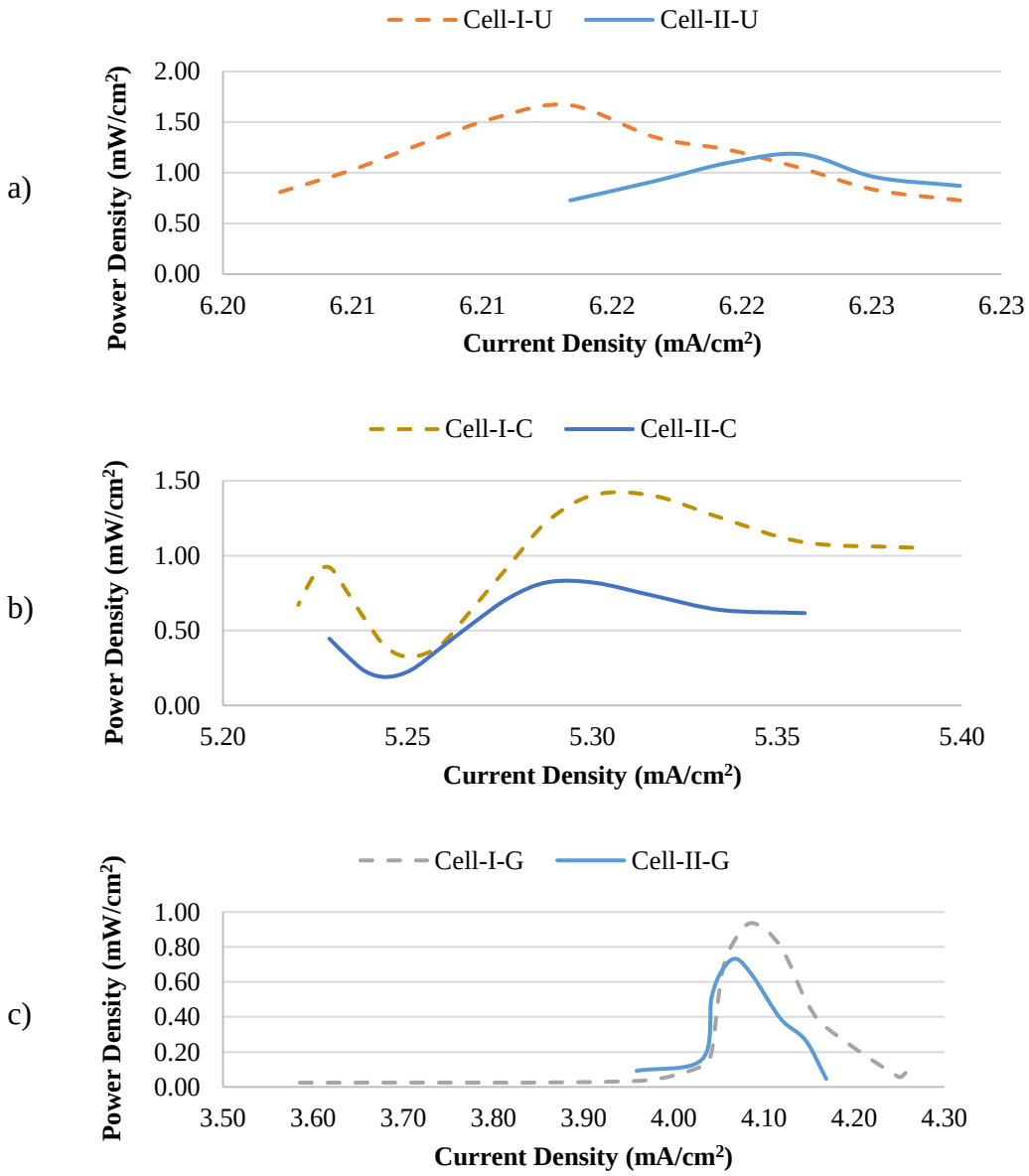


Figure 5-4: Phases I and II polarization comparison of a) Cell-U, b) Cell-C, and c) Cell-G.

The obtained $Pd_{max}$ from the examined MFCs (Cell-U, Cell-C, and Cell-G) for phases I and II were compared with the literature based on the utilized substrate, as depicted in Figure 5-5. The electricity production from the substrates used in this study was found to be relatively high compared to the reported power density in the literature [13],[47],[36],[102]-[103]. The highest average $Pd_{max}$ from the literature was reported

using simple non-acetate compounds as a substrate (23 mW/cm$^2$) which was 46, 57, 39, 65, 60 and 66% higher than Cell-I-U, Cell-II-U, Cell-I-C, Cell-II-C, Cell-I-G and Cell-II-G, respectively. Moreover, the surface power density of Cell-I-U was found to be higher than acetate (38%), domestic wastewater (79%), industrial wastewater (16%), swine wastewater (89%), and leachate (63%). Similarly, Cell-I-C was found to be higher than acetate (39%), domestic wastewater (63%), swine wastewater (87%), and leachate (57%). On the other hand, the power output of Cell-I-G was higher than domestic wastewater (63%), swine wastewater (81%), and leachate (35%). Phase II cells were found to be 17 to 84% higher than domestic wastewater, swine wastewater, and landfill leachate. As mentioned earlier, no studies were conducted on the treatment and nutrient recovery of greywater and centrate in MFCs; hence no comparison of the electricity data was performed for these substrates. The surface power density values of the current study for the utilized substrate were found to be within the range of the literature which proves the efficiency of the MFC in terms of electricity generations capability.

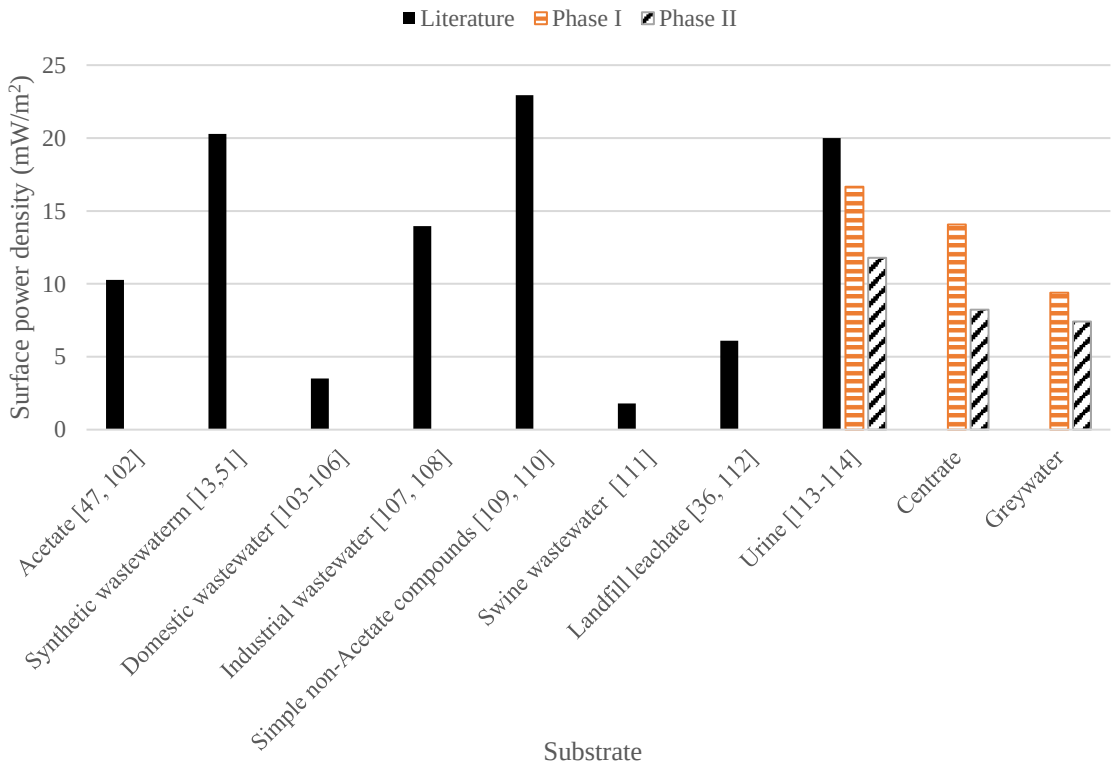


Figure 5-5: Maximum power density in the present experiment compared to previous studies.

## 5.4. Struvite Recovery

The theoretical phosphate recovery was calculated based on the precipitated struvite, compared to the actual recovered phosphate, as shown in Figure 5-6 for a volume of 700 mL. Cell-II-U produced the highest precipitate quantity (1.7 g), followed by Cell-I-U (1.5 g), Cell-I-C (1.3 g) and Cell-I-G (0.3 g) as depicted inFigure 5-7. The physical characteristics of all samples were similar in which all were in powder form, however the urine precipitate exhibited darker color (brownish). The theoretical potential phosphate recovered was calculated as the phosphate removal amounts. The phosphate recovery efficiency was found to be 56% for Cell-I-U, 23% for Cell-II-U, 36% for Cell-I-C, and 48% for Cell-I-G. Such low efficiency can be attributed to the losses of the precipitate that were washed out during reactor decanting. Improving the decanting mechanism is expected to increase the phosphate recovery as reported in the literature, where the efficiency of recovery can reach 90% [68].

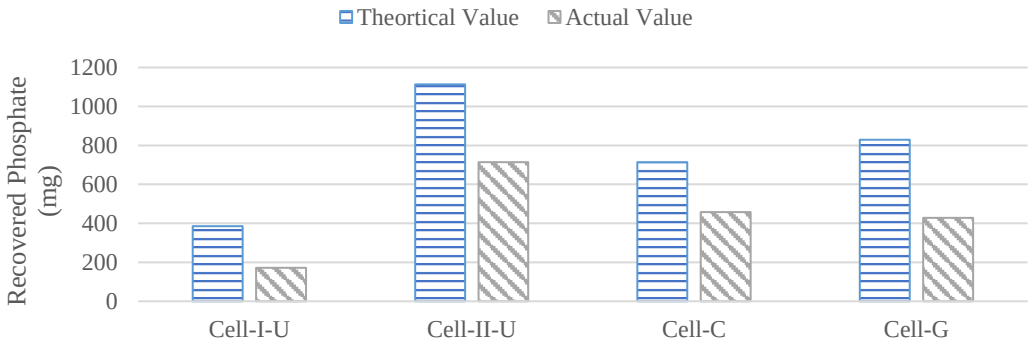


Figure 5-6: Comparison between theoretical and actual recovered phosphate.

Figure 5-7: Samples of struvite recovered from greywater, centrate, urine (phase I), and urine (phase II) in order from left.

## 5.5. Struvite Morphology Analysis

Figure 5-8 shows the XRD results of the precipitate formed in Cell-I-U, Cell-I-C, and Cell-I-G. The XRD was used to indicate the composition of the collected precipitate

using a known struvite sample as the reference. The results revealed that the dominant elements in all samples were P, Mg, and N, which constitute the composition of a typical struvite sample [76]. The elements P, Mg, and N had similar intensity counts for all tested precipitate samples. Moreover, the peaks were similar in all tested samples; nevertheless, the centrate had a distinguished relatively high peak at 2θ. The peaks between 23 and 25 kα represent $NH_4^+$, whereas the range between 19.4 to 20.8 represent magnesium element [104]. Moreover, peaks at a kα greater than 26 up to 28 represent phosphorus.

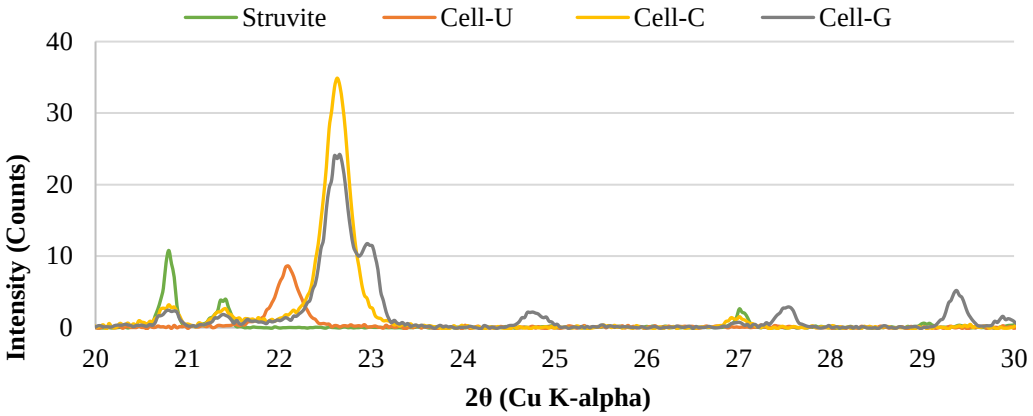


Figure 5-8: X-ray diffraction sample analysis of the anolyte, catholyte and precipitate analysis.

To verify the XRD results, the precipitate samples were further analyzed using XRF spectroscopy, shown in Figure 5-9. The dominantly present elements included Mg, P, N, Zn, Ca, and K. For the nitrogen, the highest concentration was detected in Cell-I-G, followed by Cell-I-C and Cell-I-U. The quality of Cell-I-G was relatively higher compared to Cell-I-U and Cell-I-C as the P, N, and Mg were highly detected compared to other elements. The presence of Zn in Cell-I-U can be justified by the typical presence of Zinc in concentrated fresh urine with a concentration of 15 mg/L [105]. Moreover, it also exists in high concentrations (up to 700 mg/L) in detergents present in greywater [106]. It should be noted that the fluorescence counts indicate the presence of the element in the sample as it has emitted X-rays.

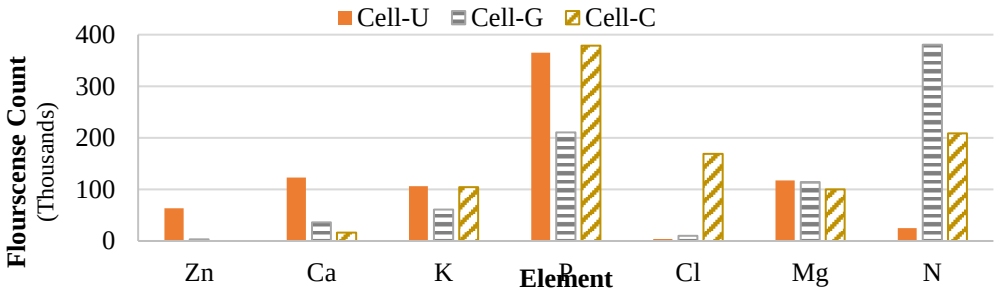


Figure 5-9: X-ray fluorescence analysis of precipitated struvite for urine, centrate, and greywater samples.

The precipitates were also verified using FTIR analysis, where Cell-I-U, Cell-I-C, and Cell-I-G samples were compared to a reference struvite sample, as shown in Figure 5-10. The peaks from 3,430 to 3,370 $cm^{-1}$ and 2,600 to 3,780 $cm^{-1}$ represented the water in the sample [107]. All three curves showed a peak between 1,081 and 1,085 $cm^{-1}$ indicating the presence of $PO_4^{3-}$ in the samples. Furthermore, peaks at wavelengths of 1,414 and 1,457 $cm^{-1}$ were observed, representing the N-H bond. The wavelengths between 2,850 and 2,935 $cm^{-1}$ demonstrated the $NH_4^+$ spectrum [108]. The peaks and drops in all three samples were similar, with a difference in the transmittance percentage. Cell-I-G sample had the lowest transmittance in the spectrum between 2,350 and 3,350 $cm^{-1}$, indicating lower concentrations of the aforementioned functional groups. Overall, the present functional groups in the FTIR-analysed precipitates indicated the absorption of the struvite sample.

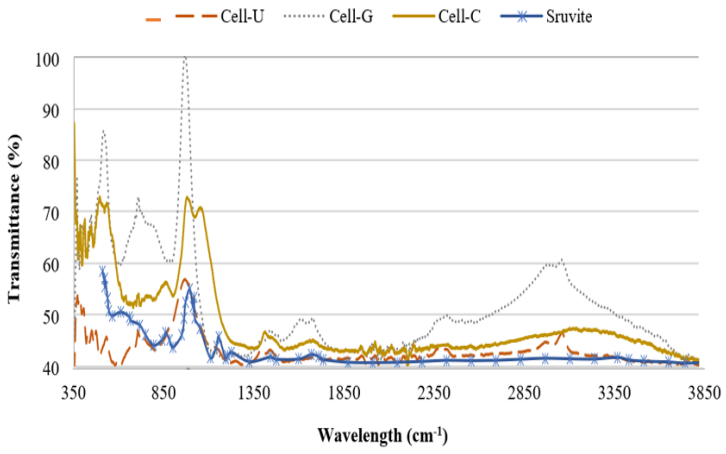


Figure 5-10: Comparison of the Fourier transform-infrared spectroscopy results for reference struvite with tested precipitate samples.

The morphology and elemental composition analysis of the precipitated samples were conducted using SEM-EDS. Figure 5-11a and b show the SEM images of the struvite sample collected from Cell-I-U. According to Damalerio et al. [109], a pure struvite sample exhibits a rectangular shape, while Rahman et al. [110] asserted that struvite could also have a rod-like or irregular shape [75, 76]. The sample collected from Cell-I-U showed an elongated structure (needle shape) with a length of 16.6 μm which is typical of struvite samples [74]. The precipitate formed in Cell-I-U was impure due to the fine glass filter paper used during sample collection. The shape and purity of the struvite crystal was mainly affected by the presence of $Ca^{2+}$ [111]. Moreover, Figure 5-11c shows the EDS analysis, where the composition included O, Mg, P, and N, in addition to other competitive ions such as Na, Ca, and Cl, are indicated. Other pollutants available in the sample included Si, B, and Al. The analysed sample contained almost 50% B, 27% O, 13% C, 1% of Mg, N, and P. In this sample, high level of impurity could be detected which was reflected by the high concentration of B in the sample which originates from the silicon sealant of the operated reactors.

The SEM-EDS analysis was also performed for the sample precipitated at Cell-II-U; the 2$^{nd}$ stage constituted nutrient recovery using recirculated anolyte. The SEM images and the corresponding EDS analysis are presented in Figure 5-12. The formed struvite varied from small needle-like shape (7 μm) to larger rod-like crystals (11 μm). The size was relatively small compared to Cell-I-U which can be attributed to the high percentage of $Ca^{2+}$ (2.5%) compared to 0.3% for Cell-I-U [111]. The major composition of the sample included O (50%), C (20%), P (13%), Mg (11%), and Ca (2%). The SEM images shown in Figure 5- 13a and b for the samples that precipitated in the cathodic chamber of Cell-I-C revealed a more defined rod-like crystals, compared to Cell-I-U, with a length ranging from 50 to 70 μm. The elemental composition depicted in Figure 5- 13c showed a higher absorbance of P and Mg than the Cell-I-U sample. Moreover, Ca, K, Cl, Na, and C were found with similar absorbance compared to Cell-I-U composition analysis. The composition of the sample mainly contained O (53%), P (13%), Mg (12%), C (11%), N (4%), Na (3%), Cl (2%), and Ca (0.3%) The purity of Cell-I-C sample was higher compared to Cell-I-U as the percentage of competitive ions were relatively less. The SEM-EDS analysis of the Cell-I-G precipitates exhibited different properties to those of Cell-I-U and Cell-I-C in terms of crystal shape, length, and elemental composition, as shown in Figure 5-14. The crystal morphology showed

a smooth surface with a length of 30 μm and a cube-like structure. Moreover, oxygen constituted 52% of the total sample by weight, followed by C (12%), Mg (10%), and P (9.2%). The Si, Na, K, Al, and Ca elements were found at less than 9%. Wang et al. [112] reported that EDS measurements of nitrogen are inaccurate as they are characterized by low emissions measured in electronvolts (keV).

a)

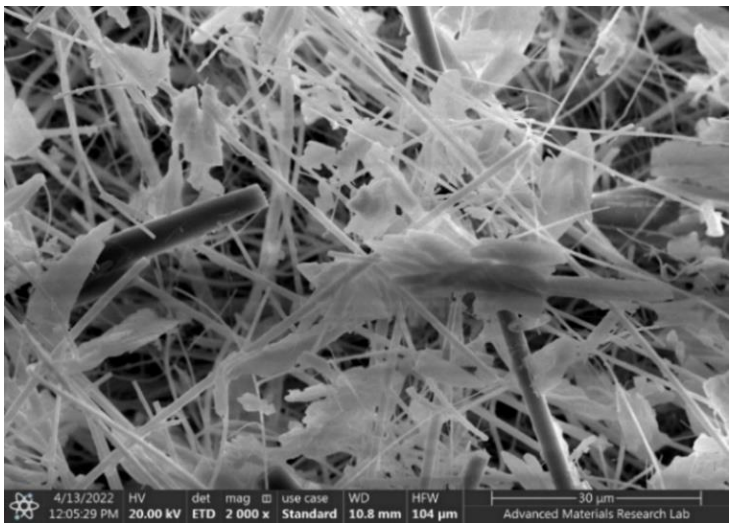


b)

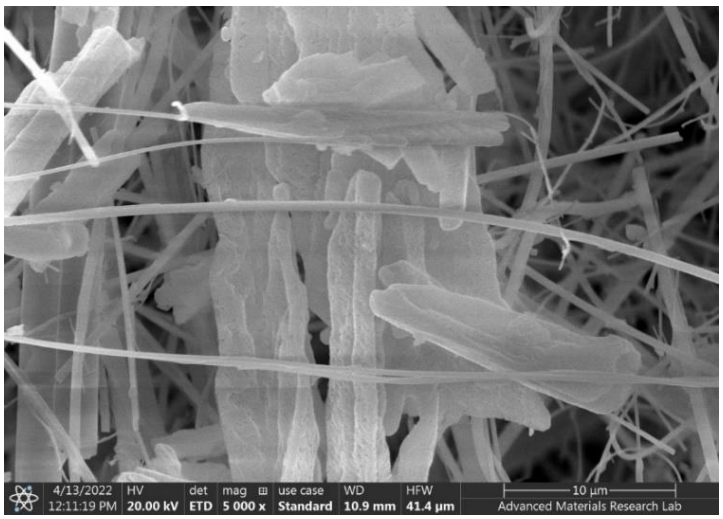

c)

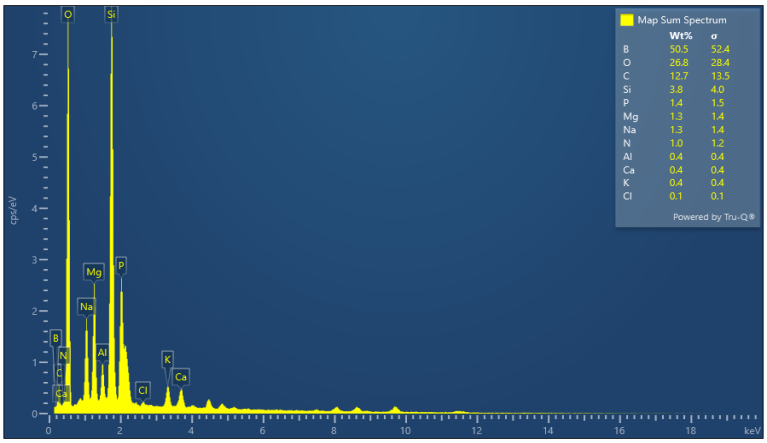


Figure 5-11: Scanning electron microscope images of Cell-I-U precipitate with a horizontal field width of a) 104 µm, b) 41.4 µm, and c) energy-dispersive spectroscopy analysis.

a)

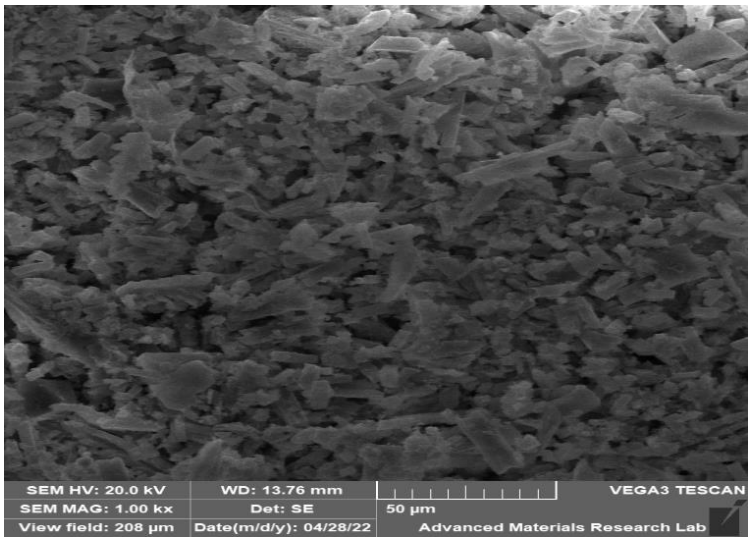


b)

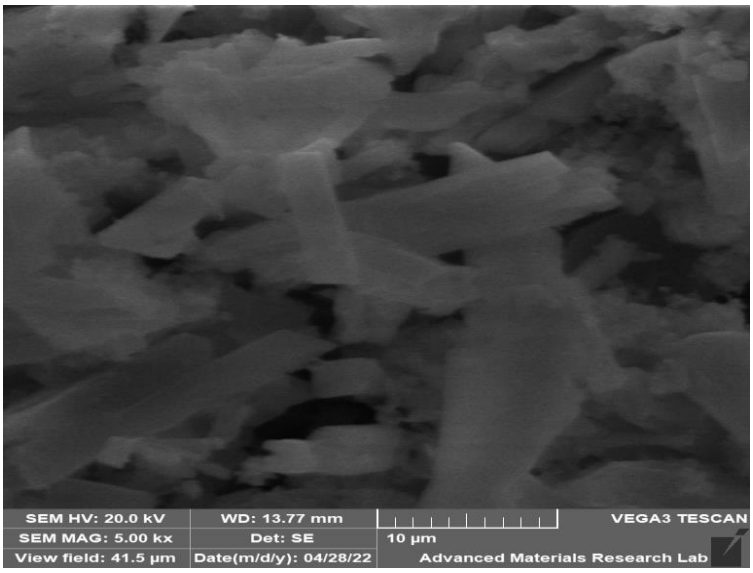

c)

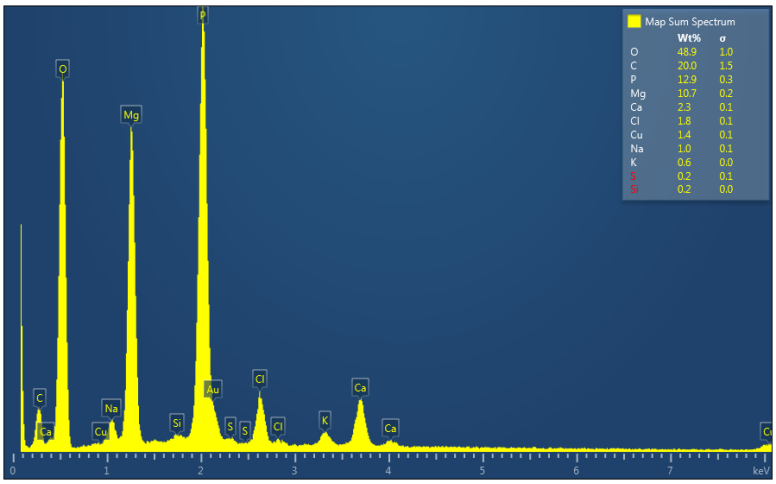


Figure 5-12: Scanning electron microscope images of Cell-II-U precipitate with a horizontal field width of a) 208 µm, b) 41.5 µm, and c) energy-dispersive spectroscopy analysis.

a)

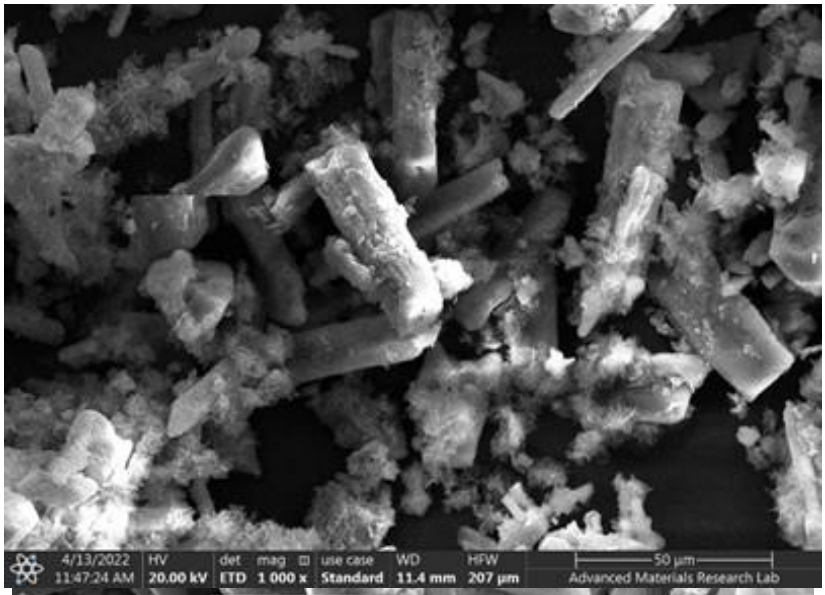


b)

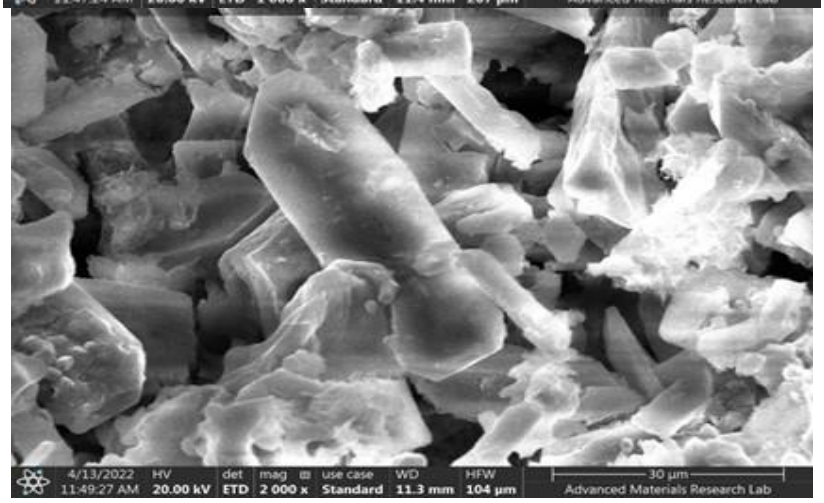

c)

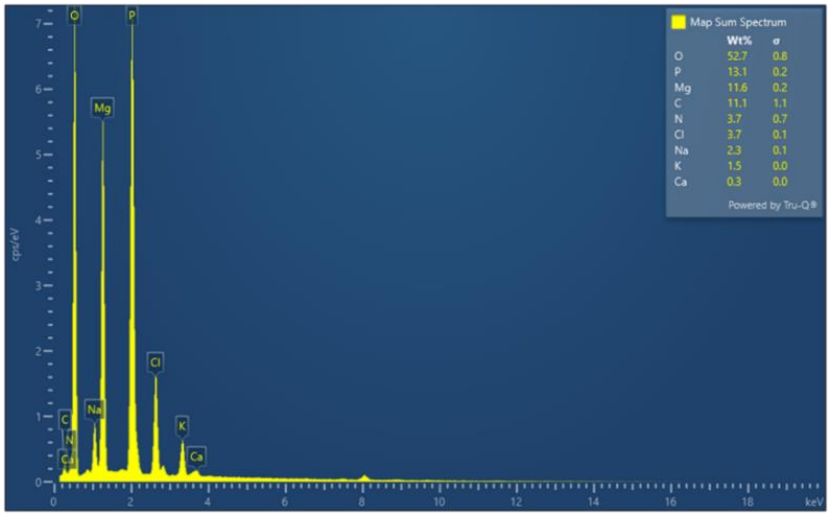


Figure 5- 13: Scanning electron microscope images of Cell-I-C precipitate with a horizontal field width of a) 207 µm, b) 104 µm, and c) energy-dispersive spectroscopy analysis.

a)

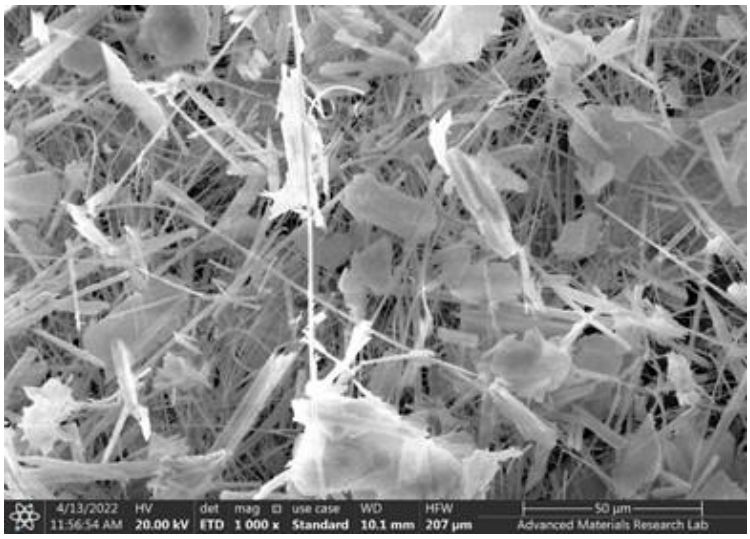


b)

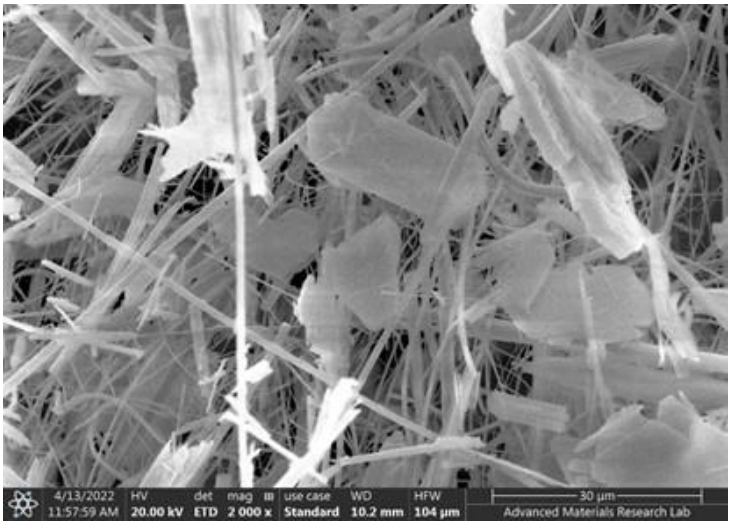

c)

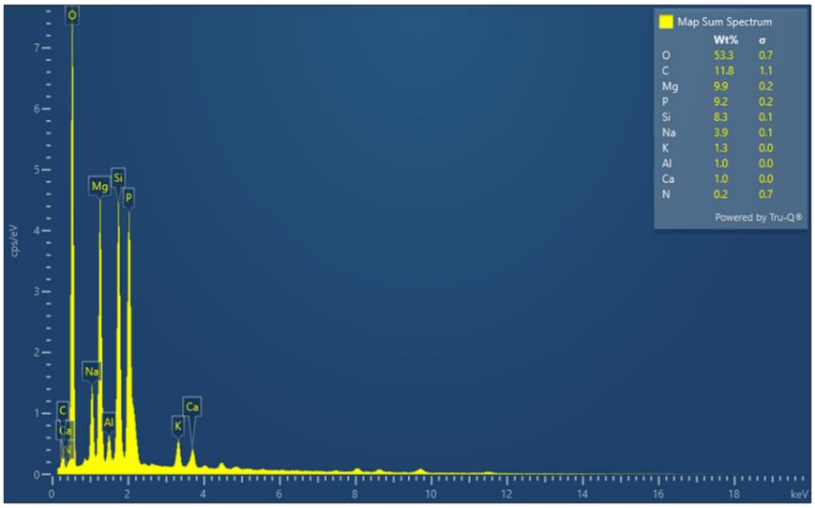


Figure 5-14: Scanning electron microscope images of Cell-I-G precipitate with a horizontal field width of a) 207 µm, b) 104 µm, and c) energy-dispersive spectroscopy analysis.

# Chapter 6. Conclusion and Future Work

Phosphorus is essential to sustain natural life as well as many industries, however, this element suffers from the excessive consumption and depletion of its finite rock reserves. As wastewater is an abundant source of phosphorus, the demand for sustainable treatment technologies that can recover phosphorus, particularly in the form of struvite, has increased. Considering that wastewater treatment is also known to be an energy-intensive process, MFCs have emerged as a potential technology for concurrent energy harvesting, organic treatment, and more recently, nutrient recovery.

In this study, single-batch and sequencing batch operating mechanisms were investigated using dual-chamber MFCs to identify the optimum configuration for phosphorus recovery as struvite. In addition, the effect of various substrates, namely urine, centrate, and greywater, on struvite formation was assessed. The MFC performance was evaluated based on electricity generation, organic removal efficiency, and struvite recovery. The treated effluents were characterized, and solid precipitates were analyzed using SEM-EDX, FTIR, and XRF to detect and characterize the morphology of the formed struvite. The main outcomes of the current experimental research work are summarized as follows:

1. The general **characterization** tests showed that the TS and VS content was the highest in urine with values of 40 and 34 mg/L, respectively. The collected urine samples contained the highest fraction of readily biodegradable organics at 41%, followed by the centrate at 34%, while the greywater had the lowest fraction (8%). Results indicated the presence of relatively higher organic content in urine. The examined substrates were alkaline, with the urine being within the recommended pH range of 8-9.5 for nutrient recovery.
2. Based on the **electrochemical** measurements, the EC analysis revealed that the three substrates were highly conductive, with urine being slightly higher (17.85 μS/cm) than greywater (15.49 μS/cm) and centrate (15.38 μS/cm). The centrate had the highest ORP, which could lead to a higher electron transfer between the anolyte and catholyte.
3. The **nutrient** results revealed that relatively high $NH4^{+}$, $PO_4^{3-}$, and $Mg^{2+}$ concentrations were found in urine and centrate, with the highest in the urine samples. The greywater was deficient in both phosphorus and ammonia, which

was attributed to the use of phosphorus-free detergent and the exclusion of feces and urine. In all the MFC reactors, $NH_4^+$ showed the highest removal efficiency among other nutrients. The removal of $NH_4^+$ from greywater was the highest (99.2%), followed by urine (92.4%) and centrate (92.2%). The high removal efficiency of $NH_4^+$ at the catholyte of the urine fed MFC was attributed to the accelerated urea hydrolysis of ammonium ions. The removal of $Mg^{2+}$ was the lowest in all scenarios, as it is considered the limiting nutrient in most of the substrates. $Mg^{2+}$ removal in centrate was the highest, followed by greywater and urine at 80.4, 74.7, and 64.9%, respectively. The removal efficiencies of $PO_4^{3-}$ and $Mg^{2+}$ at the catholyte of the greywater-fed cell were in close proximity at 76.4 and 74.7%, respectively. The relatively lower removals found in the greywater and centrate cells can be due to the lower $PO_4^{3-}$ concentrations in those samples.

4. The **organic** analyses indicated that the COD was highest in centrate (4,135 mg/L), followed by urine (1,343 mg/L) and greywater (210 mg/L). The soluble fraction of COD was highest in urine, in which it comprised 40% of the total COD, followed by centrate (34%) and greywater (8%). The organics removal - in terms of sCOD - at the anolyte of the greywater-fed MFC was the lowest (58.8%) due to the complex organic compounds contained in greywater resulting in a relatively longer lag period and shorter stable electricity output phase. The sCOD removal of centrate-fed MFC was found to be the highest, where it declined from 1390 to 32 mg/l, which can be attributed to the high soluble organic content of the centrate.
5. The **electrical** measurements showed that the daily voltage readings for greywater-fed MFC lasted for the longest duration in the lag phase (23 days) compared to 15 days in the urine and centrate-fed MFC. The highest voltages recorded from the urine, centrate, and greywater-fed cells were 381, 590, and 439 mV, respectively. The stationary growth phase lasted longer in the MFC with urine substrate (18 days) as a result of the readily biodegradable organics, compared to 11 and 7 days for greywater and centrate, respectively.
6. The **phosphate** recovery was measured and also theoretically calculated based on the struvite precipitation experiments. The greywater fed MFC produced (actual) the highest precipitate quantity (1.5 g), followed by centrate (1.3 g) and

urine (0.3 g). The phosphate recovery efficiency was found to be 56% for the MFC with urine as substrate, 36% for centrate, and 48% for greywater as well as 23% for the urine samples during phase II.

7. The struvite precipitate **morphology** analysis using XRD revealed that the dominant elements in all samples are Ca, K, P, Mg, and N, which constitute the composition of pure struvite. The XRF analysis revealed that the dominant elements included Mg, P, N, Zn, Cl, and K. The highest N concentration was detected for the greywater sample, followed by centrate and urine samples. The FTIR curves showed the presence of water molecules, $PO_4^{3-}$, and the N-H bond at their specific wavelengths. The SEM images showed a difference in struvite crystal shape, where the urine sample was needle-like with a length of 16.6 μm, compared to rod-like crystals (50 to 70 μm in length) in the centrate sample, and smooth surface with a 30 μm length and a cube-like structure in the greywater sample. Phase II analysis resulted in variation of the formed struvite varied from the small needle-like shape (7 μm) to the larger rod-like crystals (11 μm). Phase II was characterized by relatively smaller precipitate size compared to struvite from phase I as a result of the high percentage of $Ca^{2+}$. The EDS analysis of the three samples showed that the elemental composition included O, Mg, P, and N in addition to traces of Na, Ca, and Cl.
8. The treatment efficiency of the MFC was based on the removal of COD and the final effluent concentration which was highest for the greywater with removal efficiency of 98% and final effluent concentration of 4 mg/L.
9. The performance of MFC in terms of electricity output was determined compared to the previous literature which was found to be in range for all substrates.
10. The success of struvite recovery from the MFC was based on morphology analysis results that were confirmed with the literature.

Based on these findings, the main aim of the current study was achieved and a key gap in the literature was filled with regard to the comparative experimental assessment between batch single-stage and sequencing two-stage (using recirculated anolyte) operation modes as well as the performance of MFC in terms of electricity generation, treatment efficiency, and struvite recovery using unconventional substrates. Such outcomes are expected to prompt research on the potential of struvite recovery using

nutrient-rich substrates such as centrate. Moreover, the results of the present study show the potential of cost savings upon the replacement of conventional chemical buffers in the MFC to recirculated anolyte in the two-stage operation mode.

The present study shows the potential cost-savings from the recovery of struvite using the implemented MFCs, therefore future financial analysis can be carried out. Moreover, the reduction of chemical use during MFC operation (recirculated anolyte) also has the potential of improving the environmental performance. In order to support such results a comprehensive environmental and financial life cycle analyses are recommended. In terms of MFC operation, additional exploration of the two-stage mode is required to study the effect of the catholyte pH on the overall cell performance. Other areas of research that need to be explored, include the effect of the different greywater compositions on the treatment efficiency and electricity generation potential of the MFC as well as the corresponding impact on nutrient recovery. Moreover, the work conducted on studying the different operating modes using lab-scale MFC reactors will facilitate up-scaling to pilot- and full-scale stacked MFCs towards the commercialization of the technology.

References

[1] M. Maktabifard, E. Zaborowska, and J. Makinia, “Achieving Energy Neutrality In Wastewater Treatment Plants Through Energy Savings and Enhancing Renewable Energy Production,” *Reviews in Environmental Science and Biotechnology*, vol. 17, no. 4, pp. 655–689, 2018.

[2] International Energy Agency, “World Energy Outlook,” 2019, [online]. Available: https://www.iea.org/reports/world-energy-outlook-2019.

[3] A. S. Mathuriya, D. A. Jadhav, and M. M. Ghangrekar, “Architectural Adaptations of Microbial Fuel Cells,” *Applied Microbiology and Biotechnology*, vol. 102, no. 22, pp. 9419–9432, 2018.

[4] W. He, X. Zhang, J. Liu, X. Zhu, Y. Feng, and B. E. Logan, “Microbial Fuel Cells With an Integrated Spacer and Separate Anode and Cathode Modules,” *Environmental Science: Water Research and Technology*, vol. 2, no. 1, pp. 357–373, 2015.

[5] S. Elhenawy, M. Khraisheh, F. Almomani, M. Al-Ghouti, and M. K. Hassan, “From Waste to Watts: Updates on Key Applications of Microbial Fuel Cells in Wastewater Treatment and Energy Production,” *Sustainability*, vol. 14, no. 2, pp. 955, 2022.

[6] R. Kaur, A. Marwaha, V. A. Chhabra, K. H. Kim, and S. K. Tripathi, “Recent Developments on Functional Nanomaterial-based Electrodes for Microbial Fuel Cells,” *Renewable and Sustainable Energy Reviews*, vol. 119, p. 109551, 2020.

[7] S. G. A. Flimban, I. M. I. Ismail, T. Kim, and S. E. Oh, “Overview of Recent Advancements in The Microbial Fuel Cell from Fundamentals to Applications: Design, Major Elements, and Scalability,” *Energies*, vol. 12, no. 17, PP. 3390 2019.

[8] J. M. Sonawane, A. Gupta, and P. C. Ghosh, “Multi-electrode Microbial Fuel Cell (MEMFC): A Close Analysis Towards Large Scale System Architecture,” *International Journal of Hydrogen Energy*, vol. 38, no. 12, pp. 5106–5114, 2013.

[9] M. Rahimnejad, A. A. Ghoreyshi, G. D. Najafpour, H. Younesi, and M. Shakeri, “A Novel Microbial Fuel Cell Stack for Continuous Production of Clean Energy,” *International Journal of Hydrogen Energy*, vol. 37, no. 7, pp. 5992-6000, 2012.

[10] R. Goswami and V. K. Mishra, “A Review of Design, Operational Conditions and Applications of Microbial Fuel Cells,” *Biofuels*, vol. 9, no. 2, pp. 203–220, 2017.

[11] Y. Ye *et al.*, “Nutrient Recovery from Wastewater: From Technology to Economy,” *Bioresource Technology Reports*, vol. 11, pp. 100425, 2020.

[12] Y. hua Li, H. bo Li, X. yang Xu, S. yao Xiao, S. qi Wang, and S. cong Xu, "Fate of Nitrogen in Subsurface Infiltration System for Treating Secondary Effluent," *Water Science and Engineering*, vol. 10, no. 3, pp. 217–224, 2017.

[13] G. L. Zang *et al.*, "Nutrient Removal and Energy Production in A Urine Treatment Process Using Magnesium Ammonium Phosphate Precipitation and A Microbial Fuel Cell Technique," *Physical Chemistry Chemical Physics*, vol. 14, no. 6, pp. 1978–1984, 2012.

[14] M. Faragò *et al.*, "From Wastewater Treatment to Water Resource Recovery: Environmental and Economic Impacts of Full-Scale Implementation," *Water Research*, vol. 204, pp. 117554, 2021.

[15] B. Li *et al.*, "Phosphorous Recovery through Struvite Crystallization: Challenges for Future Design," *Science of the Total Environment*, vol. 648, pp. 1244–1256, 2019.

[16] C. M. Mehta and D. J. Batstone, "Nucleation and Growth Kinetics of Struvite Crystallization," *Water Research*, vol. 47, no. 8, pp. 2890–2900, 2013.

[17] A. Siciliano, C. Limonti, G. M. Curcio, and R. Molinari, "Advances in Struvite Precipitation Technologies for Nutrients Removal and Recovery from Aqueous Waste and Wastewater," *Sustainability*, vol. 12, no. 18, pp. 7538, 2020.

[18] K. P. Fattah, "Assessing Struvite Formation Potential at Wastewater Treatment Plants," *International Journal of Environmental Science and Development*, vol. 3, no. 6, pp. 548–552, 2012.

[19] M. H. Do *et al.*, "Challenges in The Application of Microbial Fuel Cells to Wastewater Treatment and Energy Production: A Mini Review," *Science of The Total Environment*, vol. 639, pp. 910–920, 2018.

[20] N. Duteanu, B. Erable, S. M. Senthil Kumar, M. M. Ghangrekar, and K. Scott, "Effect of Chemically Modified Vulcan XC-72R on The Performance of Air-Breathing Cathode in A Single-Chamber Microbial Fuel Cell," *Bioresource Technology*, vol. 101, no. 14, pp. 5250–5255, 2010.

[21] L. Wang, P. Liang, J. Zhang, and X. Huang, "Activity and Stability of Pyrolyzed Iron Ethylenediaminetetraacetic Acid As Cathode Catalyst in Microbial Fuel Cells," *Bioresource Technology*, vol. 102, no. 8, pp. 5093–5097, 2011.

[22] L. Birry, P. Mehta, F. Jaouen, J. P. Dodelet, S. R. Guiot, and B. Tartakovsky, "Application of Iron-based Cathode Catalysts in A Microbial Fuel Cell," *Electrochimica Acta*, vol. 56, no. 3, pp. 1505–1511, 2011.

[23] Y. Zhang *et al.*, "Effect of A Mixed Anionic-Nonionic Surfactant Adsorption on Bentonite Structure and on Distribution of Pentachlorophenol," *Applied Clay Science*, vol. 69, pp. 93–98, 2012.

[24] J. Ramirez-Nava *et al.*, "The Implications of Membranes used As Separators in Microbial Fuel Cells," *Membranes*, vol. 11, no. 10, pp. 738, 2021.

[25] M. Rahimnejad, G. Bakeri, M. Ghasemi, and A. Zirepour, "A Review on The Role of Proton Exchange Membrane on The Performance of Microbial Fuel Cell," *Polymers for Advanced Technologies*, vol. 25, no. 12, pp. 1426–1432, 2014.

[26] H. M. Singh, A. K. Pathak, K. Chopra, V. V. Tyagi, S. Anand, and R. Kothari, "Microbial Fuel Cells: A Sustainable Solution for Bioelectricity Generation and Wastewater Treatment," *Biofuels*, vol. 10, no. 1, pp. 11–31, 2018.

[27] G. Bhargavi, V. Venu, and S. Renganathan, "Microbial Fuel Cells: Recent Developments in Design and Materials," *IOP Conference Series: Materials Science and Engineering*, vol. 330, no. 1, 2018.

[28] L. He *et al.*, "Advances in Microbial Fuel Cells for Wastewater Treatment," *Renewable and Sustainable Energy Reviews*, vol. 71, pp. 388–403, 2017.

[29] B. E. Logan, "Essential Data and Techniques for Conducting Microbial Fuel Cell and Other Types of Bioelectrochemical System Experiments," *ChemSusChem*, vol. 5, no. 6, pp. 988–994, 2012.

[30] A. Nawaz *et al.*, "Upscaling Feasibility of A Graphite-Based Truncated Conical Microbial Fuel Cell for Bioelectrogenesis through Organic Wastewater Treatment," *Journal of Colloid and Interface Science*, vol. 570, pp. 99–108, 2020.

[31] M. Jiang, T. Xu, and S. Chen, "A Mechanical Rechargeable Small-Size Microbial Fuel Cell with Long-Term and Stable Power Output," *Applied Energy*, vol. 260, p. 114336, 2020.

[32] H. Liu, S. Cheng, L. Huang, and B. E. Logan, "Scale-up of Membrane-free single-chamber Microbial Fuel Cells," *Journal of Power Sources*, vol. 179, no. 1, pp. 274–279, 2008.

[33] C. Feng, A. Hu, S. Chen, and C. P. Yu, "A Decentralized Wastewater Treatment System using Microbial Fuel Cell Techniques and Its Response to A Copper Shock Load," *Bioresource Technology*, vol. 143, pp. 76–82, 2013.

[34] H. Hiegemann *et al.*, "An Integrated 45 L Pilot Microbial Fuel Cell System at A Full-Scale Wastewater Treatment Plant," *Bioresource Technology*, vol. 218, pp. 115–122, 2016.

[35] P. Clauwaert, S. Mulenga, P. Aelterman, and W. Verstraete, “Litre-scale Microbial Fuel Cells Operated in A Complete Loop,” *Applied Microbiology and Biotechnology*, vol. 83, no. 2, pp. 241–247, 2009, doi: 10.1007/s00253-009-1876-0.

[36] K. Ganesh and J. R. Jambeck, “Treatment of Landfill Leachate using Microbial Fuel Cells : Alternative Anodes and Semi-continuous Operation,” *Bioresource Technology*, vol. 139, pp. 383–387, 2013.

[37] P. Liang, R. Duan, Y. Jiang, X. Zhang, Y. Qiu, and X. Huang, “One-year Operation of 1000-L Modularized Microbial Fuel Cell for Municipal Wastewater Treatment,” *Water Research*, vol. 141, pp. 1–8, 2018.

[38] A. Dekker, A. Ter Heijne, M. Saakes, H. V. M. Hamelers, and C. J. N. Buisman, “Analysis and Improvement of a Scaled-up and Stacked Microbial Fuel Cell,” *Environmental Science and Technology*, vol. 43, no. 23, pp. 9038–9042, 2009.

[39] S. Wu *et al.*, “A novel Pilot-scale Stacked Microbial Fuel Cell for Efficient Electricity Generation and Wastewater Treatment,” *Water Research*, vol. 98, pp. 396–403, 2016.

[40] H. Liu, B. Zhang, Y. Liu, Z. Wang, and L. Hao, “Continuous Bioelectricity Generation with Simultaneous Sulfide and Organics Removals in An Anaerobic Baffled Stacking Microbial Fuel Cell,” *International Journal of Hydrogen Energy*, vol. 40, no. 25, pp. 8128–8136, 2015.

[41] E. B. Estrada-arriaga, Y. Guillen-alonso, C. Morales-morales, and L. A. Pliego, “Performance of Air-cathode Stacked Microbial Fuel Cells Systems for Wastewater Treatment and Electricity Production,” *Water Science amd Technology*, vol. 76, no. 3, pp. 683-693, 2017.

[42] J. R. Kim, J. Rodr, F. R. Hawkes, R. M. Dinsdale, and J. Guwy, “Increasing Power Recovery and Organic Removal Efficiency using Extended Longitudinal Tubular Microbial Fuel Cell (MFC) Reactors,” *Energy and Enviroenmtnal Science*, vol. 4, pp. 459–465, 2011.

[43] M. Rahimnejad, A. A. Ghoreyshi, G. D. Najafpour, H. Younesi, and M. Shakeri, “A Novel Microbial Fuel Cell Stack for Continuous Production of Clean Energy,” *International Journal of Hydrogen Energy*, vol. 37, no. 7, pp. 5992–6000, 2012.

[44] P. Aelterman, “Microbial Fuel Cells for The Treatment of Waste Streams with Energy Recovery,” PhD, Ghent University, 2009.

[45] B. Min and B. E. Logan, “Continuous Electricity Generation from Domestic Wastewater and Organic Substrates in a Flat Plate Microbial Fuel Cell,” *Environmental Science and Technology*, vol. 38, no. 21, pp. 5809–5814, 2004.

[46] D. Akman, K. Cirik, S. Ozdemir, B. Ozkaya, and O. Cinar, “Bioelectricity generation in Continuously-fed Microbial Fuel Cell: Effects of Anode Electrode Material and Hydraulic Retention Time,” *Bioresource Technology*, vol. 149, pp. 459-464, 2013.

[47] F. Vicari, M. Albamonte, A. Galia, and O. Scialdone, “Effect of Mode of Operation, Substrate, and Final Electron Acceptor on Single-Chamber Membraneless Microbial Fuel Cell Operating with a Mixed Community,” *Journal of Electroanalytical Chemistry*, vol. 814, pp. 104–110, 2018.

[48] D. Pant, G. Van Bogaert, L. Diels, and K. Vanbroekhoven, “A Review of the Substrates used in Microbial Fuel Cells (MFCs) for Sustainable Energy Production,” *Bioresource Technology*, vol. 101, no. 6, pp. 1533–1543, 2010.

[49] J. Yu, J. Seon, Y. Park, S. Cho, and T. Lee, “Electricity Generation and Microbial Community in a Submerged-exchangeable Microbial Fuel Cell System for Low-strength Domestic Wastewater Treatment,” *Bioresource Technology*, vol. 117, pp. 172–179, 2012.

[50] I. Shizas and D. M. Bagley, “Experimental Determination of Energy Content of Unknown Organics in Municipal Wastewater Streams,” *Journal of Energy Engineering*, vol. 130, no. 2, pp. 45–53, 2004.

[51] A. Sotres, L. Tey, A. Bonmatí, and M. Viñas, “Microbial Community Dynamics in Continuous Microbial Fuel Cells Fed with Synthetic Wastewater and Pig Slurry,” *Bioelectrochemistry*, vol. 111, pp. 70–82, 2016.

[52] Y. V. Nancharaiah, S. Venkata Mohan, and P. N. L. Lens, “Recent Advances in Nutrient Removal and Recovery in Biological and Bioelectrochemical Systems,” *Bioresource Technology*, vol. 215, pp. 173–185, 2016.

[53] L. Pastor, D. Mangin, R. Barat, and A. Seco, “A Pilot-scale Study of Struvite Precipitation in a Stirred Tank Reactor : Conditions Influencing The Process,” *Bioresource Technology*, vol. 99, pp. 6285–6291, 2008.

[54] M. Hanhoun, L. Montastruc, C. Azzaro-pantel, B. Biscans, M. Frèche, and L. Pibouleau, “Temperature Impact Assessment on Struvite Solubility Product : A Thermodynamic Modeling Approach,” *Chemical Engineering Journal*, vol. 167, no. 1, pp. 50–58, 2011.

[55] D. Kim, K. J. Min, K. Lee, M. S. Yu, and K. Y. Park, “Effects of pH , Molar Ratios and Pre-Treatment on Phosphorus Recovery through Struvite Crystallization from Effluent of Anaerobically Digested Swine Wastewater,” *Environmental Engineering Research*, vol. 22, no. 1, pp. 12–18, 2017.

[56] H. Saidou, S. Ben Moussa, and M. Ben Amor, "Influence of Airflow Rate and Substrate Nature on Heterogeneous Struvite Precipitation," *Envrioenmtal Technology*, vol. 3330, no. 1, pp. 75-83, 2015.

[57] L. Peng, H. Dai, Y. Wu, Y. Peng, and X. Lu, "A Comprehensive Review of the Available Media and Approaches for Phosphorus Recovery from Wastewater," *Water, Air, and Soil Pollution*, vol. 229, no. 4, 2018.

[58] W. Tao, K. P. Fattah, and M. P. Huchzermeier, "Struvite Recovery from Anaerobically Digested Dairy Manure: A Review of Application Potential and Hindrances," *Journal of Environmental Management*, vol. 169, pp. 46–57, 2016.

[59] C. Vaneeckhaute *et al.*, "Nutrient Recovery from Digestate: Systematic Technology Review and Product Classification," *Waste and Biomass Valorization*, vol. 8, no. 1, pp. 21–40, 2017.

[60] M. Molinos-Senante, F. Hernández-Sancho, R. Sala-Garrido, and M. Garrido-Baserba, "Economic Feasibility Study for Phosphorus Recovery Processes," *AMBIO* vol. 40, no. 4, pp. 408–416, 2011.

[61] J. You, J. Greenman, C. Melhuish, and I. Ieropoulos, "Electricity Generation and Struvite Recovery from Human Urine using Microbial Fuel Cells," *Journal of Chemical Technology and Biotechnology*, vol. 91, no. 3, pp. 647–654, 2016.

[62] S. Ghosh, "Optimization of Phosphorus Recovery from Anaerobic Digester Supernatant Through a Struvite Crystallization Fluidized Bed Reactor," MSc Thesis, University of British Columbia, 2016.

[63] R. Baur, N. Cullen, and B. Laney, "Nutrient Recovery: One Million Pounds Recovered - With Benefits," In *Proceedings of the Water Environment Federation*, vol. 2011, no. 18, pp. 223–235, 2012.

[64] J. Oleszkiewicz, D. J. Kruk, T. Devlin, M. Lashkarizadeh, and Q. Yuan, "Options for Improved Nutrient Removal and Recovery from Municipal Wastewater in the Canadian Context," *Environmental Technology*, vol. 20, no. 7, pp. 681–695, 2015.

[65] E. Desmidt *et al.*, "Global Phosphorus Scarcity and Full-Scale P-Recovery Techniques: A Review," *Critical Reviews in Environmental Science and Technology*, vol. 45, no. 4, pp. 336–384, 2015.

[66] PAQUES Cases, "PHOSPAQ." [Online]. Available: https://en.paques.nl/products/other/phospaq

[67] T. Pepè Sciarria, G. Vacca, F. Tambone, L. Trombino, and F. Adani, "Nutrient Recovery and Energy Production from Digestate using Microbial Electrochemical

Technologies (METs)," *Journal of Cleaner Production*, vol. 208, pp. 1022–1029, 2019.

[68] P. Sharma and S. Mutnuri, "Nutrient Recovery and Microbial Diversity in Human Urine Fed Microbial Fuel Cell," *Water Science and Technology*, vol. 79, no. 4, pp. 718–730, 2019.

[69] K. Orner *et al.*, "Energy Recovery and Nitrogen Management from Struvite Precipitation Effluent via Microbial Fuel Cells," *Journal of Environmental Engineering*, vol. 145, no. 3, pp. 1–7, 2019.

[70] F. Fischer, C. Bastian, M. Happe, E. Mabillard, and N. Schmidt, "Microbial Fuel Cell Enables Phosphate Recovery from Digested Sewage Sludge as Struvite," *Bioresource Technology*, vol. 102, no. 10, pp. 5824–5830, 2011.

[71] A. Almatouq and A. O. Babatunde, "Identifying Optimized Conditions for Concurrent Electricity Production and Phosphorus Recovery in A Mediator-less Dual Chamber Microbial Fuel Cell," *Applied Energy*, vol. 230, pp. 122–134, 2018.

[72] A. Almatouq and A. O. Babatunde, "Concurrent Phosphorus Recovery and Energy Generation in Mediator-less Dual Chamber Microbial Fuel Cells: Mechanisms and Influencing Factors," *International Journal of Environmental Research and Public Health*, vol. 13, no. 4, 2016.

[73] M. Happe *et al.*, "Scale-up of Phosphate Remobilization from Sewage Sludge in a Microbial Fuel Cell," *Bioresource Technology*, vol. 200, pp. 435–443, 2016.

[74] Q. Tao, S. Zhou, J. Luo, and J. Yuan, "Nutrient Removal and Electricity Production from Wastewater using Microbial Fuel Cell Technique," *Desalination*, vol. 365, pp. 92–98, 20151.

[75] B. Kim, N. Jang, M. Lee, J. Kyung Jang, and I. Seop Chang, "Microbial Fuel Cell Driven Mineral Rich Wastewater Treatment Process for Circular Economy by Creating Virtuous Cycles," *Bioresource Technology*, vol. 320, pp. 124254, 2020

[76] Y. Ye *et al.*, "Feasibility Study on a Double Chamber Microbial Fuel Cell for Nutrient Recovery from Municipal Wastewater," *Chemical Engineering Journal*, vol. 358, pp. 236–242, 2019.

[77] I. Merino-Jimenez, V. Celorrio, D. J. Fermin, J. Greenman, and I. Ieropoulos, "Enhanced MFC Power Production and Struvite Recovery by The Addition of Sea Salts to Urine," *Water Research*, vol. 109, pp. 46–53, 2017.

[78] K. Hirooka and O. Ichihashi, "Phosphorus Recovery from Artificial Wastewater by Microbial Fuel Cell and Its Effect on Power Generation," *Bioresource Technology*, vol. 137, pp. 368–375, 2013.

[79] O. Ichihashi and K. Hirooka, “Removal and Recovery of Phosphorus As Struvite from Swine Wastewater using Microbial Fuel Cell,” *Bioresource Technology*, vol. 114, pp. 303–307, 2012.

[80] W. T. Tang, J. Dai, R. Liu, and G. H. Chen, “Microbial Ureolysis in the Seawater-catalysed Urine Phosphorus Recovery System: Kinetic Study and Reactor verification,” *Water Research*, vol. 87, pp. 10–19, 2015.

[81] L. Zhuang, S. Zhou, Y. Li, and Y. Yuan, “Enhanced Performance of Air-cathode Two-chamber Microbial Fuel Cells with High-pH Anode and Low-pH Cathode,” *Bioresource Technology*, vol. 101, no. 10, pp. 3514–3519, 2010.

[82] O. Ichihashi and K. Hirooka, “Deterioration in The Cathode Performance during Operation of The Microbial Fuel Cells and The Restoration of The Performance by The Immersion Treatment,” *Journal of Microbial and Biochemical Technology*, vol. 5, no. 2, 2013.

[83] M. Oteng-peprah and K. Nanne, “Greywater Characteristics, Treatment Systems, Reuse Strategies, and User Perception; a Review,” *Water, Air, and Soil Polution* vol. 229, no. 255, 2018.

[84] Metrohm Autolab, “NOVA,” 2022. [Online], Available: https://metrohm-autolab.com/Products/Echem/Software/Nova.html.

[85] C. Sánchez, P. Dessì, M. Duffy, and P. N. L. Lens, “Microbial Electrochemical Technologies: Electronic Circuitry and Characterization Tools,” *Biosensors and Bioelectronics*, vol. 150, pp. 111884, 2020.

[86] T. A. Shepherd, R. T. Burns, L. B. Moody, D. R. Raman, and K. J. Stalder, “Investigating Conductivity to Predict Magnesium Addition Requirements for Struvite Precipitation in Swine Manure Slurries,” *Applied Engineering in Agriculture*, vol. 25, no. 1, pp. 103–108, 2009.

[87] E. C. C. Rose, A. Parker, and B. Jefferson, “The Characterization of Feces and Urine: A Review of the Literature to Inform Advanced Treatment Technology,” *Critical Reviews in Environmental Science and Technology*, vol. 45, pp. 1827–1879, 2015.

[88] Z. Liu, Q. Zhao, K. Wang, D. Lee, W. Qiu, And J. Wang, “Urea Hydrolysis and Recovery of Nitrogen and Phosphorous As MAP From Stale Human Urine,” *Journal of Environmental Sciences*, vol. 20, no. 8, pp. 1018–1024, 2008.

[89] F. Li, K. Wichmann, and R. Otterpohl, “Review of the Technological Approaches for Grey Water Treatment and Reuses,” *Science of the Total Environment*, vol. 407, no. 11, pp. 3439–3449, 2009.

[90] Y. Li *et al.*, "Characterization of a Microalga Chlorella Sp. Well Adapted to Highly Concentrated Municipal Wastewater for Nutrient Removal and Biodiesel Production," *Bioresource Technology*, vol. 102, no. 8, pp. 5138–5144, 2011.

[91] P. Kuntke *et al.*, "Ammonium Recovery and Energy Production from Urine by a Microbial Fuel Cell," *Water Research*, vol. 46, no. 8, pp. 2627–2636, 2012.

[92] W. Dabrowski, B. Karolinczak, P. Malinowski, and D. Boruszko, "Modeling of Pollutants Removal in Subsurface Vertical Flow and Horizontal Flow Constructed Wetlands," *Water*, vol. 11, no. 1, 2019.

[93] M. B. Vanotti, A. A. Szogi, P. G. Hunt, A. Q. Ellison, P. D. Millner, and F. J. Humenik, "Development of an Environmentally Superior Treatment System for Replacing Anaerobic Swine Waste Lagoons," In *Proceedings of the Water Environment Federation*, vol. 2005, no. 12, pp. 4073–4092, 2012.

[94] E. Eriksson, K. Auffarth, M. Henze, and A. Ledin, "Characteristics of Grey Wastewater," *Urban Water*, vol. 4, no. 1, pp. 85–104, 2002.

[95] F. Li, K. Wichmann, and R. Otterpohl, "Review of the Technological Approaches for Grey Water Treatment and Reuses," *Science of the Total Environment*, vol. 407, no. 11, pp. 3439–3449, 2009.

[96] S. Johansson, M. Ruscalleda, B. Saerens, and J. Colprim, "Potassium Recovery from Centrate: Taking Advantage of Autotrophic Nitrogen Removal for Multi-Nutrient Recovery," *Journal of Chemical Technology and Biotechnology*, vol. 94, no. 3, pp. 819–828, 2019.

[97] J. Grandgirard, D. Poinsot, L. Krespi, J. P. Nénon, and A. M. Cortesero, "Costs of Secondary Parasitism in the Facultative Hyperparasitoid Pachycrepoideus Dubius: Does host size matter?," *Entomologia Experimentalis et Applicata*, vol. 103, no. 3, pp. 239–248, 2002.

[98] World Health Organization, "World health statistics overview 2019: monitoring health for the SDGs, sustainable development goals.," 2019, [Online]. Available: https://www.who.int/publications/i/item/9789241565707.

[99] I. M. Hassana, B. A. Omotayo, I. M. Hassana, and B. A. Omotayo, "Heavy Metals Accumulation in Edible Part of Vegetables Irrigated with Untreated Municipal Wastewater in Tropical Savannah zone, Nigeria," *African Journal of Environmental Science and Technology*, vol. 8, no. 8, pp. 460–463, 2014.

[100] A. Thomas, B. R. K. Mantha, and C. C. Menassa, "A Framework to Evaluate the Life Cycle Costs and Environmental Impacts of Water Pipelines," In *American Society of Civil Engineers* On *Piplines*, July 2016, pp. 1721–1731.

[101] T. E. Igboamalu, N. Bezuidenhout, M. Thomas Matsena, and E. M. Nkhalambayausi Chirwa, "Microbial Fuel Cell Power Output and Growth: Effect of pH on Anaerobic Microbe Consortium," *Chemical Engineering Transactions*, vol. 76, pp. 1381–1386, 2019.

[102] S. Ong and K. Yamagiwa, "Evaluation on the Electricity Generation using Membrane-Less Fixed-Bed Upflow Microbial Fuel Cell," *Rendiconti Lincei-Scienze Fisiche E Naturali*, vol. 29, pp. 103–107, 2018.

[103] M. J. Salar-García, V. M. Ortiz-Martínez, I. Gajda, J. Greenman, F. J. Hernández-Fernández, and I. A. Ieropoulos, "Electricity Production from Human Urine in Ceramic Microbial Fuel Cells with Alternative Non-fluorinated Polymer Binders for Cathode Construction," *Separation and Purification Technology*, vol. 187, pp. 436–442, 2017.

[104] R. C. de S. Meira, S. P. A. da Paz, and J. A. M. Corrêa, "XRD-Rietveld Analysis As a Tool for Monitoring Struvite Analog Precipitation from Wastewater: P, Mg, N and K Recovery for Fertilizer Production," *Journal of Materials Research and Technology*, vol. 9, no. 6, pp. 15202–15213, 2020.

[105] K. Pfrimer, R. F. Micheletto, J. S. Marchini, G. J. Padovan, J. cesar Moriguti, and E. Ferriolli, "Impact of Aging on Urinary Excretion of Iron and Zinc," *Nutrition and Metabolic Insights*, vol. 7, 2014.

[106] S. Ren, "Probabilistic Risk Assessment for Zinc in Some Commercial Dishwashing Detergents: The Nitrification Processes in US POTWs," *Chemosphere*, vol. 68, no. 8, pp. 1474–1488, 2007.

[107] S. H. Mohamed Ameen and A. Syed Mohamed, "Study of the Inhibitory Effect of Tamarind, Routula Aquatica and Routula Terrastrica on Struvite Urinary Crystals," *Asian Academic Journal of Multidiciplinary*, vol. 1, no. 19, pp. 521–533, 2014.

[108] D. Sidorczuk, M. Kozanecki, B. Civalleri, K. Pernal, and J. Prywer, "Structural and Optical Properties of Struvite. Elucidating Structure of Infrared Spectrum in High Frequency Range," *Journal of Physical Chemistry A*, vol. 124, no. 42, pp. 8668–8678, 2020.

[109] K. Linderholm, A. M. Tillman, and J. E. Mattsson, "Life Cycle Assessment of Phosphorus Alternatives for Swedish Agriculture," *Resources, Conservation and Recycling*, vol. 66, pp. 27–39, 2012.

[110] M. M. Rahman, M. A. M. Salleh, U. Rashid, A. Ahsan, M. M. Hossain, and C. S. Ra, "Production of Slow Release Crystal Fertilizer from Wastewaters through Struvite Crystallization - A review," *Arabian Journal of Chemistry*, vol. 7, no. 1, pp. 139–155, 2014.

[111] K. S. Le Corre, E. Valsami-Jones, P. Hobbs, and S. A. Parsons, “Impact of Calcium on Struvite Crystal Size, Shape and Purity,” *Journal of Crystal Growth*, vol. 283, no. 3–4, pp. 514–522, 2005.

[112] C. C. Wang, X. D. Hao, G. S. Guo, and M. C. M. van Loosdrecht, “Formation of Pure Struvite at Neutral pH by Electrochemical Deposition,” *Chemical Engineering Journal*, vol. 159, no. 1–3, pp. 280–283, 2010.

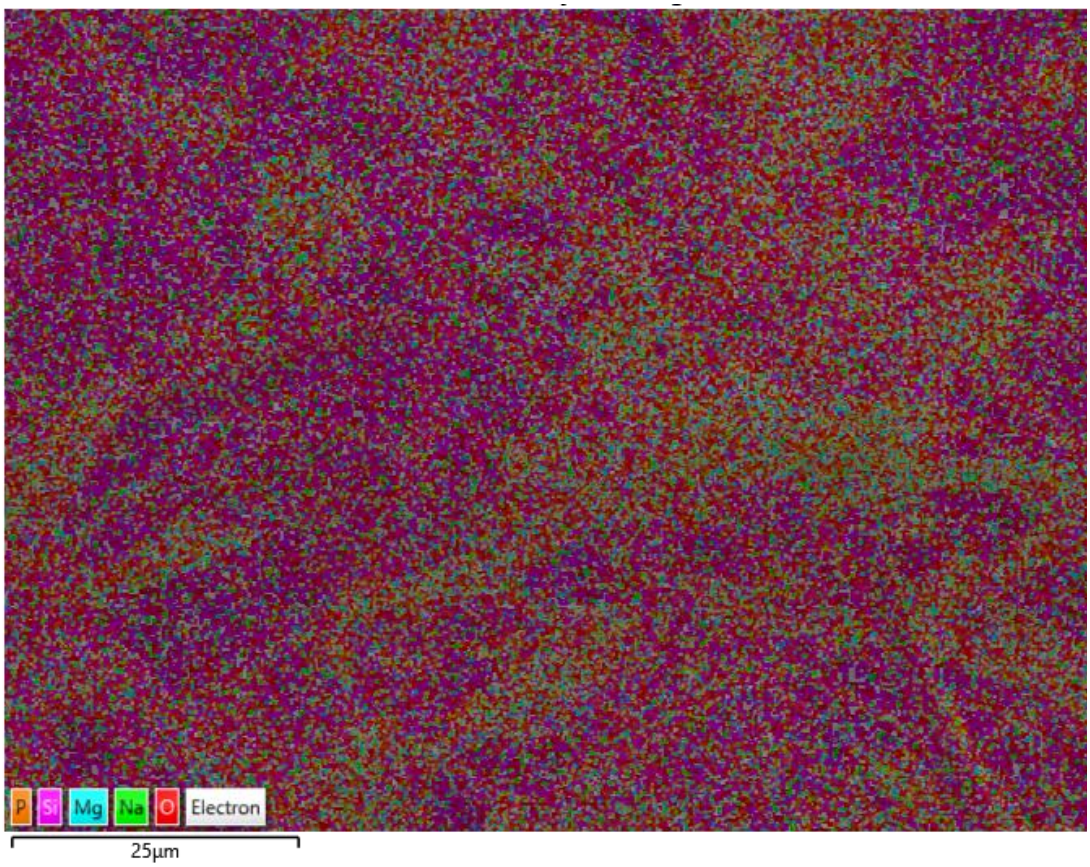
P
Si
Mg
Na
O
Electron
25µm

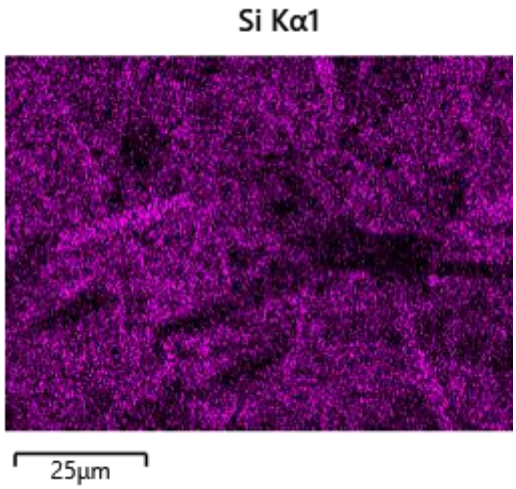
Si Kα1
25µm

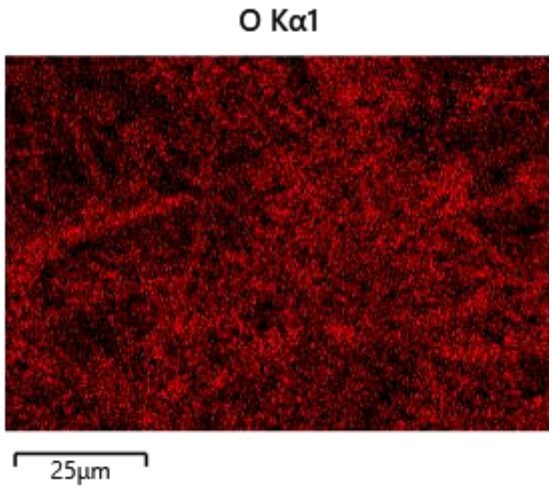
O Kα1
25µm

Mg Kα1,2

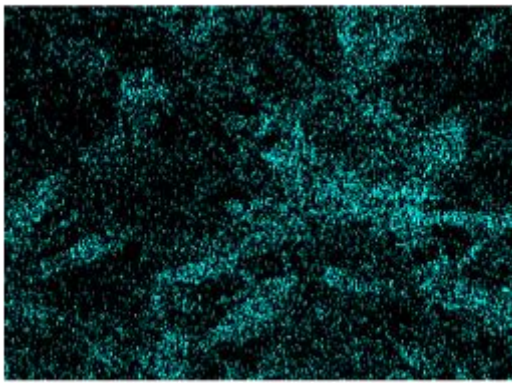


P Kα1

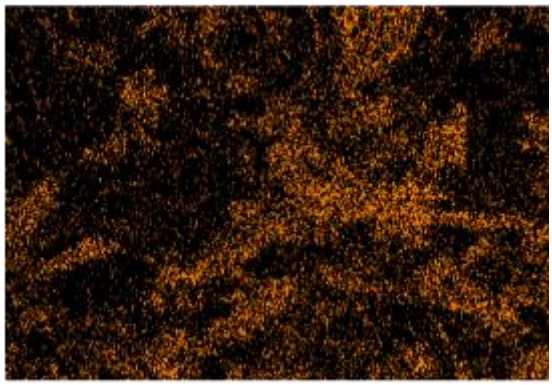


Na Kα1,2

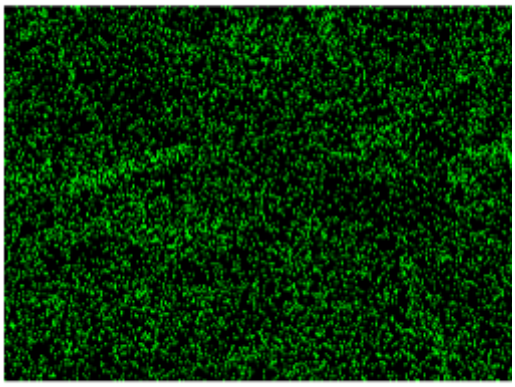


K Kα1

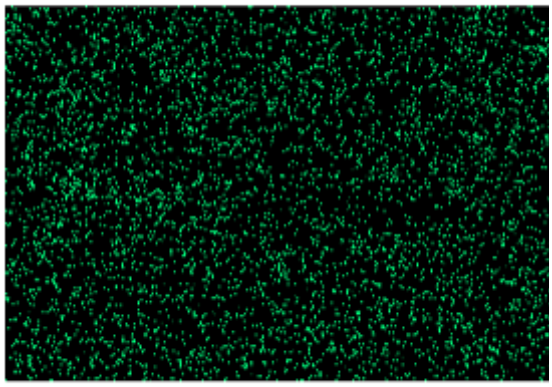


Ca Kα1

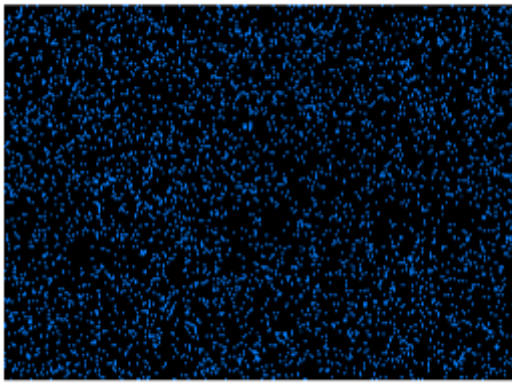


Al Kα1

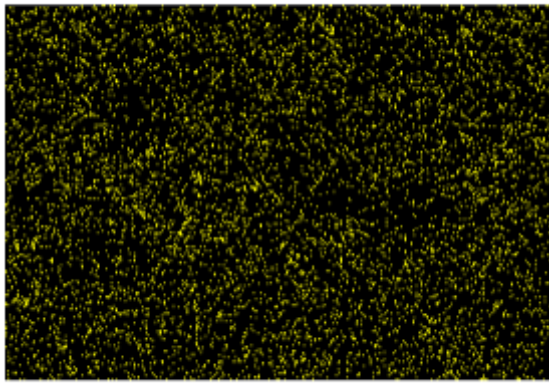

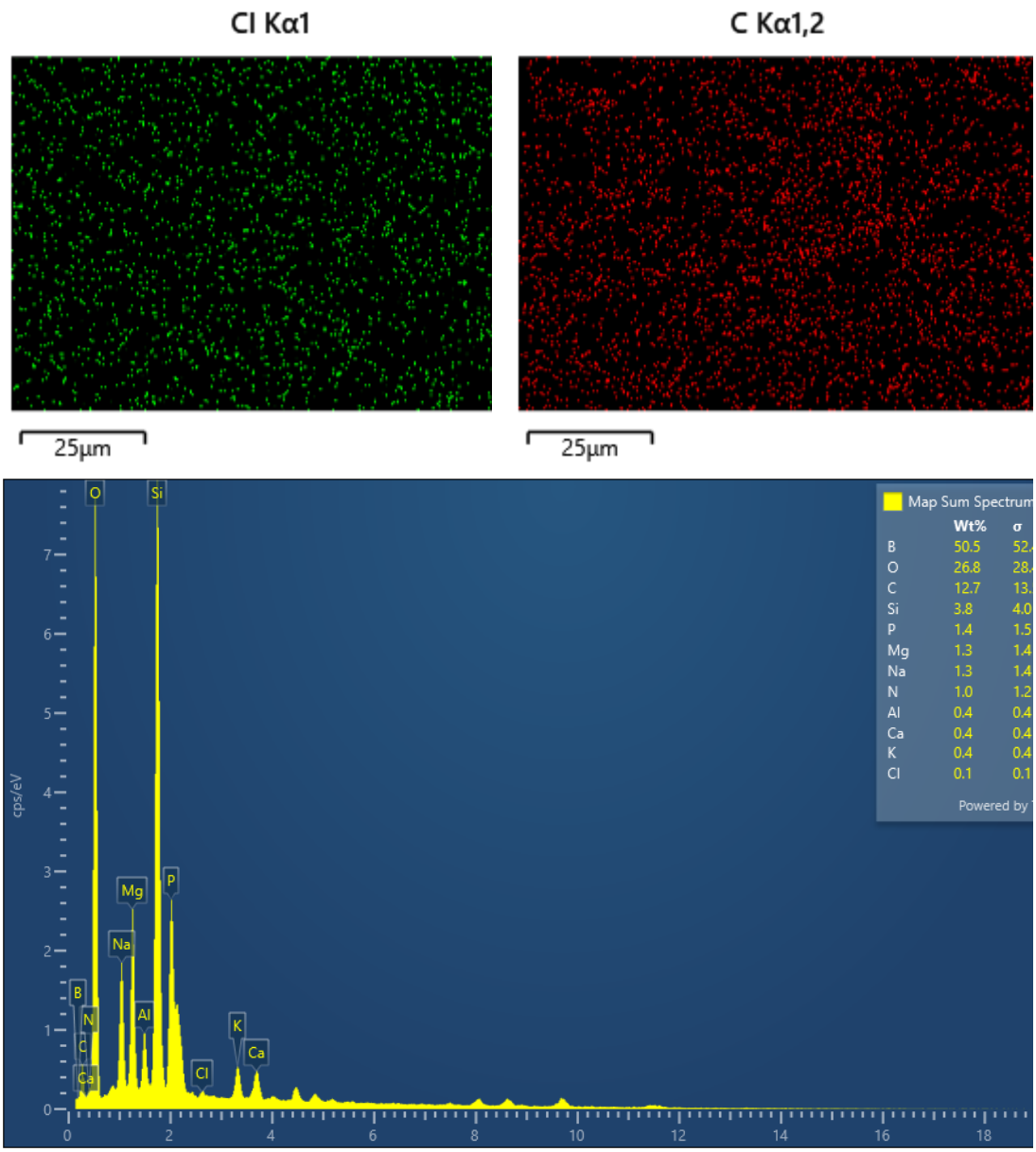


Figure S 1. Scanning electron microscope results for urine sample during operation phase I.

EDS Layered Image 1


Si Kα1

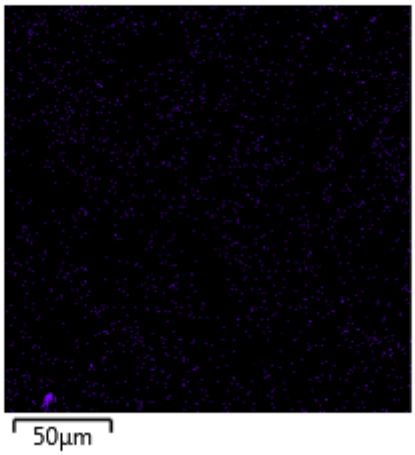


Mg Kα1_2

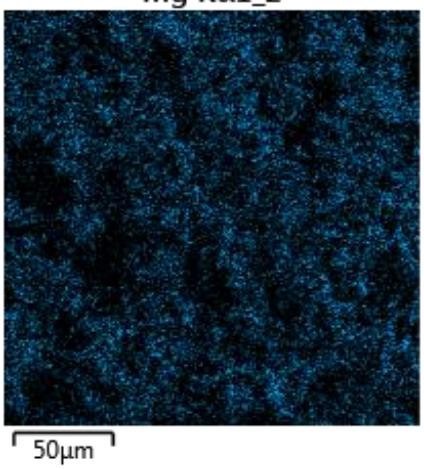


S Kα1

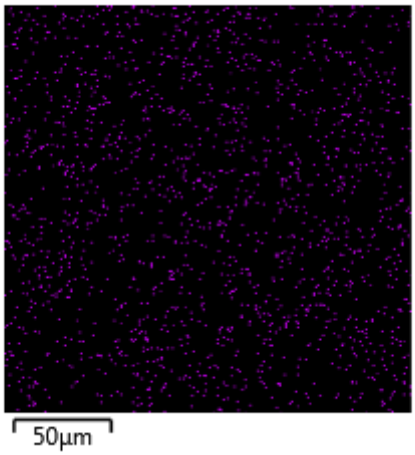


C Kα1_2

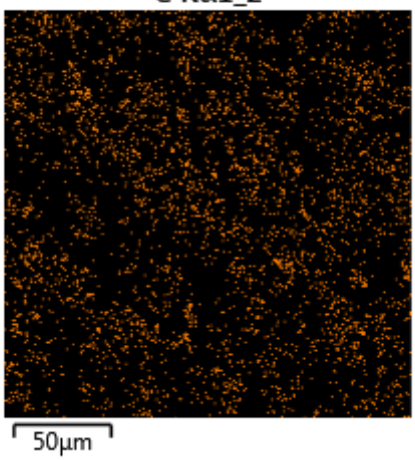

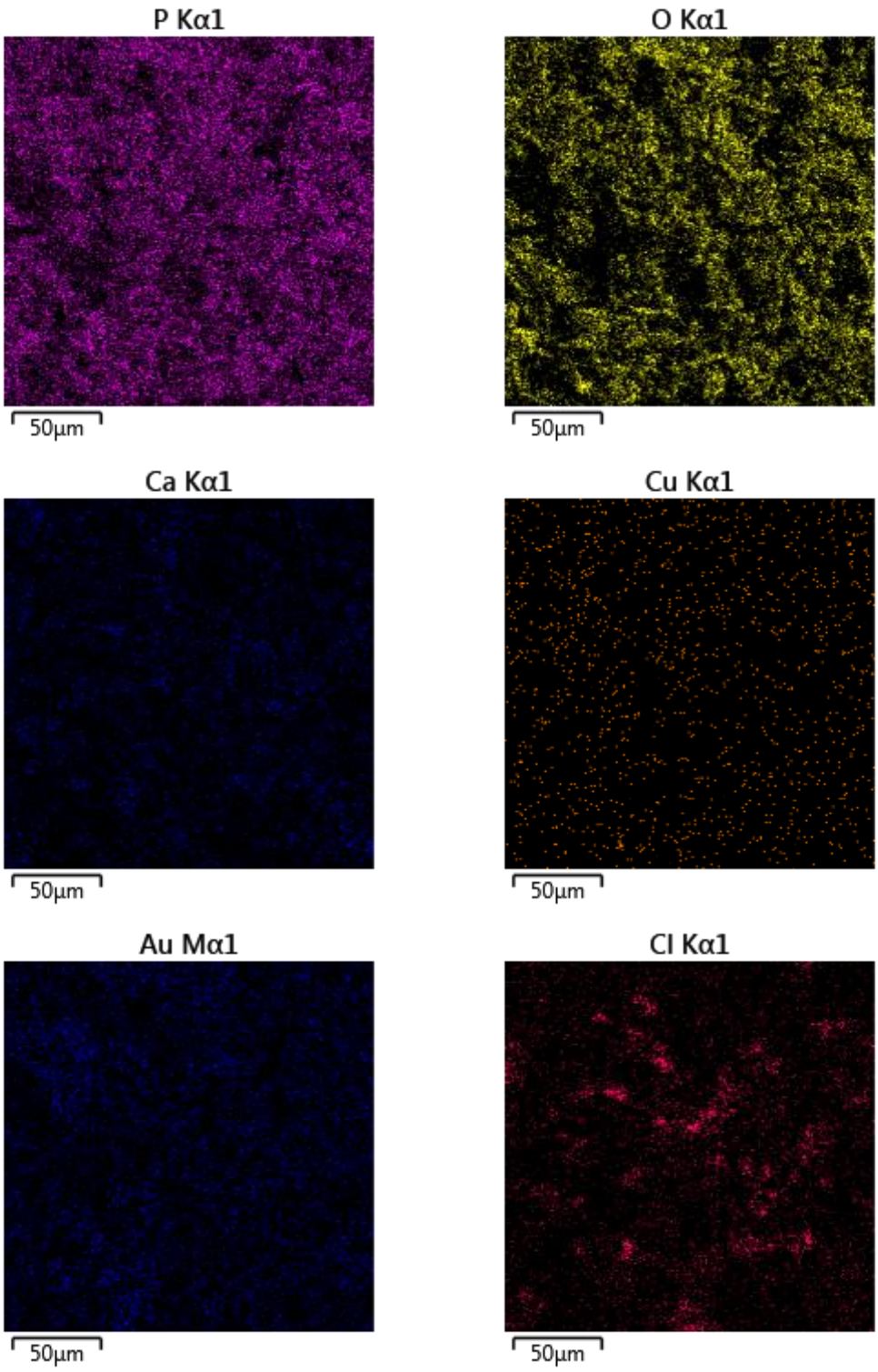
P Kα1
50µm
O Kα1
50µm
Ca Kα1
50µm
Cu Kα1
50µm
Au Mα1
50µm
Cl Kα1
50µm

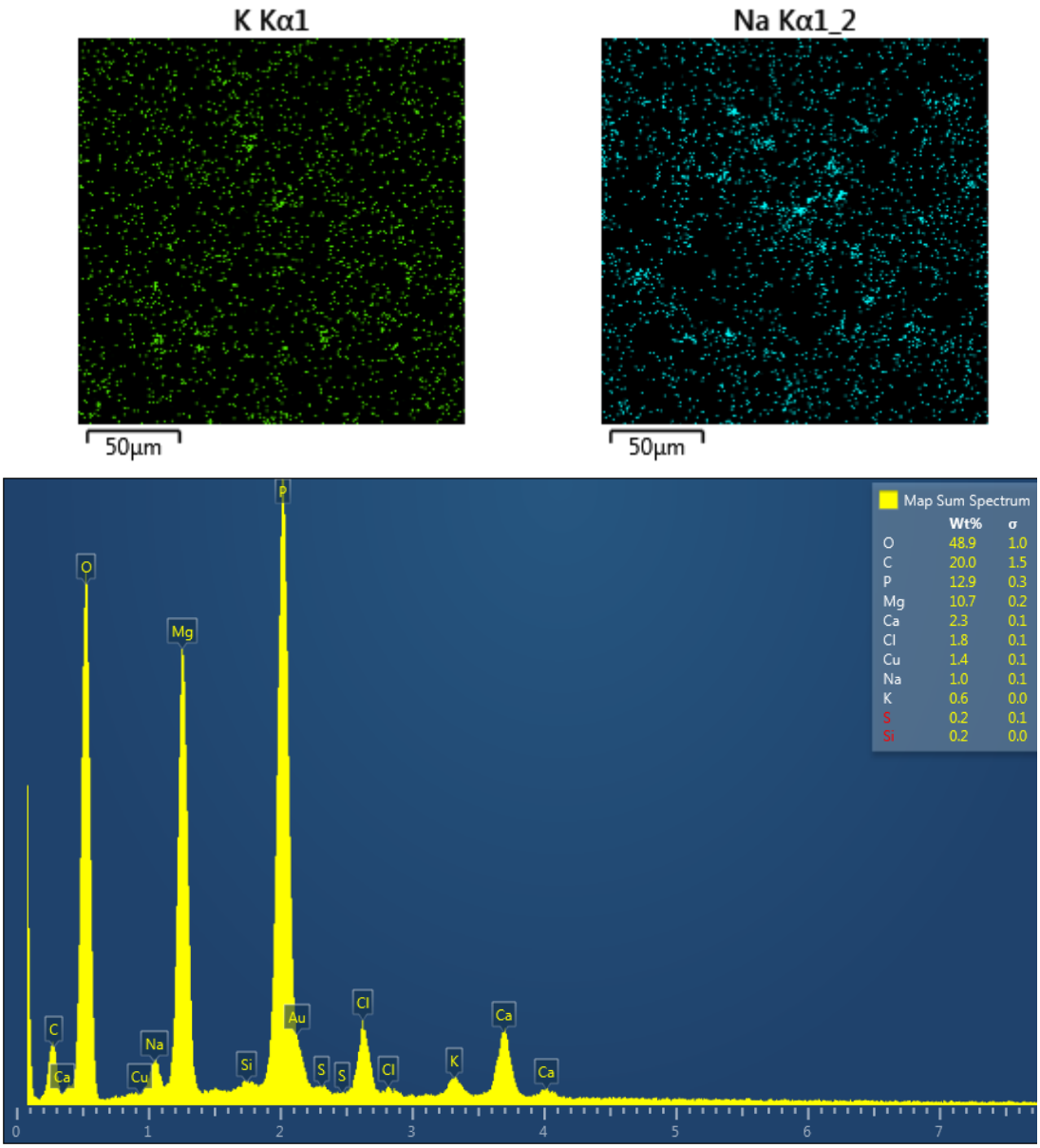


Figure S 2. Scanning electron microscope results for urine sample during operation phase II.

EDS Layered Image 1

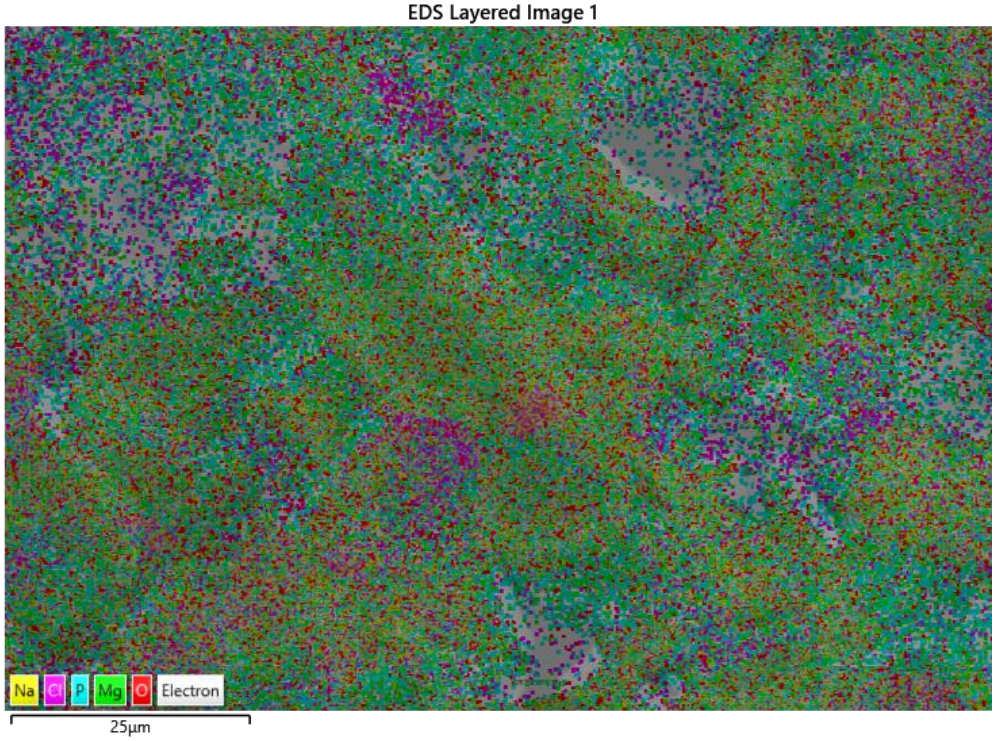


P Kα1

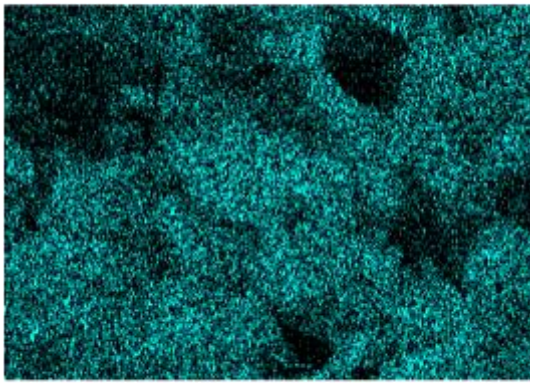


O Kα1

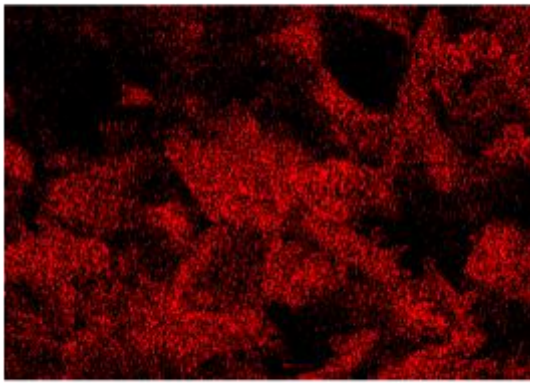


Mg Kα1,2

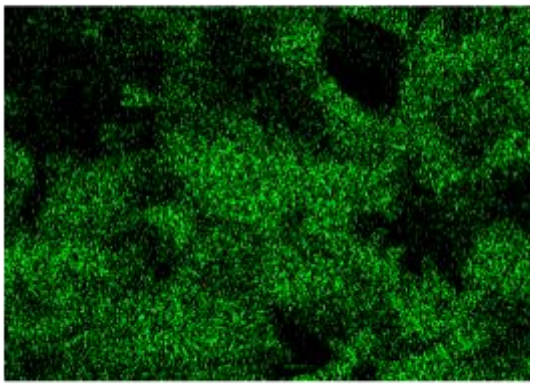


Cl Kα1

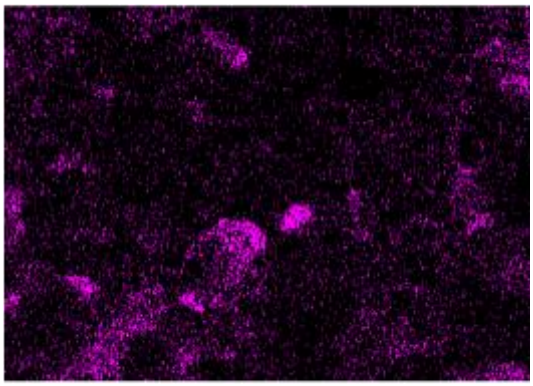

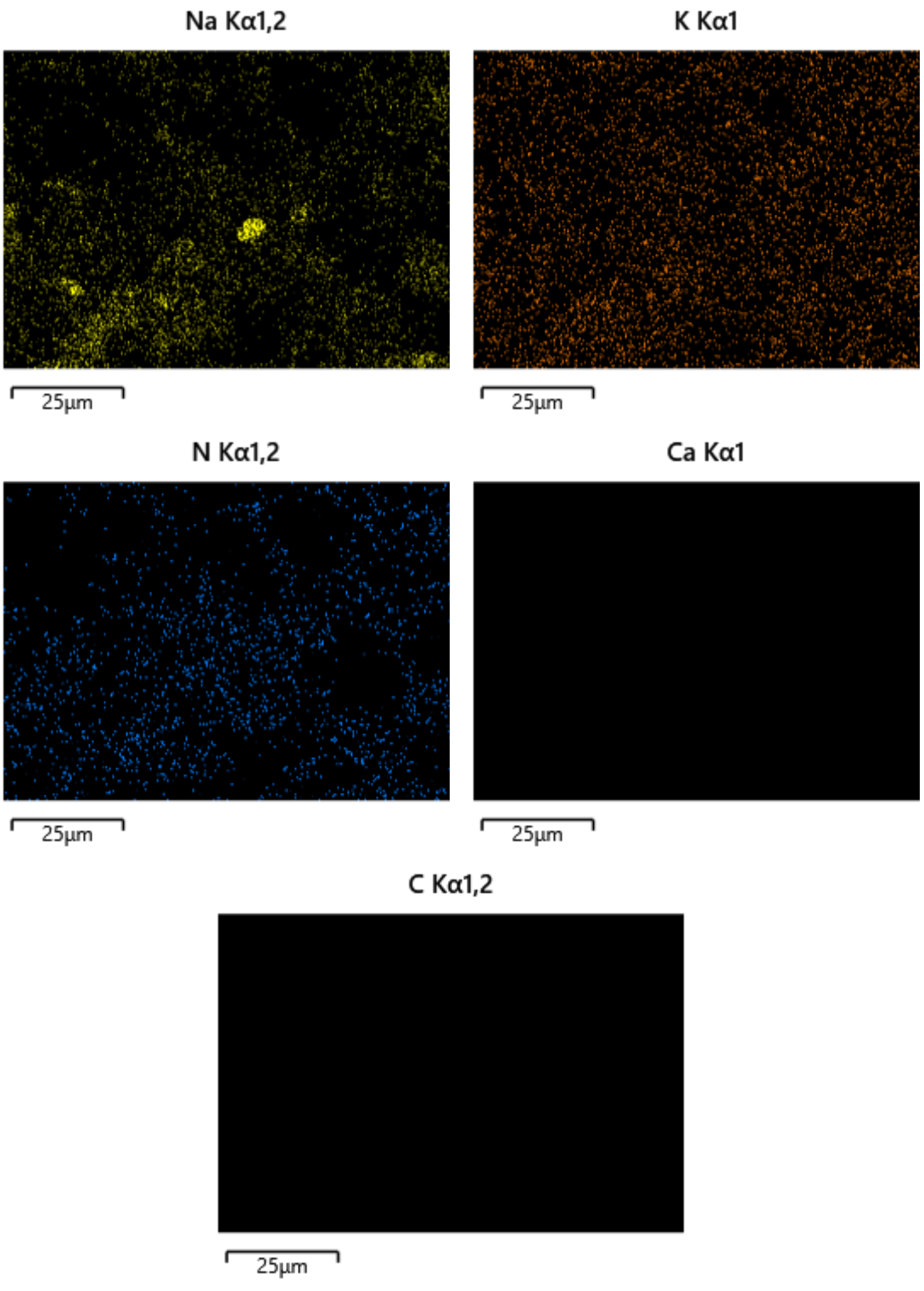
Na Kα1,2
K Kα1
25µm
25µm
N Kα1,2
Ca Kα1
25µm
25µm
C Kα1,2
25µm

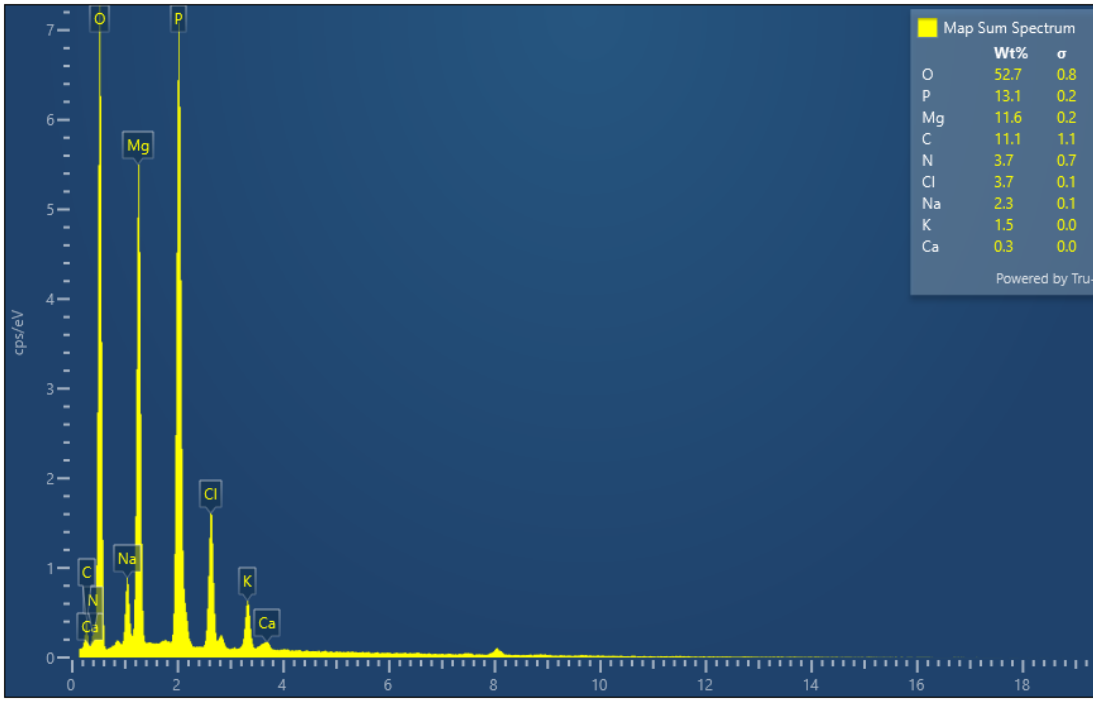


Figure S 3. Scanning electron microscope results for centrate sample during operation phase I.

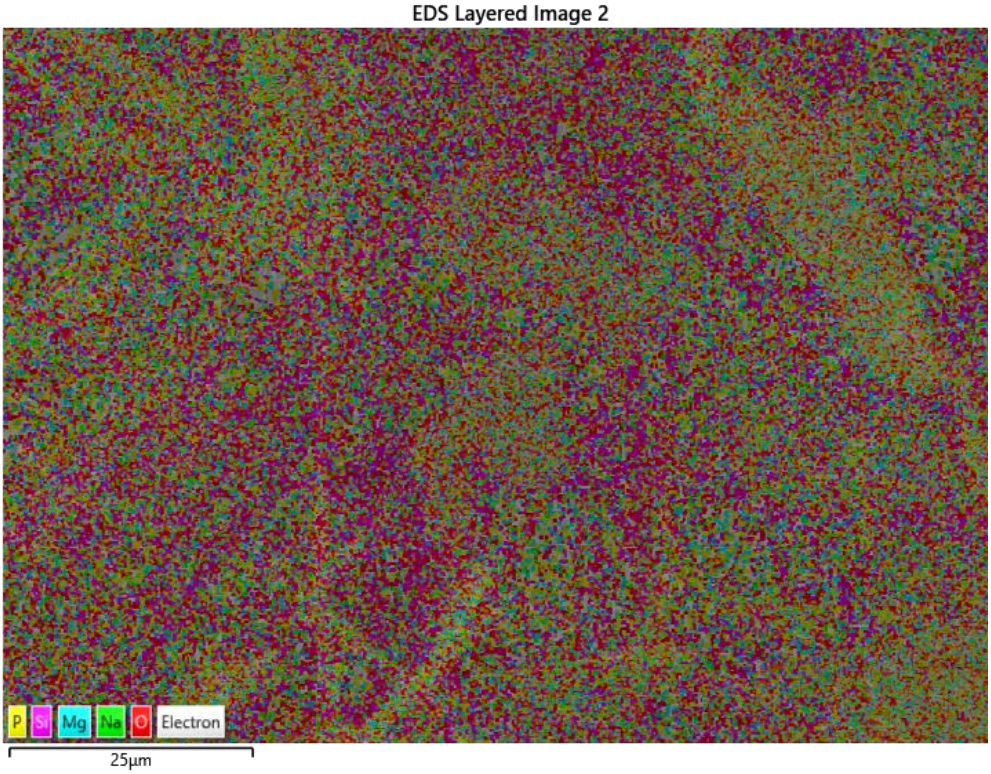

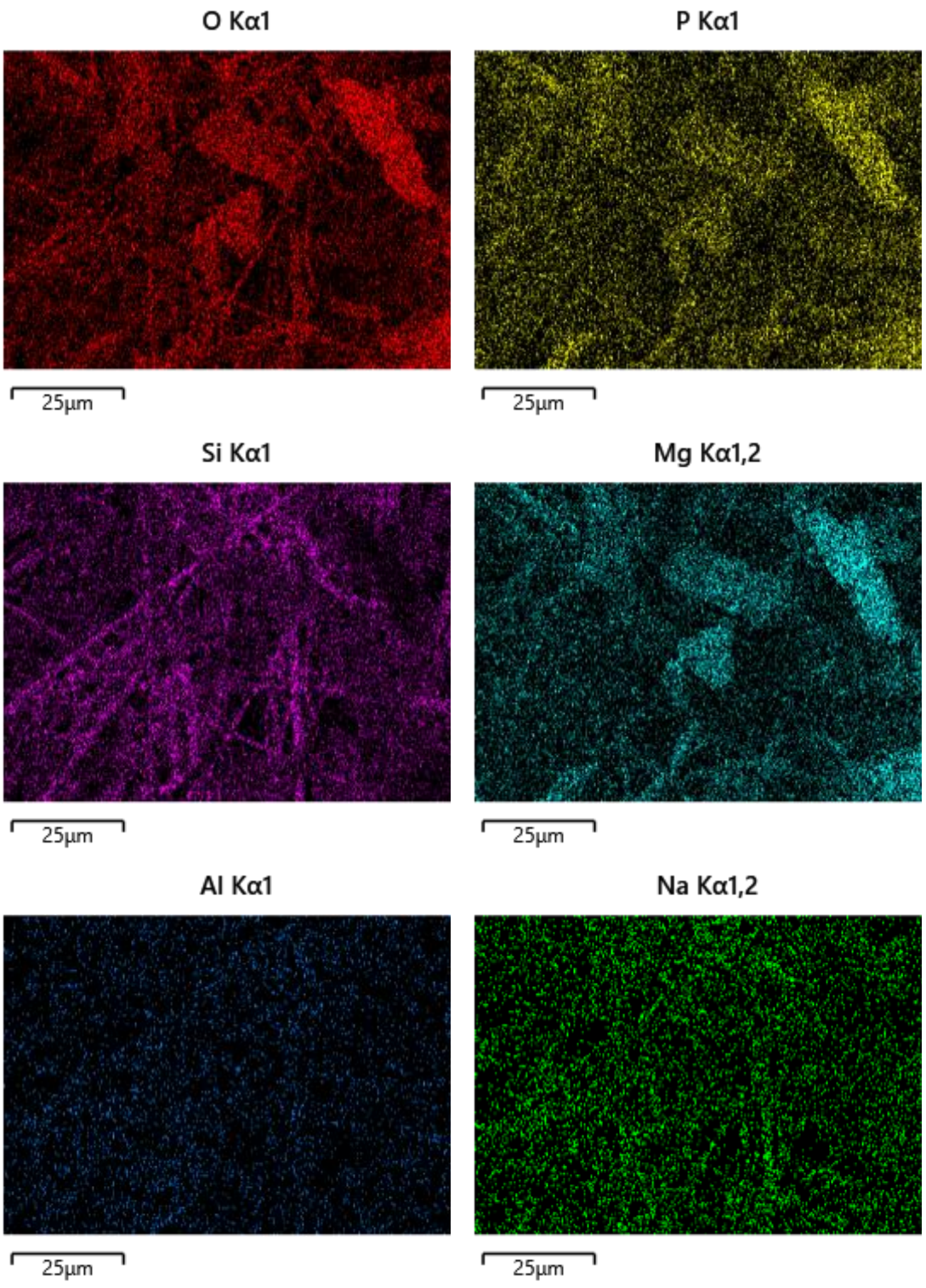
O Kα1
P Kα1
25µm
25µm
Si Kα1
Mg Kα1,2
25µm
25µm
Al Kα1
Na Kα1,2
25µm
25µm

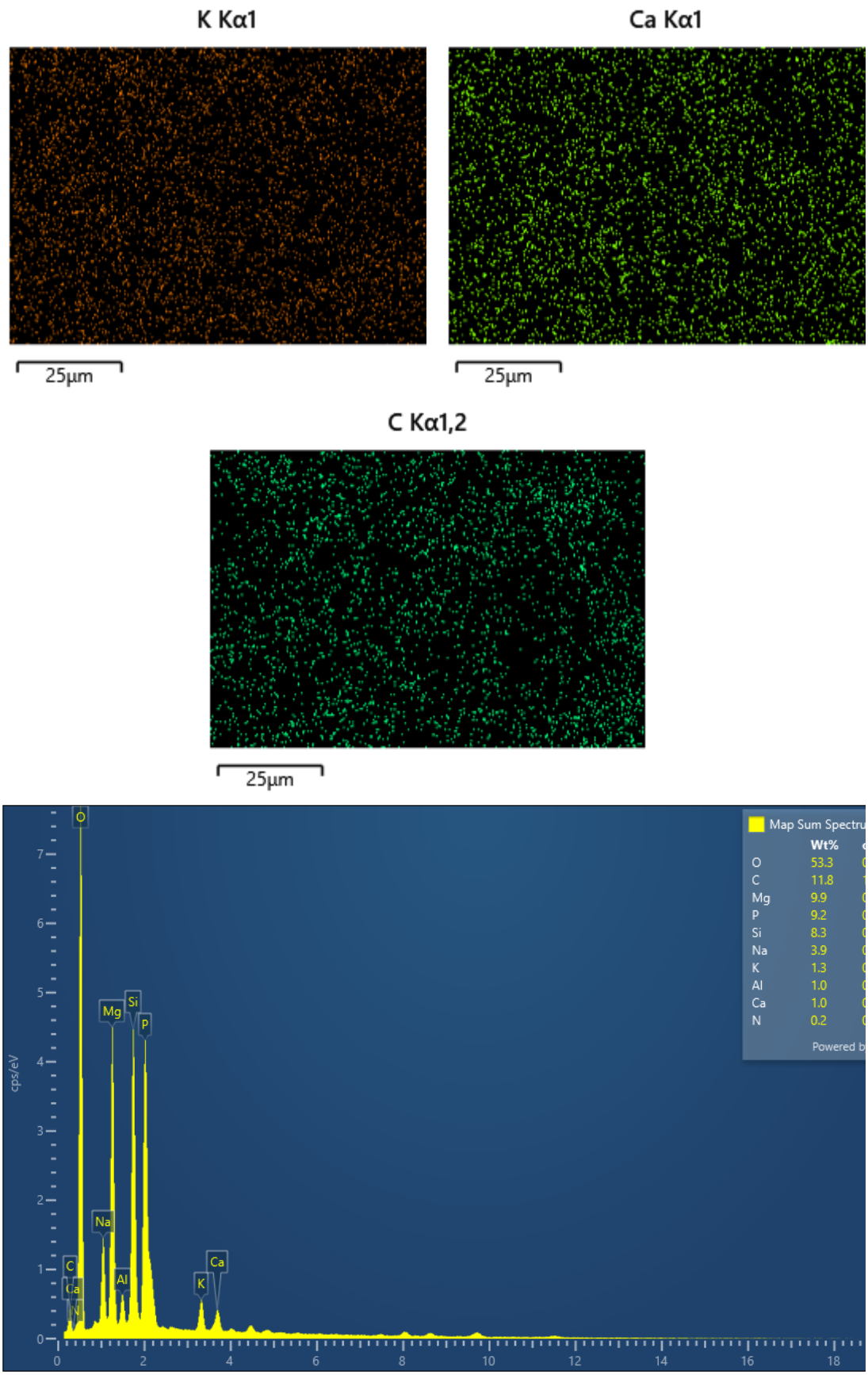


Figure S 4. Scanning electron microscope results for greywater sample during operation phase I.

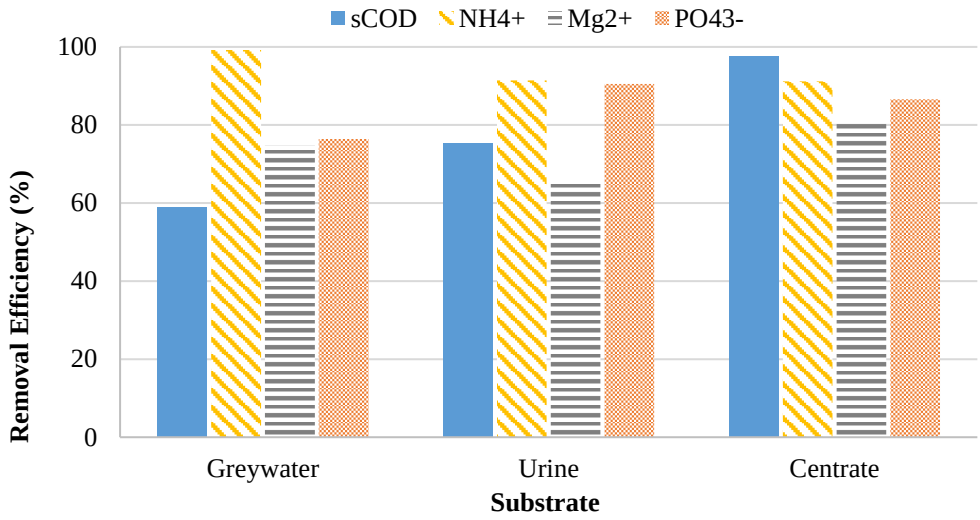


Figure S 5. Removal efficiencies of sCOD, $NH_4^+$, $PO_4^{3-}$, and $Mg^{2+}$ for the examined substrates.

# Vita

Hadeer Abdalla was born in 1998, in Cairo, Egypt. She received her primary and secondary education in Abu Dhabi, UAE. She accepted his B.Sc. degree in Civil Engineering from the University of Sharjah in 2019. In September 2020, she joined the Civil Engineering master's program at the American University of Sharjah as a graduate teaching and research assistant. During the last two years, she co-authored three journal papers, “Eco-efficiency analysis of integrated grey and black water management systems,” “Environmental footprint and economics of a full-scale 3D-printed house”, and “Artificial intelligence applications in solid waste management: A systematic research review” which were all published in top peer-reviewed journals, in addition to three conference papers presented in international indexed conferences. Her research interests are waste-to-energy, microbial fuel cells, life cycle assessment, integrated waste management, artificial intelligence, and statistical modeling.